uOttawa

L'Université canadienne
Canada's university

FACULTÉ DES ÉTUDES SUPÉRIEURES ET POSTOCTORALES

uOttawa

L'Université canadienne
Canada's university

FACULTY OF GRADUATE AND POSDOCTORAL STUDIES

Keegan Lobo
AUTEUR DE LA THÈSE / AUTHOR OF THESIS

M.A.Sc. (Mechanical Engineering)
GRADE / DEGREE

Faculty of Engineering, Mechanical Engineering
FACULTÉ, ÉCOLE, DÉPARTEMENT / FACULTY, SCHOOL, DEPARTMENT

Finite Element Modeling of the Natural Aortic Valve
TITRE DE LA THÈSE / TITLE OF THESIS

Michel Labrosse
DIRECTEUR (DIRECTRICE) DE LA THÈSE / THESIS SUPERVISOR

CO-DIRECTEUR (CO-DIRECTRICE) DE LA THÈSE / THESIS CO-SUPERVISOR

EXAMINATEURS (EXAMINATRICES) DE LA THÈSE / THESIS EXAMINERS

M. Yaras

G. Rouhi

Gary W. Slater
Le Doyen de la Faculté des études supérieures et postdoctorales / Dean of the Faculty of Graduate and Postdoctoral Studies

FINITE ELEMENT MODELING OF THE NATURAL AORTIC VALVE

Keegan Lobo

A thesis submitted to the Faculty of Graduate and Postdoctoral Studies in partial fulfillment of the requirements for the degree of

MASTER OF APPLIED SCIENCE

in Mechanical Engineering

Ottawa-Carleton Institute for Mechanical and Aerospace Engineering

University of Ottawa

Ottawa, Canada

May 2009

Your file Votre référence
ISBN: 978-0-494-61331-3
Our file Notre référence
ISBN: 978-0-494-61331-3

ABSTRACT

The natural aortic valve is able to outlast almost any man-made valve known to date and is a marvellous yet complex structure from a mechanical engineering perspective. However, due to repeated heavy loading, the aortic valve sometimes develops problems such as stenosis, calcification, or even tearing. To correct these pathologies, a replacement prosthesis or repair of the native aortic valve is necessary.

A new numerical benchmark model of the aortic valve was developed to ultimately study aortic valve disease, the effects of a prosthesis or the consequences of an aortic valve repair procedure. As a first step, the focus was placed on a normal aortic valve, since it is not until the mechanical behaviour of the aortic valve in normal conditions is better elucidated that pathologies and deviations from the norm can be better understood and treated.

Many challenges arise when attempting to numerically replicate the aortic valve, including the modeling of its dynamics and hyperelastic, anisotropic material properties. In the present study, a finite element model of a normal aortic valve was established and validated using experimental data obtained from a pressurization system and a left-heart simulator, as well as from published works.

Geometric orifice area and valve dynamics agreed well between experimental and simulated valve models, demonstrating that a fluid-structure interactions model is not needed. Moreover, the total states of stress and strain were determined in the whole aortic valve over the entire cardiac cycle. Significant improvements were achieved compared to previously published models.

ACKNOWLEDGEMENTS

First and foremost I am greatly indebted to my academic supervisor, Dr. Michel Labrosse. I thank him sincerely for granting me this wonderful opportunity to contribute to the field of aortic valve research, and at the same time enhance my own knowledge. He has been most patient with me throughout my studies at the University of Ottawa and I am ever grateful to him. Without his guidance and inspiration this work would not have been possible.

I would also like to thank my family and relatives for their support at every stage of my studies. My parents have never settled for anything but my best efforts and I thank them for being the greatest source of encouragement in my life. Finally, I would like to thank my friends and colleagues, both old and new, each of whom has helped me progress to this point.

TABLE OF CONTENTS

SUMMARY OF FIGURES

SUMMARY OF TABLES

CHAPTER 1 INTRODUCTION

The aortic valve is one key component in the human heart. To help emphasize the relevance of the present work, a brief review of the heart's anatomy and physiology is presented below, along with specific details on the aortic valve geometry and prevalent pathologies. Although many different medical and clinical aspects of the aortic valve are extremely interesting, the focus in this introduction is placed on what is relevant to the present work, which is essentially a mechanical engineering analysis of the aortic valve seen as a pressurized structure. The objectives and main contributions of the present work will then be announced, as well as the thesis outline.

1.1 Background on the Heart and the Aortic Valve

The heart consists of four chambers: the right atrium, the right ventricle, the left atrium and the left ventricle. Blood from all over the body is collected into the right atrium and pumped from the right ventricle to the lungs. In the lungs, carbon dioxide and other metabolic waste products are removed and blood is oxygenated again. Blood from the lungs collects into the left atrium and moves into the left ventricle. Blood is then pumped from the left ventricle to the rest of the body via the aorta.

Four valves in the heart allow blood to flow only in one direction. The tricuspid valve lies between the right atrium and the right ventricle, and the mitral valve lies between left atrium and left ventricle. These two are known as the atrioventricular valves. The cusps (flaps) of the atrioventricular valves are directly connected to the myocardium (heart muscle) and suspended by papillary muscles extending from the

endocardium (inner heart muscle). The other two valves are the pulmonary and aortic valves, which are categorized as semilunar valves. The pulmonary valve lies between the right ventricle and the pulmonary artery, whereas the aortic valve is located between the left ventricle and the aorta. Semilunar valves, as their name suggests, consists of three leaflets, each shaped like the crescent of a half moon. The leaflets of these valves are not directly connected to the myocardium; instead they are supported by the sides of the blood vessel in which the valves sit.

Specifically, the aortic valve prevents back flow of blood from the aorta to the left ventricle. During systole, when blood is pumped from the ventricles, the pressure in the ventricle rises above that of the aorta (typically 120 mmHg versus 80 mmHg, respectively, i.e. approximately 16 kPa versus 11 kPa), opening the valve and allowing blood to flow into the aorta. During this time, the stress experienced by the valve leaflets is minimal. When the ventricles begin to expand again to be replenished with blood, the pressure in the aorta is greater than that in the ventricles, causing the valve to close. This moment is quite crucial as it is when the valve comes under the greatest stress.

Because the mitral and aortic valves are on the high-pressure (left) side of the heart, they experience the largest stresses among all valves. Yet, and most notably, the aortic valve undergoes up to 40 million cycles per year, which is on the order of 3 billion cycles in a lifetime (Billiar and Sacks, 2000). Most natural aortic valves last the span of a person's life without any deterioration. To date, there exists no man-made valve of comparable performance. However, the aortic valve's performance can be hindered by disease.

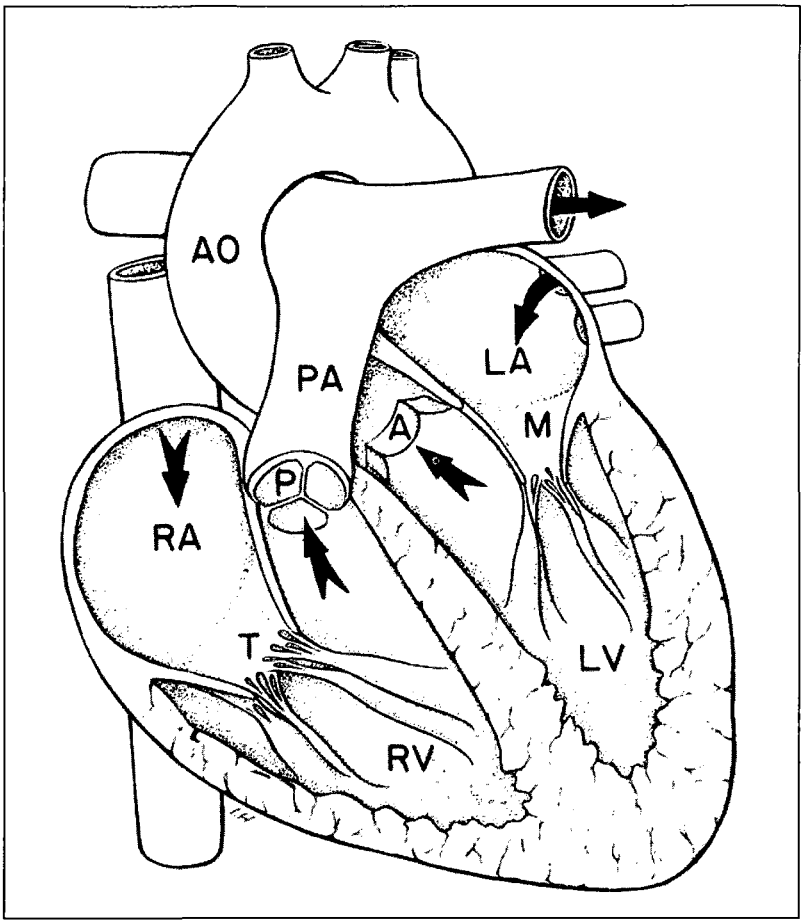

Figure 1– A schematic of the heart displaying its four chambers and valves. AO – Aorta, PA – Pulmonary Artery, RA – Right Atrium, RV – Right Ventricle, LA – Left Atrium, LV – Left Ventricle, T – Tricuspid Valve, P – Pulmonary Valve, M – Mitral Valve, A – Aortic Valve (Thubrikar 1990).

As with all natural and man-made mechanical parts, repeated stressing can cause deterioration. Development of valve deterioration is known as disease pathology and eventually results in aortic valve diseases or some form of cardiovascular disease. Certain parts of the valve experience higher stresses than others and these parts are commonly the first to become diseased. For example, some valves experience stenosis, which can be interpreted as an abnormal adaptation to high levels of mechanical stress and strain in the valve (Thubrikar, 1990; Shoen and Levy, 2005). All of these problems

result from abnormal cellular adaptations and cell deaths that arise from the inability of the tissue to handle excessive loads. Another common problem is the tearing of leaflets from their attachments to the aortic root due to high stress and strain (Thubrikar, 1990). Therefore, being able to replicate and understand the dynamics of the valve would benefit studies on pathologies or surgical modifications of the aortic valve.

1.2 Geometry and Function of the Aortic Valve

As modelling of the aortic valve will be involved, detailed knowledge of the aortic valve geometry is required. Specifically, the aortic valve is comprised of three leaflets and three corresponding sinuses (also known as the sinuses of Valsalva, which can be visualized as portions of balloons in Fig. 2). At the top of the valve, the sinuses fade into the ascending aorta and at the bottom blend into the myocardium of the left ventricle. Lower boundaries of two of the sinuses also blend into the anterior cusp of the mitral valve. In vivo, the valve is surrounded and held in position by loose connective tissue and fatty tissue. When excised from the heart, the outer structure of the valve distinctly displays three rounded sinuses. Two of these sinuses give rise to the coronary arteries that supply blood to the heart. The sinuses are consequently named left coronary sinus, right coronary sinus, and noncoronary or posterior sinus.

From the outside of the valve, the curve along which the leaflets are attached to the sinuses (attachment line) resembles a semi-circle. Following two attachment lines (from two adjacent leaflets) to their intersection brings into view a commissure. A commissure is the region where the attachment lines of two leaflets are parallel.

Commissures are located at either end of the leaflet attachment line as it proceeds towards the top of the sinuses.

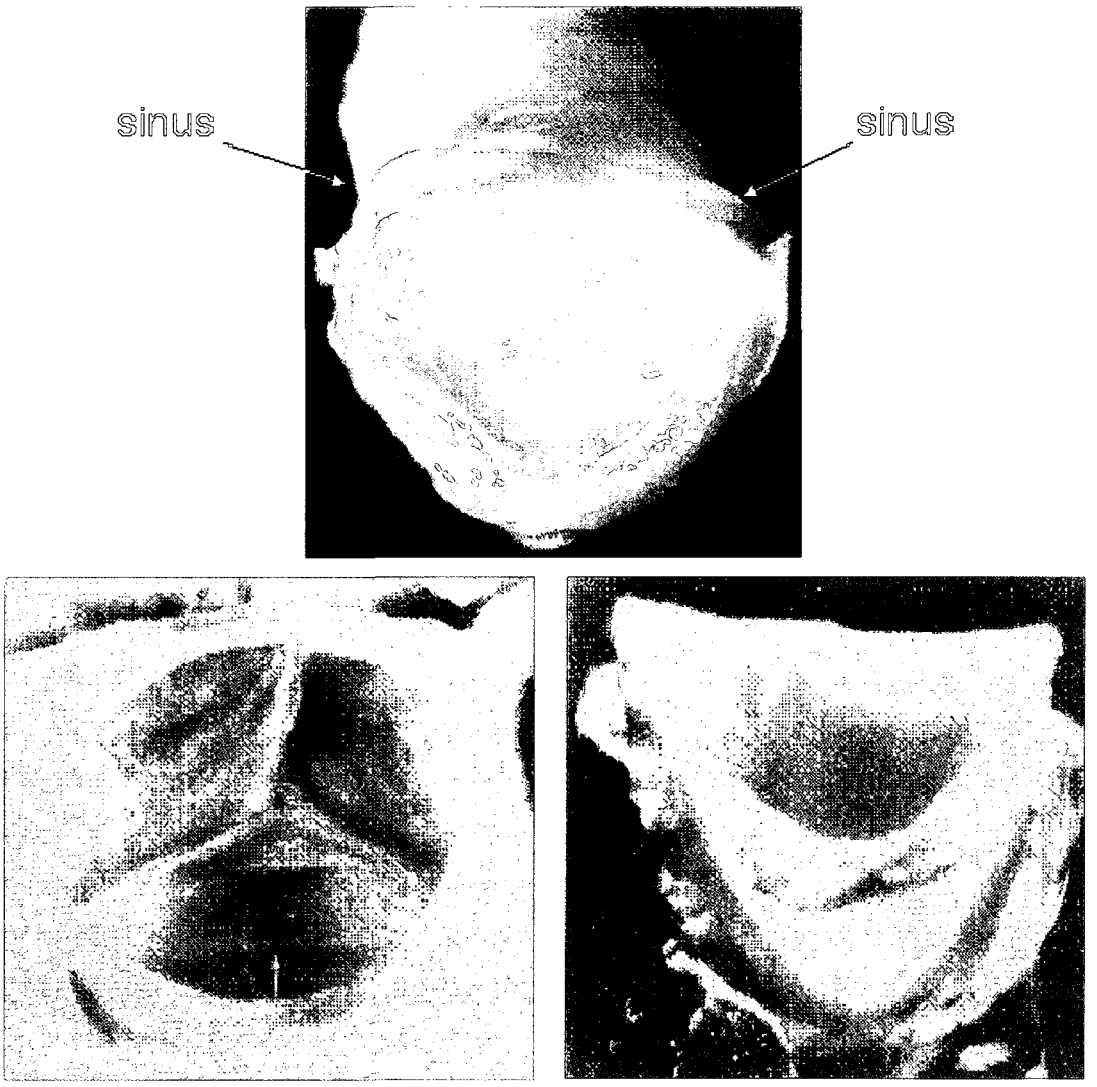

Figure 2 - Top: A view of a human aortic valve from below. The ventricular side of the load bearing portion of the leaflets can be seen, along with two sinuses and the ascending aorta. Left: A view of the leaflets from the top (aorta). Here the aortic side of the leaflets is seen. Right: A single leaflet and its corresponding sinus have been dissected. The nodule of Arantius located at the top middle of the leaflet can also be seen. The nodule is a thick elastin matrix that helps closure of the centre of the valve during diastole (Thubrikar, 1990).

In the closed position (Fig. 2, top), from the ventricular side, the bottom of the loaded leaflets can be seen slightly rounded, and closer inspection reveals that the leaflets

conform approximately to a cylindrical (Swanson and Clark, 1974, Mercer et al., 1973), not spherical, shape contrary to what is erroneously drawn in many anatomy books. From the aortic side, the three leaflets can be seen contacting each other forming a typical "Mercedes-Benz" sign (Fig. 2, left). Two distinct areas of the leaflet can be identified. The part of the leaflet whose area can be seen most separates the ventricle from the aorta and holds most of the aortic pressure. This part is called the load-bearing surface. The part that contacts the neighbouring leaflet is called the coaptation surface. Because of its position in the closed geometry the coaptation surface carries very little of the load exerted by blood.

The aortic valve is composed entirely of connective tissues. Connective tissues rely on two main structural protein components: collagen and elastin. Elastin is a material that is very compliant under stress, and one that can experience stretch ratios of up to 1.5 before breaking (Vesely and Noseworthy, 1992). Collagen fibers are much stiffer in that they can withstand high levels of stress without exhibiting much deformation. In particular the aortic valve, at zero pressure the collagen fibers are coiled up. When pressure is applied the elastin is stretched easily while the collagen fibers begin to uncoil. This is known as the low modulus region on a stress-strain curve. At some point most of the collagen fibers are uncoiled and begin to carry most of the load, increasing the overall stiffness of the tissue, withstanding more stress and less strain. The material is then said to be in the high modulus region. A typical stress strain curve for connective tissue in the aortic valve is displayed in Fig. 3.

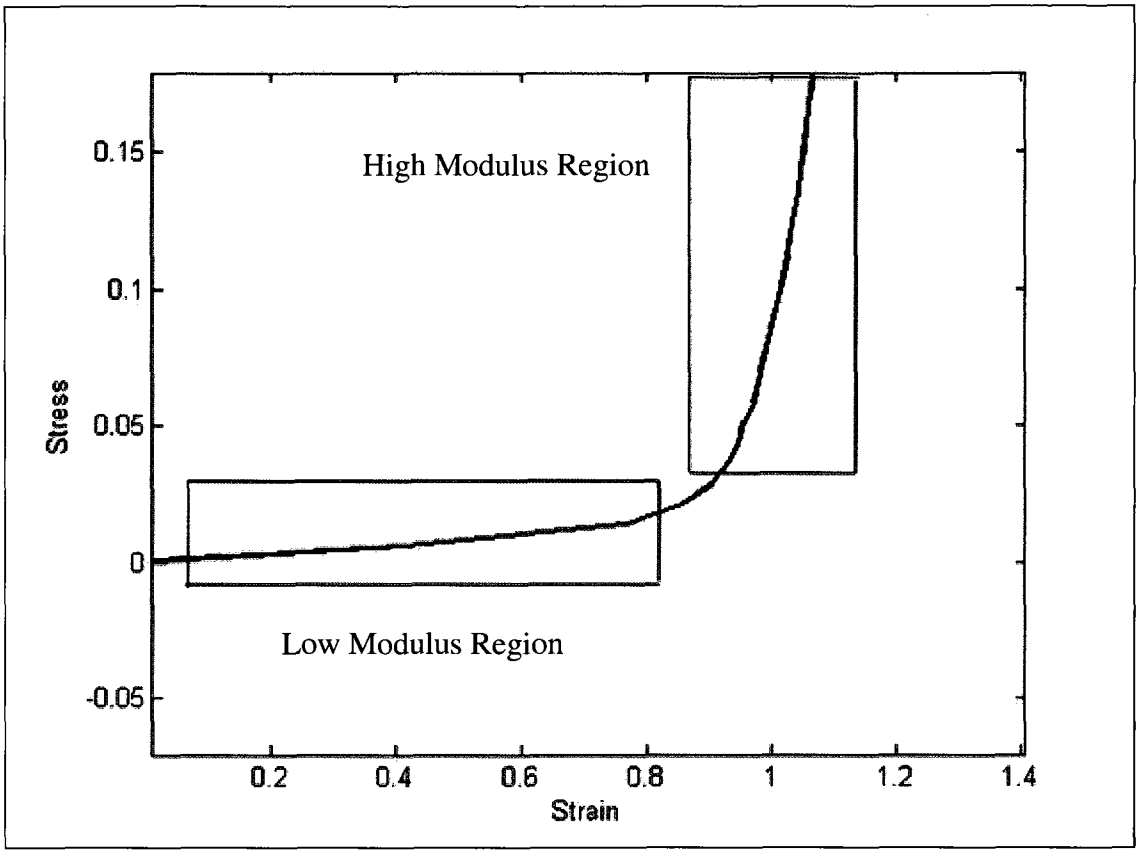

Figure 3 – A typical uniaxial stress-strain curve for connective tissue in the aortic valve. Stresses are in MPa.

The membranous leaflets of the aortic valve are quite thin (typically ranging from 0.1 to 0.6 mm, with large local differences), yet very strong. At a glance, the leaflets appear to be of uniform composition. Under back-light inspection (Fig. 4) however, one can distinctly note the existence of a network of darker fibres embedded in a pale matrix. Indeed, the leaflet consists of three distinct layers: the fibrosa, spongiosa and ventricularis. The fibrosa is predominantly comprised of thick bundles of type I collagen fibers and is positioned on the aortic side of the leaflet. The fiber bundles run generally along the circumferential direction (refer to Fig. 4).

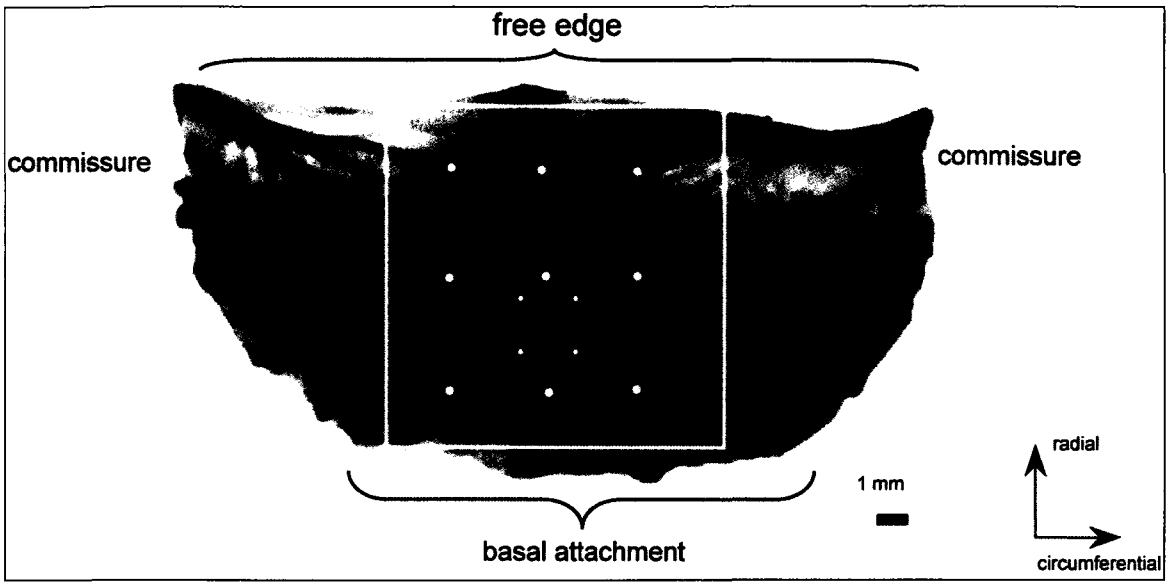

Figure 4 – A leaflet showing a concentration of fiber bundles running along the circumferential direction (Billiar and Sacks, 2000).

When unloaded, the fibrosa is highly undulated and offers little resistance to motion and deformation. During diastole the collagen fibers straighten, now acting as tensile members, thus increasing the overall stiffness of the leaflets. The ventricularis is composed of both collagen and elastin fibers. However, due to its high concentration of elastin it is considerably more extensible than the fibrosa (Stella and Sacks, 2007). The spongiosa is situated between the two layers and is composed mainly of glycosaminoglycans holding mostly water. Little is known about the purpose of the spongiosa however it is hypothesized that it facilitates local relative movement between the fibrosa and ventricularis, thereby promoting easy deflection (Stella and Sacks, 2007).

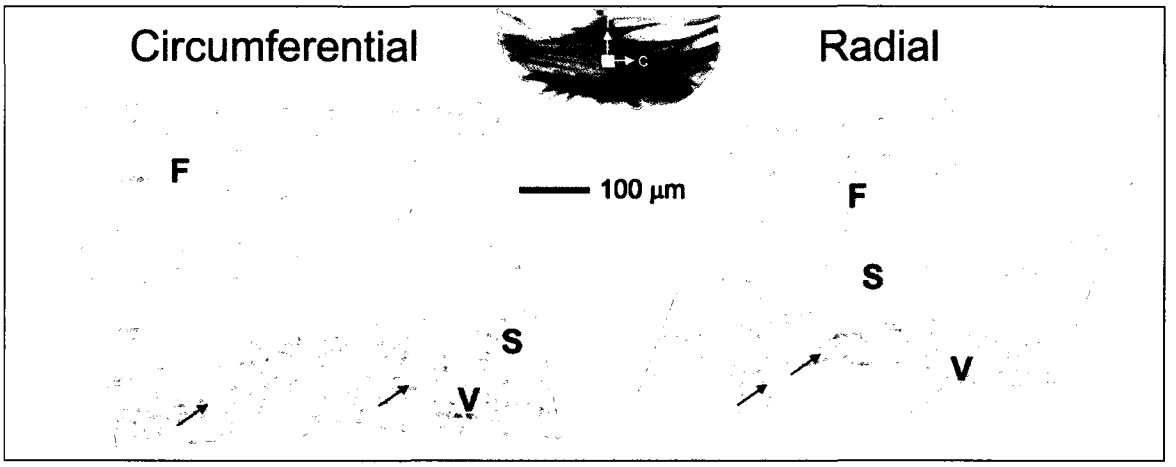

Figure 5 – The fibrosa, spongiosa and ventricularis of the leaflet shown in a cross-sectional perspective.

Before moving further, it is convenient to define coordinate systems that will be referred to quite often in the following. For the leaflets, two directions are of primary concern: radial and circumferential. The radial direction refers not to the position along the direction of thickness but rather to the other non-circumferential orientation of the leaflet. This would be from the bottom most point on the line of attachment to the nodule of Arantius at the center of the leaflet free edge. For the sinuses, ascending aorta and the base, a separate frame of reference is used. The longitudinal direction runs along the central axis of the valve, the radial direction runs across the wall thickness of the valve (outward from the central axis), and the circumferential direction as in the leaflet reference system runs transversally across the tissues at a given radius.

A normal, natural aortic valve has three leaflets whereas some abnormally developed valves sometimes have one, two or four. One and two leaflet valves more frequently develop diseases (Thubrikar, 1990). This could be because above normal amounts of flexion is required from each leaflet. Valves with four leaflets also have compromised performance as there is too much material and wrinkling can be seen in the

closed position. The advantage that the three leaflet valve has over these is that it can close with relatively little change in dimensions (Thubrikar, 1990).

As illustrated in Fig. 6, the leaflet is bounded by the free edge, the line of attachment, and the commissures. The line of attachment and the commissures are natural sites of high mechanical stress owing to the leaflet flexion taking place there as well as abrupt changes in geometry and material properties between the sinus and the leaflet. The leaflets are well equipped to handle circumferential stresses thanks to their collagen fiber reinforcement mostly in the circumferential direction.

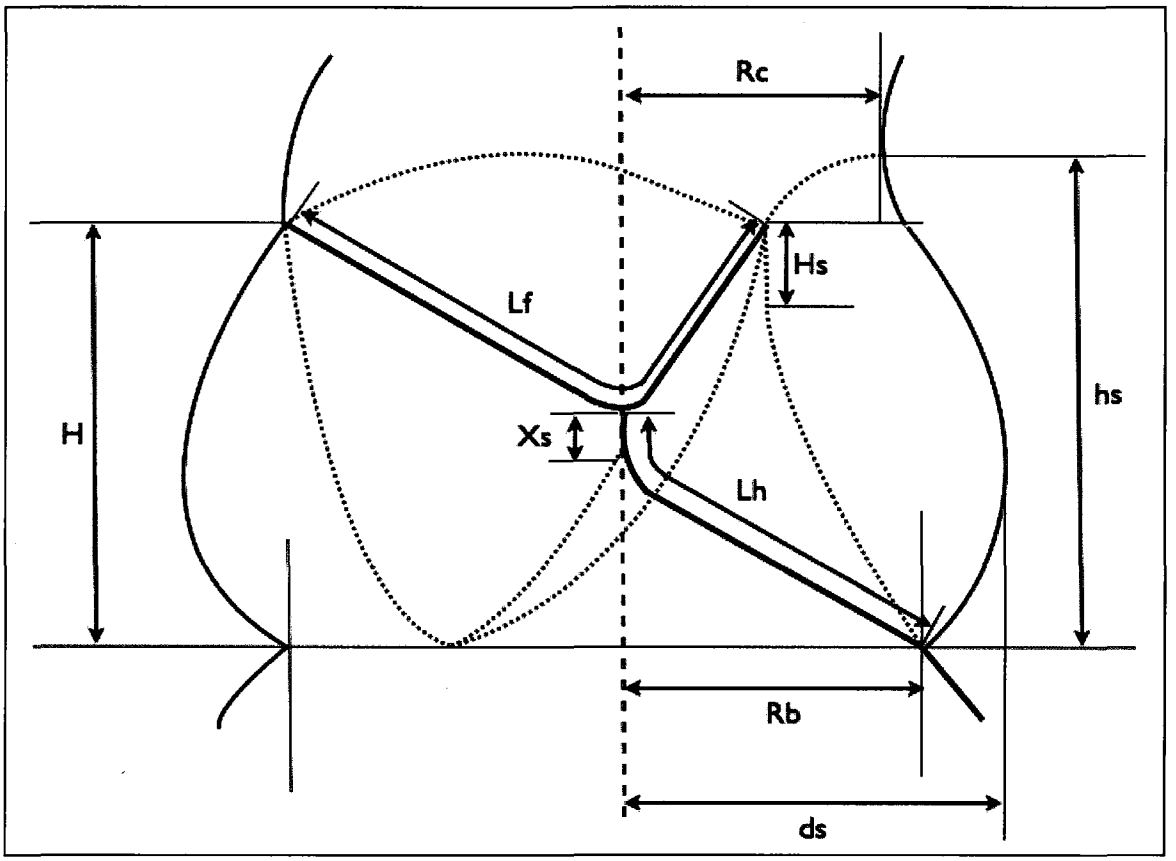

Figure 6 – A diagram displaying some of the important modeling parameters used to describe the aortic valve. R_c – Radius of the Commissures, H – Commissural Height, h_s – Sinus Height, H_s – Height of the Commissures, X_s – Coaptation Height, R_b – Radius of the base, d_s – distance of the sinus to the centre of the valve, L_h – Leaflet Height, L_f – Leaflet Free Edge Length.

An oblique cross-sectional view of a sinus and leaflet together in the closed position comes to produce a spherical structure. Spherical structures are best suited for holding pressure, which suggests that the global spherical shape of the sinus and leaflet assembly plays a very important role in smoothing the stress distribution during the diastolic phase (Beck and Thubrikar, 2001).

The coapting surface of the leaflets may seem to be redundant and insignificant. On the contrary, however, it is quite involved in proper distribution of stress as well. The leaflet experiences a lot of stress during diastole in the belly of the load-bearing surface. The coapting surface serves not only as a surface seal to counter regurgitation, but also provides support from the commissures to this highly stressed region.

The aortic valve components like other living biological tissues undergo structural maintenance and turnover, in response to repeated mechanical stress and wear. The comparatively high concentration of endoplasmic reticulum in the fibroblasts of the spongiosa suggests that the leaflets are quite active in collagen and elastin protein synthesis (Mitimo et al., 1969). Studies involving the tracing of radioactively tagged protein components also demonstrated that structural reinforcement in the aortic valve is prominent in locations of high activity and wear (Mori et al., 1967). In brief, such studies have shown that locations of high stress correspond well with areas of high collagen synthesis. Tissue renewal in the aortic valve is essential to maintain the valve structure and, consequently, functionality.

1.3 The Proposed Study

Every year thousands of people develop aortic valve diseases in Canada. The number of people that suffer from aortic valve diseases increases along with the age of patients. Aortic valve diseases among people with abnormally developed valves (two- and four-leaflet valves), is more prominent than in people with normally developed valves. All of this suggests that while the aortic valve has been studied for years, there is still much that is not known about the valve: the intricate relationship between geometry and function, how the valve's performance changes with age, or even the increased risk factors associated with abnormally developed valves. Given these concerns it is quite clear that deciphering the factors that influence the development of diseases is not at all simple. To better understand disease development and possible contributing factors, the normal aortic valve and its relationships must first be understood. Following this study, one can then examine deviations to study pathologies and abnormalities.

The overall objective of this study is to produce a numerical model of the normal aortic valve. The model will enable investigators to closely study levels of mechanical stress and strain, as well as dynamics of all the valve parts. Pressurization experiments are to be carried out from which required data for material models and validation will be obtained.

1.4 Organization of the Thesis

Much of the necessary background information about the aortic valve has been presented above. The rest of the thesis focuses primarily on modeling issues and

experimentation as it relates to modeling. The second chapter is a review of the literature devoted to existing valve models and their results. The literature review also includes the research work done on the aortic valve leaflets. Before creating a numerical simulation of the aortic valve in physiological conditions, experiments were performed to obtain some key features from a representative case: valve geometry, material properties, aortic and ventricular pressure curves. The third chapter covers these experiments in detail. The fourth chapter outlines the procedures used to construct the aortic valve geometry in commercial finite element software ANSYS. The chapter also outlines how the geometry is exported to commercial finite element software LS-Dyna using MATLAB, and how various shell and solid elements were used. The acquisition of material properties for the aortic wall, sinus and leaflets is discussed in the fifth chapter. The sixth chapter describes how the numerical model was designed to simulate conditions that are closest to physiological conditions. The final chapter compares the results obtained from simulations with the experiments performed as well as with relevant data from the literature. The valve opening and closing times, dynamics, and stress and strain behaviours are discussed there as well. The feasibility of future studies dealing with the numerical simulation of valve diseases and replacement valves is also discussed.

CHAPTER 2 LITERATURE REVIEW

A number of computational challenges have always been present in modeling the aortic valve: its complex geometry, unique material properties, large range of motion, contact between components and dynamics. Dealing with all of these issues simultaneously is quite difficult, and as the complexity of the model increases, so does the computational time. More specific modeling issues are also present. The application of fluid-structure interactions or the use of linear, instead of non-linear material properties are also subjects often debated. Significant advances have recently been made in modeling the aortic valve most of which are reviewed here.

2.1 Dry Models vs. Wet Models

Generally, two methods have been used to model the aortic valve using finite elements: "dry models" where the pressure loading is assumed, and "wet models" or fluid-structure interaction (FSI) models, where coupling between blood flow and aortic valve structure is taken into account. Dry models aim to produce the dynamic behaviour of the valve by implementing the physiological pressure gradients experienced by the valve. In such models the pressure distribution on a particular surface is spatially uniform but varies in time as the cardiac cycle proceeds. The rationale behind using dry models is that during most of the cardiac cycle, the motion of the leaflets is a passive response to the pressure gradient (or flow of blood) through the valve, while the active contraction of the heart may only marginally affect the geometry of the aortic root in which the leaflets are suspended. On the other hand, most authors who employ FSI models argue that

modeling of blood flow dynamics is required to properly simulate the motion of the leaflets. An FSI model is distinct from a computational fluid dynamics (CFD) model and a purely structural finite element (FE) model. In CFD analyses, structural components remain fixed, while in an FE model, loads must be specified before a solution can be found, therefore no coupling will take place. FSI models include the blood flow through the valve, which produces a spatially non-uniform pressure distribution. An iterative solution method is needed as the loaded structure moves and thereby affects the blood flow which, in turn, may affect the structure (two-way interaction). Compared to dry models additional information provided by FSI models includes fluid shear stress and shear strain data which some authors claim is quite significant, especially when considering the epithelial cells at the surface of the leaflets which may be very sensitive to flow conditions (Vesely and Boughner, 1989).

Various authors have obviously taken different approaches to modeling the aortic valve. The efforts have been mixed between FSI, pressure loading, non-linear and linear material properties, with all but a few models implementing all refinements at once. Many authors have also moved from using one method to another. The following will describe the evolution of various models put forth by some notable authors.

2.2 A History of Finite Element Models For the Aortic Valve

A rich stream of studies by Patterson and his colleagues began by attempting to simulate the motion and stresses encountered by the Sheffield bioprosthetic bicuspid heart valve developed by the same authors (Black et al. 1986). Huang et al. (1990) produced a two-dimensional finite element model based on experimental observations of

the Sheffield bicuspid valve. Huang et al. produced two models: one based featuring the radial cross-section and the other featuring the circumferential cross-section. The authors were able to implement the strain energy density function developed by Tong and Fung (2001) to describe the stress-strain relationship of a hyperelastic material. This was quite an advancement in the development of finite element models of heart valves and other related soft tissues.

However, some assumptions made for this study evidently had adverse effects on the results. For example, both the radial and circumferential directions were assigned the same material properties, after taking an average value for the displacements observed in experiments performed by Trowbridge et al. (1985). It is now commonly known that the radial and circumferential directions respond in different ways, which can be attributed to the direction of fiber bundle orientation in the leaflet (Billiar and Sacks, 2000). Another difficulty they encountered was with prolapse of the radial slice, a process in which the leaflet sags too much upon closing and actually creates a leak. To correct for this, the amount of pressure applied on the radial model was simply reduced. Although not mentioned in the paper, this could have been caused by improper application of boundary conditions or inadequate leaflet height. The authors only applied up to 3 kPa of pressure, which they considered to be representative of the pressure applied to a three-dimensional model in two dimensions.

Despite its drawbacks, this model still demonstrated the feasibility of applying the finite element method to the aortic valve, and the feasibility of using non-linear material properties which is arguably one of the most important features in modeling soft tissues.

The next significant development made by Patterson's group came in 1996 when they documented the development of a three dimensional finite element model of the Sheffield bicuspid valve (Thornton, 1997). For this analysis Thornton et al. used just over 2300 Belytschko-Tsai shell elements. Only the leaflets were modeled; the sinuses and aorta were left out. The leaflet attachment was assumed to be rigid, similar to a stent. The leaflets were assigned a linear Young's modulus which was varied between 3 and 8 MPa. The thickness was also varied for a constant Young's modulus of 7 MPa.

Despite the assumed symmetry of the valve, the coapting portion of the leaflets folded to one side. The author (Thornton, 1997) attributed this to the small rounding errors inherent to dynamic instabilities. The author observed the stress was lower everywhere in the leaflet except in the belly region where the opposite was true. Stresses were also reduced with reducing thickness, however not significantly so in the region of the commissures. The stress results are considered to be not completely representative given that the leaflet attachments are rigid here, whereas they would be flexible in a natural valve or somewhat flexible in a stent. With a less rigid attachment, the stresses are expected to reach significantly lower values.

Noting the importance of non-linear material properties, and the difference between these and linear material properties, Patterson and his colleagues developed a FSI model. According to Carmody et al. (2006), heart valves' work conditions have made them very difficult to study. Experimental observation is time consuming, expensive, and does not provide relevant structural data. By this logic an FSI model, as opposed to an experimental method, computational fluid dynamic (CFD) model or a structural finite element analysis (FEA), is required. This study by Patterson et al. was conducted in two

parts. The first part simulated the flow of blood into (through the mitral aperture) and out of (through aortic aperture) the left ventricle. The second part assumed the outlet flow profile as the input for the flow profile in the second model which consisted of the aortic valve and root. The ventricular model was developed from magnetic resonance image (MRI) studies, and was modeled with linear elastic material properties. The fluid control volume was modeled around the ventricle model with inlet and outlet flow reservoirs matching the mitral and aortic apertures. Pulsatile flow was simulated using two distinct methods: motion of the ventricular wall and by a direct application of pressure over time. The valve leaflets were designed using data from Thubrikar (1990) and the sinuses were modeled using data from Swanson and Clarke (1974). Shell elements employing non-linear material properties for the leaflets and linear characteristics for the aortic root walls were used. The authors unfortunately did not provide details about the non-linear material model that they applied.

The results obtained from this study were favourable in comparison to experimental methods. The valve motion corresponded well with physiological behaviour in terms of opening times and flow velocities. There was however a difference in the flow velocity profiles between the pulsatile model and the ventricular wall motion model. The ventricular wall motion model produced symmetric velocity profiles whereas the pulsatile model produced non-symmetric velocity profiles. This study was an excellent demonstration of the feasibility of FSI models and their capability to reproduce conditions in the aortic valve. The only limitation is the use of linear elastic material properties in the aortic root, as it has been demonstrated that the interaction between the

leaflets and sinuses is important to proper valve dynamics and stress distribution (Cacciola et al. 2000).

Elsewhere, a three leaflet finite element model was developed by De Hart and his colleagues (2000). These authors first developed a purely structural finite element model based on a synthetic valve designed by Cacciola et al. (2000). Only one half of a single leaflet was modeled being fixed rigidly at the attachment line to simulate fixture to a stent. The leaflet was fixed circumferentially along the leaflet height to simulate the presence of the other half of the leaflet. The synthetic valve was composed of high-performance polyethylene (HP-PE) fibres embedded in an ethylene-propylene-diene-monomer rubber matrix (EPDM). The finite element model was constructed in the same manner, with aortic and ventricular rubber sides and a fiber layer in-between. Two different fiber orientations were investigated: a sinusoidal pattern and a unidirectional circumferential pattern.

Young's moduli of 1.5 MPa and 3.0×10^3 MPa were used along with Poisson's ratios of 0.45 and 0.4 for the matrix and fiber respectively. For such a model these material properties are acceptable considering that the use of the EPDM material here is constrained to its linear range. In the fully closed state the leaflets were subjected to a maximum pressure of 4 kPa. It should be noted, however, that the normal pressure experienced by the aortic valve leaflets ranges from approximately 10.5 kPa to 13.5 kPa during diastole.

The results acquired were directly indicative of the importance of the fibers. The circumferential fiber reinforcements reduced stresses in the rubber layers by up to 60% and the sinusoidal pattern reinforcements reduced stresses by up to 30%. From this

analysis the authors hypothesized that the fiber layer began to carry most of the stress applied to the leaflet. Other notable observations include the stress concentrations at the commissures and the belly region in all layers.

Following this study, another was completed by De Hart's group (Cacciola et al. 2000), this time investigating the performance of the valve with and without stents, using the same finite element model. Geometries with stents were modelled as having a rigid attachment and geometries without stents were modelled with one half of an aortic sinus. These sinuses were modelled as linear elastic, while the rubber used in the synthetic valves was non-linear elastic. The authors mention that a Mooney-Rivlin model was appropriate for this case but was not implemented because of the difficulty in determining the material parameters. In this model as well, a maximum pressure of 4 kPa was applied to avoid numerical instability. This magnitude of pressure however, is significantly lower than the pressures witnessed in normal physiology and insufficient to carry out a complete dynamic analysis.

Despite the inability to replicate material behaviour, the authors made two significant observations. Firstly, the stentless, unidirectional, twenty-fibre configuration reduced maximum principal stress by up to 47% when compared to a stentless, non-reinforced model. Also, the stentless, sinusoidal, twenty-fibre configuration gave much lower maximum principal stresses when compared to its counterpart, the stented, sinusoidal, twenty-fibre configuration.

A few conclusions were drawn from this study. Firstly, the importance of a flexible aortic root in valve loading and dynamics was discussed. This was clearly demonstrated by the strong reduction in stresses seen between the stented configurations

and the stentless configurations. Secondly, the fibres in the unidirectional fibre-layout carried most of the amount of stresses, reducing the stresses in the matrix. The authors also note that this fibre orientation was closest to that of the natural collagen fibre distribution.

De Hart and his colleagues also developed an FSI model. The model was initially developed in two dimensions and later extended to three dimensions (De Hart et al. 2000).

Traditionally fluid and structural domains are described using two distinct formulations: the Eulerian reference frame for fluids, and the Lagrangian formulation for structures. The difference is that, in the Eulerian formulation, the material (fluid) moves through the computational domain, whereas in the Lagrangian formulation, the computational domain moves with the material (structure). Given the nature of the two domains, it can be said that both these formulations are incompatible for a simultaneous study. The authors used an arbitrary Lagrange-Eulerian (ALE) formulation as a solution to this incompatibility. It involves a continuously adapting mesh without the need to modify the mesh topology. Details about fluid domain meshing are quite complicated and lie beyond the scope of this review.

For the two-dimensional model, the structure was discretized into eight beam elements with two translations and one rotation in the plane. Linear material properties were used with an elastic modulus of 1.5×10^6 Pa and a Poisson's ratio of 0.49 allowing the leaflet to displace more in the radial direction. The two-dimensional sinus, aorta and left ventricle were assumed to be completely rigid. The structure was modeled as two walls with the leaflet attached to the base of the sinus, which protrudes out of the top

wall. The bottom wall was flat and a no-slip condition was applied, simulating a neighbouring leaflet during coaptation. As a simplification, a free outlet was enforced at the aorta and a pulsatile flow was applied at the inlet, which was modeled after conditions in an experimental set up.

The experimental apparatus consisted of a geometry similar to the one described above, except that it extended into the third dimension. The rectangular sheet simulating the leaflet was constructed from EPDM rubber having a density of 890 kg/m^3 and a Young's modulus of 1.5 MPa. The experimental leaflet was considered to be isotropic, incompressible and linearly elastic. The fluid used was a solution of 36% glycerol diluted in water, having a density of 1001 kg/m^2 and a viscosity of $4.3x10^{-3}$ kg/m.s, values that are comparable to that of blood.

The results from the numerical model and the experiment were compared using two different criteria: leaflet position and flow velocity. The leaflet in the numerical model generally lagged slightly behind the leaflet in the experiment, but was still qualitatively acceptable. The authors attribute this to the difference in fluid and leaflet mass density between the two models. The velocity vector maps also agreed quite well with the exception of a small vortex in the simulations near the leaflet attachment that hindered the sinus vortex from developing completely.

De Hart's group then focused on developing a three dimensional FSI model (De Hart et al. 2003). There, the two dimensional model was extended to three dimensions using the same ALE method as described above. Their intent was to study the effects of fluid structure interaction on valve behaviour and structural stress state. In this model, a rigid sinus and aorta were modeled with a flexible leaflet replicating a stented

configuration. Only one half of a leaflet and sinus were modeled comprising one sixth of a complete valve. The model was bounded by a plane of symmetry on one side, which ran through the middle of one whole leaflet and by a rigid contact surface on the other side where two leaflets would coapt. In this analysis, only a single systole of the cardiac cycle was implemented, for which the aortic and ventricular pressures applied were varied between 0 and 6 kPa, which is considerably lower than the normal physiological pressures. The diastolic phase was not modeled because of the excessive deformations that would result from the material's inability to withstand large pressure differences. For the leaflets, an elastic modulus of $3.0x10^{-2}$ MPa was used and the leaflets were assumed to be isotropic.

The authors commented on the alternation between tensile and compressive stresses on the aortic and ventricular surfaces of the leaflet, but gave no interpretation of this behaviour. A possible explanation of this could be the fact that this simulation started in the closed position considered as the stress-free state. Also, the authors used a relatively low elastic modulus to fit the behaviour characteristic to that of a valve in the process of opening. However, with a low modulus starting at the closed position in a stress-free state, the opening motion of the leaflet is expected to result in a stress distribution that varies between compressive and tensile stresses from the aortic to the ventricular sides of the leaflet. In actuality, the leaflets are loaded in the closed position and part of the opening motion may be an elastic response to a high deformation resulting from a high load (recoil). Either way, these stresses are far less significant compared to those witnessed during the diastole phase. However, the model does show consistency with its two-dimensional counterpart in terms of flow vorticity and dynamic behaviour.

Another group headed by Kunzelman (Grande et al. 1998), developed an asymmetric FSI model of the aortic valve that started as a pressure loaded model (Grande et al. 1998). This model is quite interesting because it is the only complete three dimensional model of the aortic valve that does not use an idealized geometry; it was developed from magnetic resonance images of natural human aortic valves, and includes the coronary ostia. Points were drawn at intervals on each cross sectional image. The points were then linked together using cubic splines and the geometry was meshed using six-noded triangular shell elements. The geometry also included varying thicknesses based on measurements taken from the magnetic resonance images and literature. The authors did not give details regarding which thicknesses were measured and which were taken from literature.

The authors also contended that the valve tissue operates primarily in the high modulus region, and applied high linear elastic modulus values. Moduli of 334 kPa and 350 kPa were used for the aortic root in the circumferential and longitudinal directions respectively. In the leaflets, 6885 kPa and 1624 kPa were used for the circumferential and radial directions respectively. Also a Poisson's ratio of 0.45 was used in the leaflets. The pressure applied to the aortic root was ramped to slightly less than 120 mmHg and tapered to approximately 80 mmHg as is normal in the aorta. Pressure applied to the leaflets was linearly raised from 0 to a maximum pressure of 100 mmHg and reduced simulating diastolic loading. The boundary conditions included contact elements along the ventricular surface of the leaflets and the inner sinus walls. The structure was constrained by assigning a displacement of zero to nodes along the bottom most layer of

the base. Longitudinal physiological stretch was also added to the top of the ascending aorta and coronary ostia by applying a corresponding tensile load (Han and Fung, 1994).

The results were validated using *in vivo* magnetic resonance images of healthy human aortic valves (average age of 26.5 years). Results from this analysis showed that the maximum stress was highest in the noncoronary sinus and corresponding leaflet. The distribution of stress corresponds well with other studies indicating high values in the belly region and along the leaflet attachment. The authors attribute the difference in stresses between leaflets to their anatomical differences. Studies show that the noncoronary leaflet among humans has the largest area, attachment length, free-edge length and thickness (Kunzelman et al. 1994). The authors argue that if the leaflet and sinus are considered together, they would produce a hemisphere. According to the Laplace law (circumferential stress equals pressure times radius divided by wall thickness) this hemisphere created by the noncoronary third will have a greater radius than the left and right coronary sections giving it a higher stress for the same physiological pressure. The fact that the stresses are highest in the noncoronary leaflet and sinus, further support the conclusion that the two parts work in tandem to manage stress in the valve. Also, the absence of a coronary ostium, which would relieve some of the blood pressure, likely contributes to the higher level of stress in the noncoronary leaflet and sinus.

Kunzelman's group then argued that an FSI model was required to completely capture and reproduce the dynamic behaviour of the valve (Nicosia et al. 2003). Their study employed the same geometry as discussed above. A few differences between the dry static model and this FSI model were present. Firstly, the FSI analysis was completed

in commercial finite element software LS-Dyna, whereas the pressure loaded solution was obtained from ANSYS. The elastic modulus was kept the same for the aortic root but was decreased for the leaflets. While Poisson's ratio was kept the same, the elastic modulus was assigned as 0.2 MPa. The authors stated that this value modeled the behaviour of the low modulus region, and consequently produced stresses during diastole that were inaccurate. In contrast to the initial dry static model, where the pressure was simply ramped to a maximum diastolic value, the pressure curves for an entire cardiac cycle were applied to this model. Due to the use of this low modulus, the diastolic pressure also had to be scaled down to prevent numerical instabilities.

In the results, cross-sectional views of the leaflet opening and closing showed that the leaflet position was acceptable at various points during the opening and closing of the valve. However, the figures exhibited an exaggerated bulge in the leaflet toward the sinus during opening. This bulge can arguably be attributed to the low modulus used for the leaflet. Another issue the model faced was related to the calculated effective orifice area. Contrary to experimental studies (Thubrikar, 1990), the model's opening motion is very gradual compared to closing. The flow visualization, however, showed that the characteristic sinus vortices and leaflet eddies were present as is in other FSI models and experimental studies (De Hart et al., 2003; Peskin and Mcqueen, 1995).

More recently, Ranga et al. (2004) developed a static model of the aortic valve. The model aimed to help study a number of aortic valve issues. The valve was developed in two configurations: open and closed. The open configuration was loaded with pressures that are typical during the systolic phase, while the closed configuration was loaded with diastolic loads. A longitudinal stretch was also applied to the whole aortic

root by pulling the top of the ascending aorta. The valve geometries were constructed using modeling relations developed by Thubrikar (1990), and data for design parameters from Swanson and Clark's study on dimensions of excised human valves (1974). The valve was given an isotropic non-linear, five parameter Mooney-Rivlin material model in ANSYS finite element package, for which the material constants were obtained from analyzing experimental stress and strain data. The model was compared to a range of simulations employing linear elastic models. It was found that the non-linear model's results corresponded best with the results of a simulation of a Young's modulus of 2000 kPa. The authors observed that as the young's modulus was increased from 250 kPa to 6000 kPa the strains experienced by the valve decreased, and expectedly the stresses increased.

Although this model showed a good potential for aortic valve modeling, some limitations exist. Ranga et al. (2004) managed to apply a Mooney-Rivlin model, however, could not apply anisotropy in ANSYS, and could not address the aortic valve dynamics either. This point in particular is the topic of the next section.

2.2 Implicit versus Explicit Methods of Solution

Leaving aside FSI problems for a moment, dry aortic valve models can be handled by two different types of finite element solvers: implicit or explicit. In statics, with an implicit finite element software, the externally applied force vector $\{F\}$ is related to the material stiffness matrix $[K]$ and displacement vector $\{U\}$ by $\{F\}=[K]\{U\}$. The displacements can be solved for by multiplying both sides by the inverted stiffness matrix. When dynamics is considered, and if material damping (e.g. originiation from

viscoelastic material behaviour) is neglected, the governing equilibrium equation is $[M]\{\ddot{U}\}+[K]\{U\}=\{F\}$, where $[M]$ represents the mass matrix, and $\{\ddot{U}\}$ is the acceleration vector. With an implicit method of solution, the displacement vector $\{U\}$ at time $t+\Delta t$ cannot be simply expressed as a function of quantities known at times t and $t-\Delta t$. Instead, heavy computational procedures based on the Newton-Raphson scheme are used to linearize the problem and find iterative solutions, which in particular, necessitates multiple inversions of the stiffness matrix $[K]$ and limits the applicability of the method when soft tissues and contact problems are involved.

By contrast, with an explicit method of solution based on the central difference scheme, the displacement vector $\{U\}$ at time $t+\Delta t$ can be simply expressed as a function of quantities known at times t and $t-\Delta t$, and this does not involve any complex matrix inversion. The displacement $\{U\}$ can therefore be solved iteratively and very efficiently as a function of time. However, one limitation of the explicit method of solution is that a small time step Δt is required, which depends on the speed of sound through the smallest element, which in turn depends on the stiffness of the material. This implies that both the element size and the material properties significantly affect the computational time.

Commercial finite element ANSYS being mostly based on implicit methods, it is now clear why the aortic valve models developed by groups such as Kunzelman's (1994) and Ranga's (2004) are limited to statics, and simplified material properties. On the other hand, commercial finite element software LS-Dyna, being mostly based on an explicit

method, has been used extensively by Patterson's group and produced dynamic models with the potential to include advanced anisotropic material properties.

2.3 Review of Design Features

While the models discussed in the literature contributed to the development of aortic valve modeling, there still remain many avenues that can be refined. A common insufficiency that led to shortcomings in many of the models discussed is the inability of available numerical methods to implement the non-linear material models developed. In some cases, even given the ability to apply appropriate material models, the finite element models used were unable to bear the stress applied to them and became numerically unstable. Also, the wide range of material models used, each having their own accuracies at various loading ranges, causes large variations in the results.

There is also a wide range of techniques used to validate the numerical models, and no clear standard of simulation performance. Regarding dynamics, many researchers prefer to compare models to *in vivo* MRI images, while others are comfortable validating against *in vitro* simulations or even other computational models. Further, depending on the models, a variety of justifications exist for the different stress values obtained in the different components of the aortic valve, without a clear consensus as to what really is expected.

Including fluid structure interactions into a finite element model is a quite worthwhile exercise. However, it most often comes at the cost of using material properties that are not suitable for modeling aortic valve tissues. While many hypotheses

exist as to the importance of the fluid-structure interactions near the leaflet and especially in the sinus, priority should be given to proper material modeling. Indeed, the shear stresses produced by fluid motion are expected to be minimal compared to the normal stress distribution developed inside the tissues (Humphrey, 2002). Valve dynamics is arguably the one area where FSI models can be appreciated. This stems from postulations that sinus vortices contribute to proper coronary circulation and force the closure of the leaflets during diastole. Other researchers, such as Patterson and his colleagues (Burriesci et al. 1999, Chew et al. 1994), have successfully argued that the motion of the leaflets is driven by the difference between the aortic and ventricular pressure and has little to do with sinus vortices.

A dynamic aortic valve model employing non-linear, anisotropic material characteristics that can be established and validated using different experimental techniques is strongly needed as a basis for further research. It is at the core of the present thesis. Extension of such a model to include fluid structure interactions could be considered at a later stage.

CHAPTER 3 IN VITRO EXPERIMENTATION

It is evident from the discussions above that aortic valve performance in numerical simulations is greatly dependent on the choice of the material models used and their implementations. However, one first step in trying to accurately reproduce the geometry and motion of the aortic valve consists in observing the behaviour and dynamics of the valve in experimental conditions that closely replicate physiological conditions. Toward this goal, a porcine aortic valve was placed into a left-heart simulator, and the valve opening and closing was observed from the aortic side. The pressure curves applied to produce these motions were recorded. Following this experiment, the aortic valve was placed in a saline bath where it was pressurized from 0 to 160 mmHg, while cross-sectional images and the position of longitudinal markers were recorded so as to establish the material properties of the aortic material. In addition, silicone rubber moulds were cast of the aortic valve under 80 mmHg pressure for further measurements. In what follows, complete details about the experimental procedures are given. Multiple experiments were run using different porcine valves in order to achieve a good control on all experimental parameters and gain confidence in the results obtained.

The aortic valve samples used in the experiments were excised from porcine hearts, which were obtained from a local abattoir. The aortic valves were carefully separated from the cardiac muscle and any excess fatty tissue was removed. The coronary ostia were blocked using wire ties and/or commercial cyanoacrylate glue. Throughout the experiments, the aortic valve was soaked with saline solution to preserve the moisture of the sample.

3.1 LEFT HEART SIMULATOR APPARATUS AND PROCEDURE

The left-heart simulator (Fig. 7) used in this procedure was manufactured by Vivitro Systems Incorporated (Victoria, British Columbia). A number of parts have been integrated to perform the function of the left-heart simulator, which in essence, is a complex system able to replicate the blood flow and pressure conditions existing in the human heart.

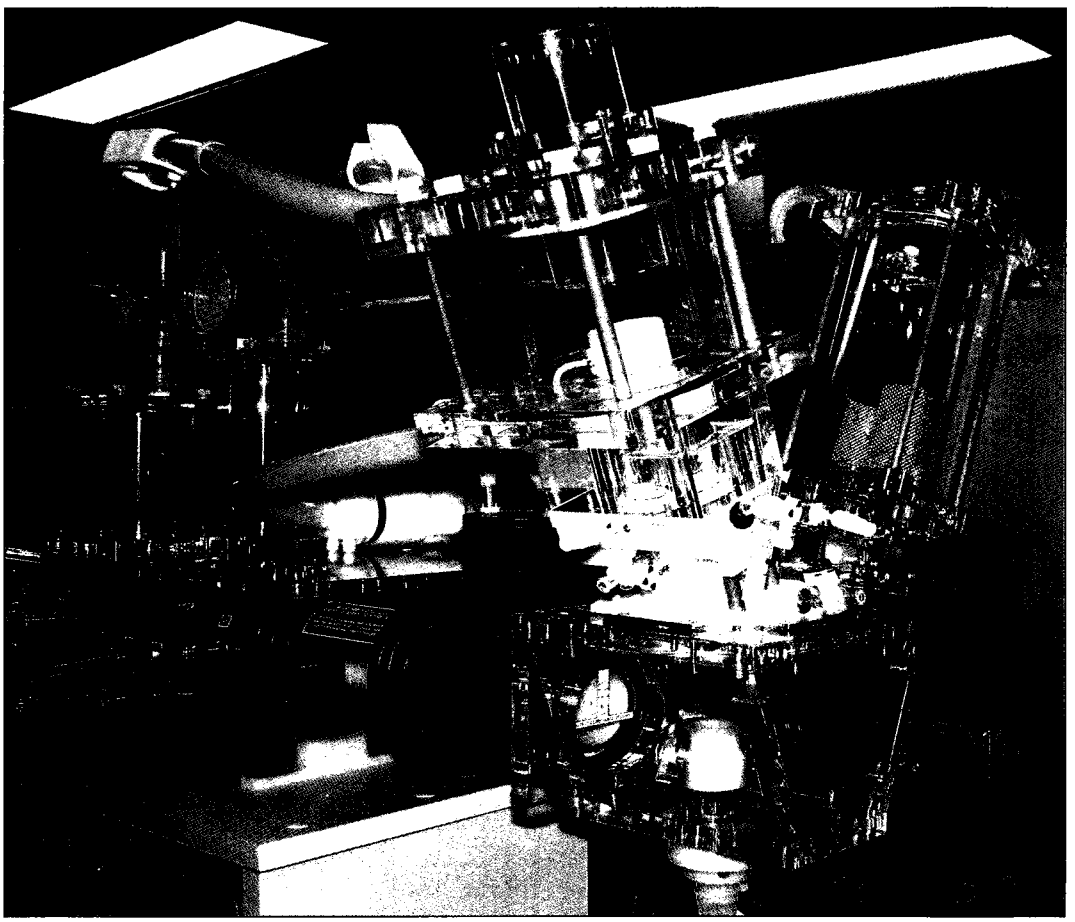

Figure 7 – Image depicting the complete left heart simulator apparatus excluding the Phantom 4.0 high speed camera and the adjustable jig. The simulator was not being operated in this figure.

A pump system is used to drive the fluid flow through a model of the left ventricle. The pump system is controlled by selecting the appropriate waveform for

position or velocity on a power amplifier. A linear actuator converts the rotary motion of the electric motor that powers the pump into linear displacements by use of a ball-screw.

Interfacing between the pump and the left-heart model is a visco-elastic impedance adapter (VIA) which dampens the pressure and flow waveforms generated by the left heart simulator to help generate physiological traces. The VIA is made up of a fixed resistive element and two adjustable compliance chambers. The system compliance can be adjusted by inserting or removing a volume of air from the source and output stop-cocks.

The left ventricular model is surrounded by water in a hydraulic chamber. The hydraulic chamber consists of transparent rigid walls that allow the functioning of the aortic and mitral valves to be visualized easily. The chamber also allows the pressure to be measured at various points, such as the aorta, left ventricle, aortic valve and mitral valve, using transducers. The left heart model is driven by the pump assemblage through the VIA. The hydraulic chamber is filled with water and any excess air is removed from the top of the chamber by a syringe through a catheter.

The model ventricle is made of a silicone rubber, the properties of which produce a near natural performance under physiological loading. The material has a density of 1.2 g/cm^3, tensile strength of 9 MPa, a quiescent volume of 133 ml and a membrane thickness of 0.584 mm. The quiescent volume is measured by pouring water into the ventricle until the level reaches the valve orifice. This volume of water can then be collected and measured to determine the quiescent volume. The ventricular volume can be adjusted by simply adding or removing fluid to the hydraulic chamber. For this experiment, 175 ml of saline fluid was used.

The left-heart simulator is typically designed for testing prosthetic and synthetic valves. Normally, mounted valves are sealed by rubber rings to prevent fluid from escaping the apparatus. Natural valves or roots cannot be fixed to the simulator without some adjustment. To accommodate this challenge, a special adjustable jig was designed (Lzeik, 2007). As seen in Fig. 8, the jig consists of two horizontal plates inserted into the system using screws at the four corners of the plates. In the center of the plates, stepped holes are present to allow the cannulas to be placed. The total height of the jig can be adjusted by moving the plates farther or closer together on the screws. This also allows a stretch to be applied to any root that is placed in the jig. For this experiment, a longitudinal stretch ratio of 1.2 was applied. This stretch is characteristic of a porcine aortic root *in vivo* and would produce dynamics that were closer to the actual physiology. This will be fully justified in Chapter 6.

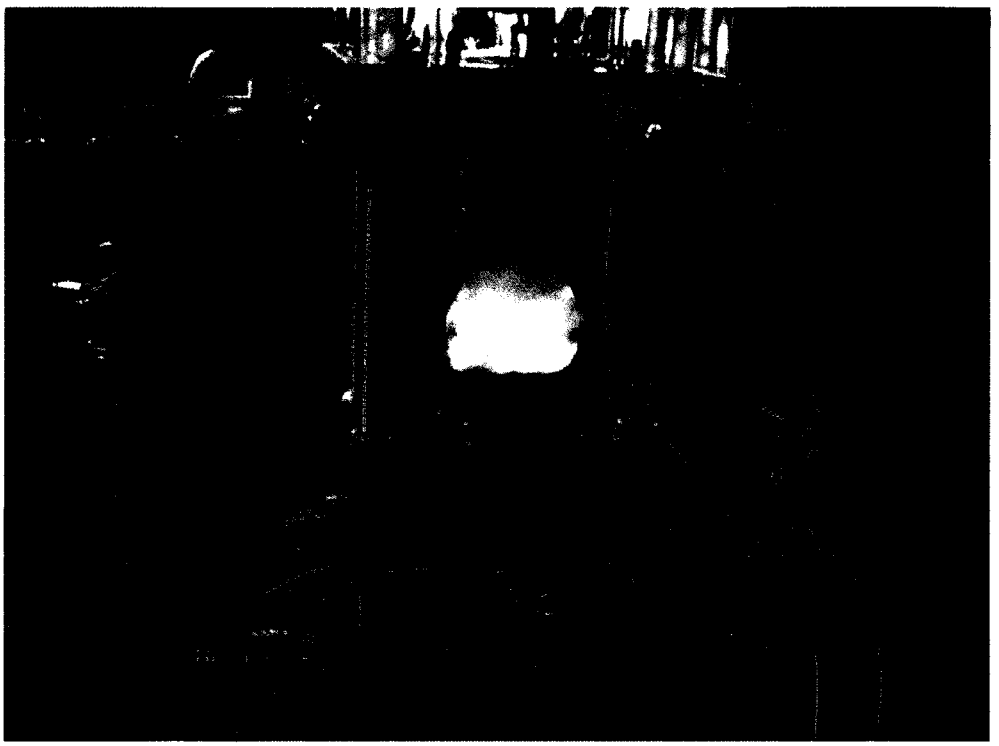

Figure 8 – A porcine aortic root mounted in the custom test jig. The jig height is adjusted by altering the length of the screws (Lzeik, 2007).

A flow measuring system measures the cardiac output in ml/min. An electromagnetic flow probe is inserted at the aortic aperture. A pressure measurement system is also used to measure conditions in the simulator. For this, the system uses amplifiers and transducers designed specifically for in-vitro environments. The transducers are very sensitive and could be damaged by extreme pressures. The pressure transducers may be calibrated by adjusting gains and shifts, and they are zeroed at each experiment, while their relative height difference, if any, is recorded for correction of the pressure readings to account for possible hydrostatic pressure differences.

A high-speed camera was mounted at the top of the hydraulic chamber and captures the motion of the aortic valve leaflets. The camera has a maximum frame rate of 2000 frames per second which was quite adequate to acquire relevant images. For a

closer view, an endoscope was extended from the camera towards the aortic root. A light source at the end of the endoscope illuminated the valve and root. Using the high-speed camera, video images of the valve motion were recorded and processed to extract still images with accurate time information (see Fig. 9). These images and videos were later used for quantative and qualitative analyses of the finite element valve dynamics.

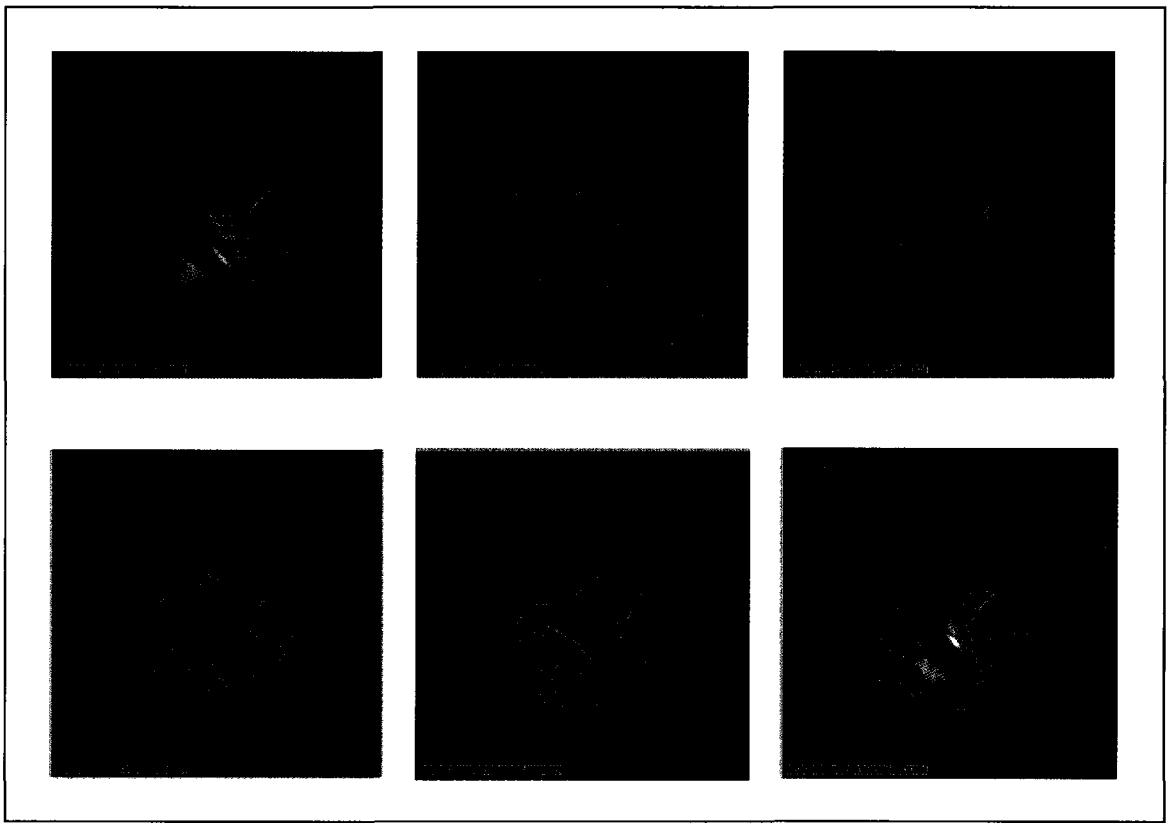

Figure 9 – In order from the top left to the bottom right, an evolution of the opening and closing motion of the valve through one cardiac cycle.

3.2 Aortic Root Pressurization Procedure and Apparatus

Aside from capturing valve dynamics, data had also to be collected to establish the aortic material properties to be used in the finite element model. Note that the leaflets

were not tested given the very good data already published in the literature by Billiar and Sacks (2000). To obtain relevant data such as dilation, extension and change in wall thickness, the aortic root was subjected to pressurization from 0 to 160 mmHg.

The information about valve dynamics gathered in the previous section was sample specific. Therefore, to maintain consistency of the data, after testing in the left-heart simulator, the very same sample was placed in a saline bath for quasi-static pressurization testing. The root was blocked with a stopper about 5 cm above the sinotubular junction (see Fig. 10). The base of the valve was fitted with a threaded cannula that was screwed on to the opening of a pipe inlet. A large syringe was then used to pump saline into the root to increase the internal pressure. As the pressure was increased and measured by a digital manometer, the root dilated radially and extended longitudinally. The pressure was kept constant for a brief period at every increment of 20 mmHg from 0 to 160 mmHg. To measure the longitudinal extension of the ascending aorta at the exit of the aortic root, red chalk markers were placed at the sinotubular junction and about 1 cm above into the ascending aorta. The markers were digitally photographed at each pressure reading for later processing to yield the longitudinal stretch ratio. To allow the measurement of the aortic wall thickness and the circumferential stretch, an ultrasound probe captured cross-sectional images at a constant level between the longitudinal markers.

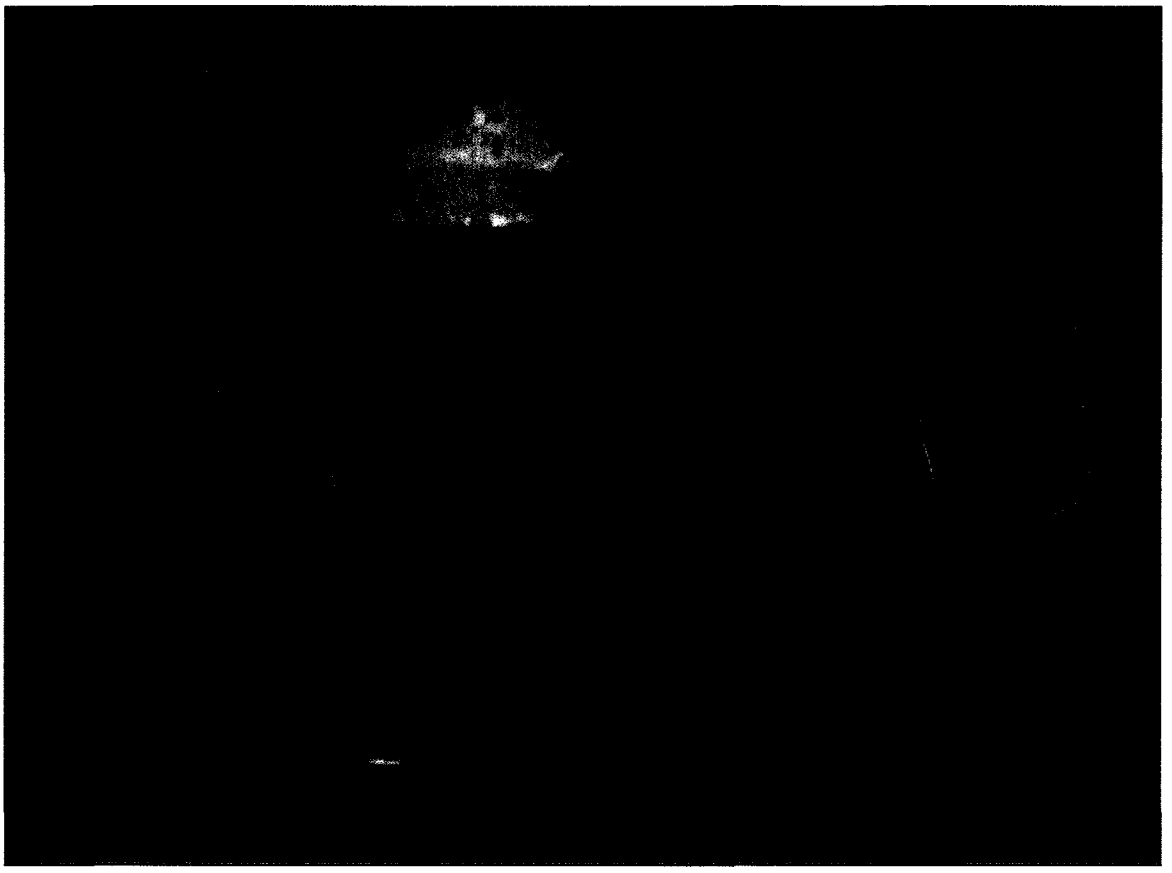

Figure 10 – The same aortic root used in the left heart simulator is removed from the custom test jig and pressurized (100 mmHg in this figure) in a saline bath. Note the ultrasound camera placed just above the sinotubular junction. The root is blocked past the sinotubular junction (left of the root) and saline is allowed to flow in from the pipe at the base of the valve (right of the root). Also note the red chalk placed as markers at the sinotubular junction and the commissures.

Once data had been recorded at various pressures, a procedure to establish the valve dimensions was started. A solution of silicone rubber was poured into the valve and a static (diastolic) pressure of 80 mmHg was applied to the mould and valve overnight. The aortic valve tissue was then stripped away to produce a silicone rubber mould of the valve leaflets, sinuses, and commissures in the closed position at 80 mmHg pressure (see Figs. 11, 12). The mould was cut along the leaflet free edges to reveal various important parameters; the most important being free edge length, leaflet height and width, as well as

commissure and valve height. Processing of the collected data and the resulting values are discussed in Chapter 6.

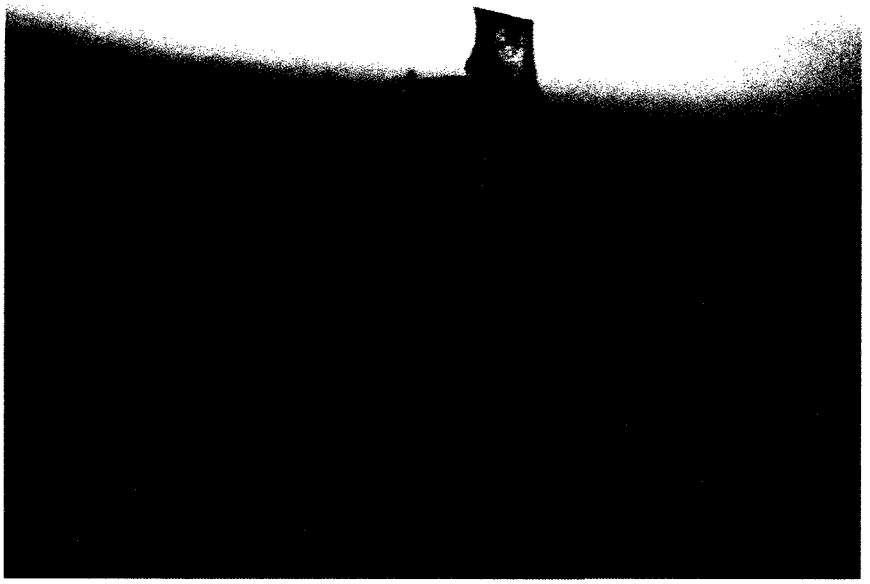

Figure 11 – A perspective of the aortic valve used in the pressurization testing, after the sinuses were cut away and the mould was separated from the valve. What is left, therefore, is dried up tissues which have become transparent but yet help visualize the aortic valve structure.

Figure 12 – The silicone rubber mould that was removed from the aortic root tested. This is a ventricular perspective of the valve leaflets. The mould was further cut along the free edges of the leaflets for measurement of the leaflet dimensions.

CHAPTER 4 GEOMETRIC MODELING

Detailed dimensions of the different components of the aortic valve have been studied by different researchers (Mercer et al., 1973; Swanson and Clark, 1974; Thubrikar, 1990; Kunzelman, 1994; Labrosse et al., 2006). The main thrust for all these studies is to understand the relationships between the different valve dimensions in order to produce a scalable design for an efficient, leak-free valve. In particular, Thubrikar (1990) brought forward some basic criteria regarding the limits and relationships between geometric parameters to ensure proper coaptation and optimal valve dynamics. Specifically, an appropriate valve height-to-diameter ratio was proposed to minimize dead space, prevent folds in the leaflets and minimize leaflet flexion to promote an efficient use of energy. One of the goals of the present work was to build a scalable (i.e. dimensionally parameterized) finite element model of the aortic valve. Given, say the diameters at the base and top of the valve, and the height of the valve, what should be the leaflet dimensions for proper valve function? This problem was studied by Labrosse et al (2006), and their approach was adopted as detailed below to build a scalable skeleton for the finite element model.

4.1 Assumptions and Design Principles Used in Modeling the Aortic Valve

The three sinuses and leaflets of the aortic valve are somewhat similar but not symmetrical in general. However, for the sake of simplicity, the model developed herein assumed an idealized, symmetrical geometry. Therefore, only one sinus and leaflet was modeled as an average of the three from a single valve. An average of the physical

dimensions was taken and the sinuses were assumed to be 120 degrees from each other in the circumferential direction. Additionally, assuming symmetry in the radial-longitudinal plane, only one half of a single leaflet and sinus was modeled. This was done to save computational resources.

Another assumption related to the geometry was the exclusion of the coronary ostia. The coronary ostia lie in the middle of two of three sinuses and are the origins of the coronary arteries. The model developed assumed a sinus without the coronary ostia (non-coronary sinus). The height of each sinus is also variable and was therefore averaged from the three sinuses of a single valve. It was also assumed that the planes passing through the base of the valve and the top of the commissures were parallel.

Next, based on two experimental observations noted by Mercer et al. (1973) and Thubrikar (1990), the load-bearing surface of the leaflet in closed position was considered to be approximately cylindrical in shape, and the attachment line of the leaflet was assumed to lie in a plane that serves as a reflection plane for the load-bearing surface when considering the fully closed and fully open configurations. Additionally, following Thubrikar (1990) and Swanson and Clark (1974), the leaflet free edge length and leaflet height can be considered to be unchanged between the open and closed positions. The result of these three design principles is illustrated in Figs. 13 and 14 where *B* represents the outermost position of the leaflet free edge from the valve centreline in the open position, and *B'* represents where *B* moves to in closed position. Key parameters used in modelling the aortic valve are shown in Fig 15 (complete details are given in a publication in Labrosse et al. 2006).

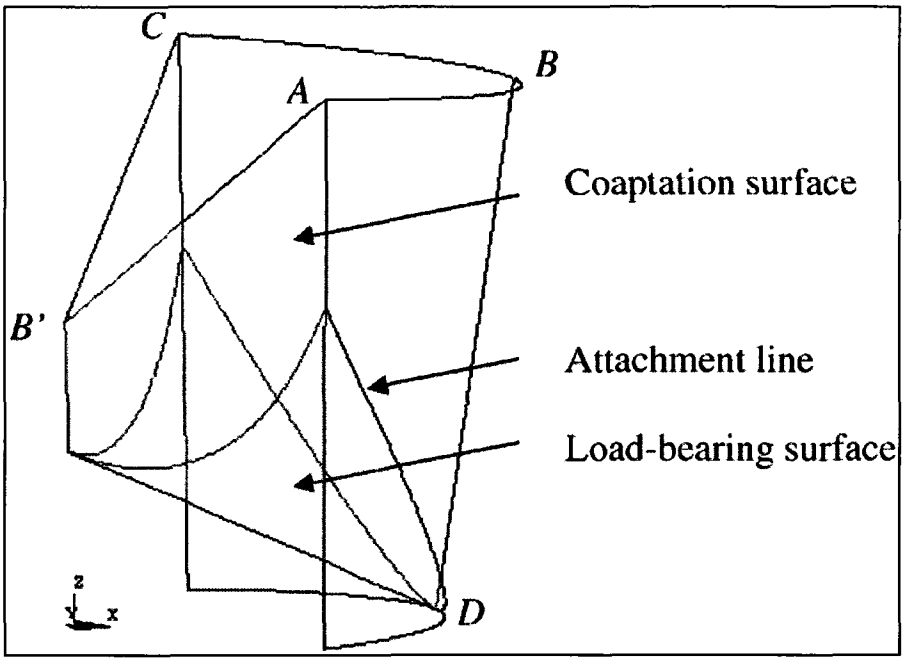

Figure 13 – A perspective of the leaflet displaying the open and closed positions (Labrosse et al., 2006).

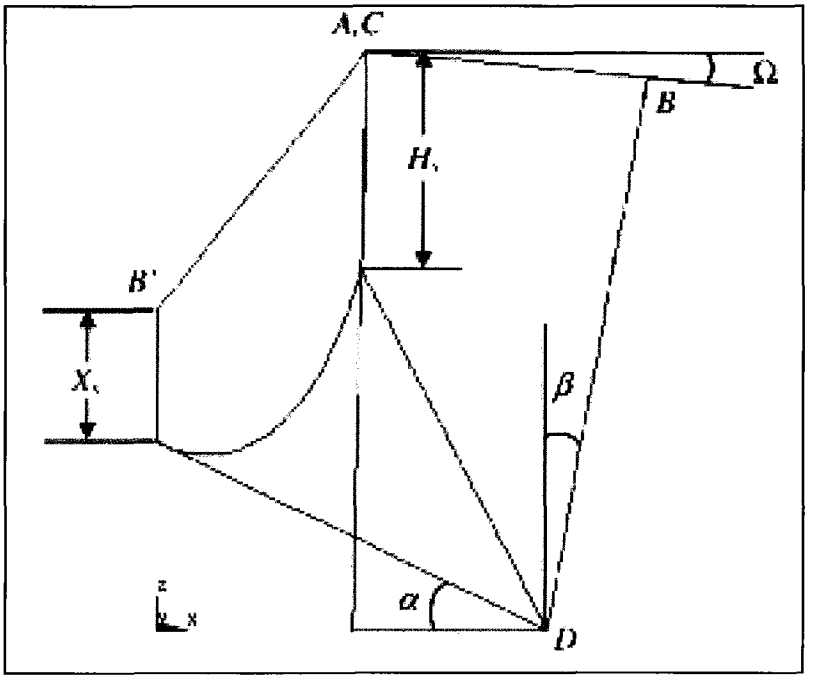

Figure 14 – A side view of the leaflet, again shown in both open and closed positions, with associated design parameters. The coaptation height and the commissural height are labelled as Xs and Hs respectively. The angle of the closed leaflet with the horizontal is α, whereas the angle of the open leaflet with the vertical is β. The angle of the free-edge with the horizontal in open position is Ω. Letters *A-D* are the same as in Fig. 13 (Labrosse et al., 2006).

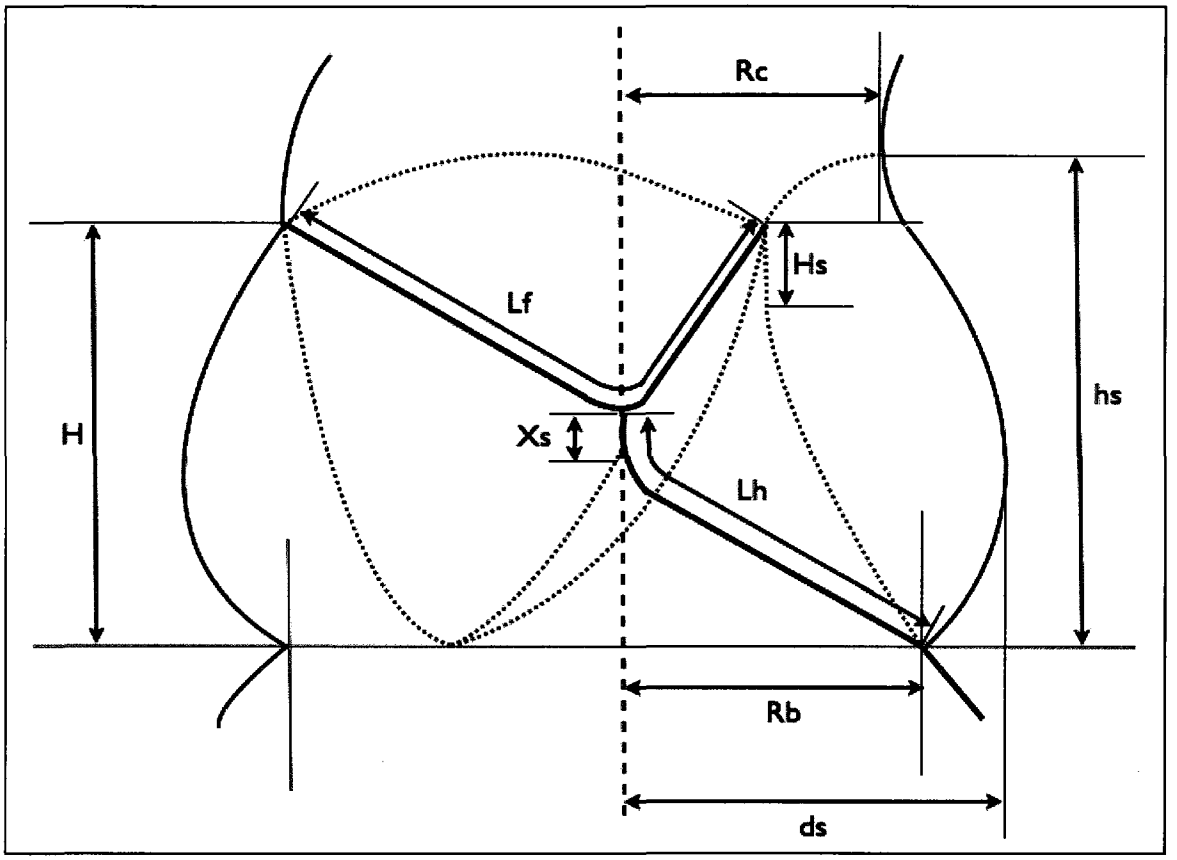

Figure 15 – A diagram displaying some of the important modeling parameters uses to describe the aortic valve. R_c : Radius of the Commissures, H : Commissural Height, h_s :Sinus Height, H_s : Height of the Commissures, X_s : Coaptation Height, R_b : Radius of the base, d_s : distance of the sinus belly to the centre of the valve, L_h : Leaflet Height, L_f : Leaflet Free Edge Length.

4.2 Geometric Relations

The parameters and design principles presented above are translated into analytical equations used to model the three-dimensional valve. The equations derived involve the primary parameters discussed as well as additional secondary parameters.

Note that experimental values are often described in terms of diameters, while radii are used to develop the analytical equations.

Recalling the open position of the leaflet in Figs. 13 and 14, note that the leaflet is represented by a section of an approximately cylindrical surface. The free-edge of the leaflet, represented by arc *ABC*, lies along the top edge of this surface. The free-edge length L_f spans this edge and lies in a plane at an angle Ω to commissural plane. The radius of this arc is denoted as R, and d is the location of the centre of the arc, in the same plane as radius R, with respect to the middle of the top of the commissures A and C. Due to the circular symmetry of the valve, the distance between commissures A and C is $\sqrt{3}R_c$. Following Labrosse et al. 2006, free-edge length L_f is expressed in terms of d and R_c as

$$L_f = 2\sqrt{d^2 + \frac{3R_c^2}{4}}\arctan\left(\frac{\sqrt{3}}{2}\frac{R_c}{d}\right) \qquad \text{if } L_f \le \pi\frac{\sqrt{3}}{2}R_c, \qquad \text{Eq. (1a)}$$

$$\text{or} \quad L_f = 2\sqrt{d^2 + \frac{3R_c^2}{4}}\left\{\pi - \arctan\left(\frac{\sqrt{3}}{2}\frac{R_c}{d}\right)\right\} \qquad \text{if } L_f > \pi\frac{\sqrt{3}}{2}R_c. \qquad \text{Eq. (1b)}$$

If L_f and R_c are measured from a sample aortic root then d can be solved for numerically. The radius of the free-edge arc can then be obtained through the relation

$$R = \sqrt{d^2 + \frac{3R_c^2}{4}}. \qquad \text{Eq. (2)}$$

To ensure that the leaflet has a wrinkle-free straight form of nearly cylindrical shape, point B along the free-edge must lie at a specific distance from the base of the valve. The coordinates of B can be described in a rectangular coordinate system centered on the intersection between the valve centerline and the basal plane, and with the x-direction

running through the middle of the leaflet and the z-direction running along the centreline of the valve. The coordinates of B are then given as $(\frac{1}{2}R_c + X_B\cos\Omega, 0, H + X_B\sin\Omega)$, where

$$X_B = R - d \qquad \text{if } L_f \le \pi\frac{\sqrt{3}}{2}R_c, \qquad \text{Eq. (3a)}$$

$$\text{or } X_B = R + d \qquad \text{if } L_f > \pi\frac{\sqrt{3}}{2}R_c. \qquad \text{Eq. (3b)}$$

Note that B must lie on a circle of radius L_h centered on point D of coordinates (R_b, 0, 0) using the same rectangular coordinate system and reference. With this, after some derivation, the angle Ω between the free-edge and the commissural plane can be expressed as

$$\Omega = \arcsin\left\{\frac{L_h^2 - \left[\left(R_b - \frac{R_c}{2}\right)^2 + H^2 + X_B^2\right]}{2X_B\sqrt{\left(R_b - \frac{R_c}{2}\right)^2 + H^2}}\right\} + \arctan\left\{\frac{R_b - \frac{R_c}{2}}{H}\right\} \qquad \text{Eq. (4)}$$

Also, the angle of the open leaflet to the z-axis obtained as

$$\beta = \arcsin\left\{\frac{X_B\cos\Omega - \left(R_b - \frac{R_c}{2}\right)}{L_h}\right\} \qquad \text{Eq. (5)}$$

In closed position, the leaflet free-edge and length are now described respectively by

$$\begin{cases} L_f^2 = 4\left[R_c^2 + (H - X_s - R_b \tan\alpha)^2\right] \\ L_h = X_s + \dfrac{R_b}{\cos\alpha} \end{cases} \qquad \text{Eq. (6)}$$

where L_f represents the length of the two straight line segments of the free-edge extending from the centreline to the two commissures; and L_h sums the coaptation height and the length of the load-bearing surface along the centre of the valve. Given inputs the unknowns X_s and α can be solved for numerically.

At this stage, only the plane on which the leaflet attachment line lies remains to be defined. Design principles discussed above dictate that this plane must act as a reflection plane for the load-bearing surface of the leaflet, between the open and closed positions. If θ is defined as the angle between the open and closed leaflet then the plane lies at an angle of $\alpha + \frac{\theta}{2}$ to the basal plane, thus yielding $\theta = \frac{\pi}{2} + \beta - \alpha$. Note that the height of the commissures, H_s, is the difference between the commissural height H and the longitudinal distance between the lowest point on the attachment line (at the valve base) and the upper most point of the attachment line (at the junction between the commissures and the attachment line). This gives the height of the commissures H_s to be

$$H_s = H - \left(R_b - \frac{R_c}{2}\right)\tan\left[\frac{1}{2}\left(\alpha + \beta + \frac{\pi}{2}\right)\right] \qquad \text{Eq. (7)}$$

as the commissures run parallel to the centreline of the valve (Labrosse et al. 2006).

From the above purely geometric modeling (the leaflet material is not supposed to stretch, and the leaflet support is considered rigid), important relationships could be developed to make a pre-selection of dimensions that are compatible with correct valve

function, pending further analysis of the whole deformable valve. These relationships also provide a rationale for scaling the design of the aortic valve model.

4.3 Construction of the Aortic Valve Model in ANSYS 11.0

ANSYS has a very powerful pre-processor which allows the user to parameterize a geometric construction involving Boolean operations (such as intersections of different surfaces in three dimensions). In addition or in replacement of using a graphic-user interface, the user can write a script that directly builds the model, making the use of ANSYS as a geometric builder quite attractive. To begin construction of one aortic valve model, values for the parameters discussed above had to be decided upon. Some of these values were obtained experimentally and used to calculate other parameters, while other values were assumed from the literature.

The experimental values obtained for R_b and R_c were 11.7 mm and 9.0 mm respectively, at 0 mmHg pressure. These measurements were taken from the ultrasound images of the aortic root cross-section during pressurization. The radii obtained were then compared to those obtained by Swanson and Clark (1974) on pressurized human aortic roots, and matched well with their series number 7. Key design dimensions of multiple aortic valve samples were measured by Swanson and Clark and recorded; each valve sample was labelled as a data series. Measurements from the silicone rubber mould of the porcine root further reinforced this match to Swanson and Clark series 7 yielding comparable radii at 80 mmHg. Based on these observations, series 7 measurements for leaflet height and free-edge length were taken as 13.1 mm and 28.0 mm respectively. Swanson and Clark leaflet measurements were used instead of those obtained in the

present study because it was difficult to obtain leaflet dimensions at 0 mmHg pressure from the root sample. The measurements obtained by Swanson and Clark were deemed preferable because these authors developed a high degree of skill and precision in making such measurements.

The dimensions of the sinus, particularly sinus height h_s, maximum depth and longitudinal location of the maximum depth, were measured from the silicone rubber mould and ultrasound images. Sinus height was measured to be 21.0 mm from the base, and maximum depth as 17.16 mm from the centreline at a height of 4 mm from the base. The height of the commissures was found to be 8.02 mm by numerically solving Eq. 7. Equations 6 for leaflet height and free-edge length were also solved numerically for coaptation height X_s and commissural height H yielding 3.9 mm and 17.8 mm respectively. Finally, Eqs. 4 and 5 were solved to yield angles Ω and β. The parameter values are summarized in Table 1.

Table 1 – A summary of key valve parameters used as inputs in constructing the aortic valve model.

Base Radius	R_b	11.75 mm
Commissural Radius	R_c	9.1 mm
Commissural Height	H	17.8 mm
Height of Commissures	H_s	8.02 mm
Leaflet Height	l_h	13.1 mm
Leaflet Free-edge	l_w	28.0 mm
Coaptation Height	X_s	3.90 mm
Leaflet Opening Angle	β	8.23 degrees
Sinus Height	h_s	21 mm
Maximum Sinus Depth	d_s	17.16 mm
Maximum Depth Location	z_s	4 mm

The construction of the aortic valve model in ANSYS started with inputting the values for the parameters presented above (see Appendix A for complete ANSYS 11.0 script). Only one half of a single leaflet and sinus were built. First a frustum upon which the left ventricular outflow tract (LVOT) was built by rotating a line about the valve centerline. A plane defining where the line of attachment should intersect this frustum was then defined (Fig. 16). The area above the attachment plane was then removed allowing the leaflet to be built in its place. The commissures were built by extending a vertical line from the top of the attachment line to the commissural height. The leaflet free-edge was then defined by an arc of radius R given by Eq. 2. The leaflet area was then lofted between the attachment line, commissures and free-edge (Fig. 17). The LVOT was then reshaped by adding a cylindrical section below the existing LV tract. This concluded the construction of the inner leaflet and inner LVOT geometry (Fig. 18, left).

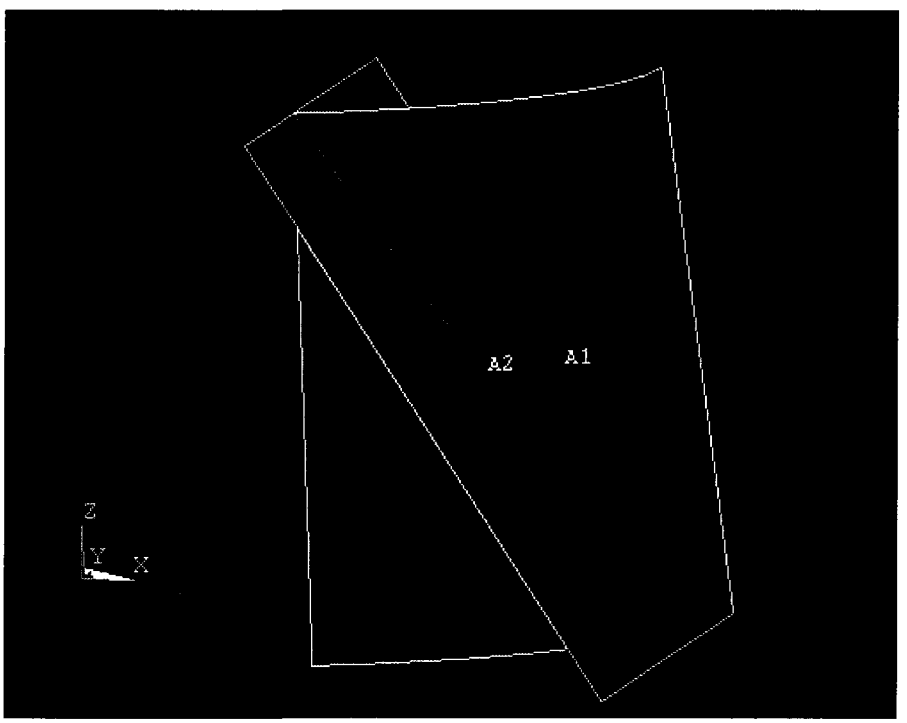

Figure 16 – The intersection of the frustum defining the LV tract and the plane on which the line of attachment lies.

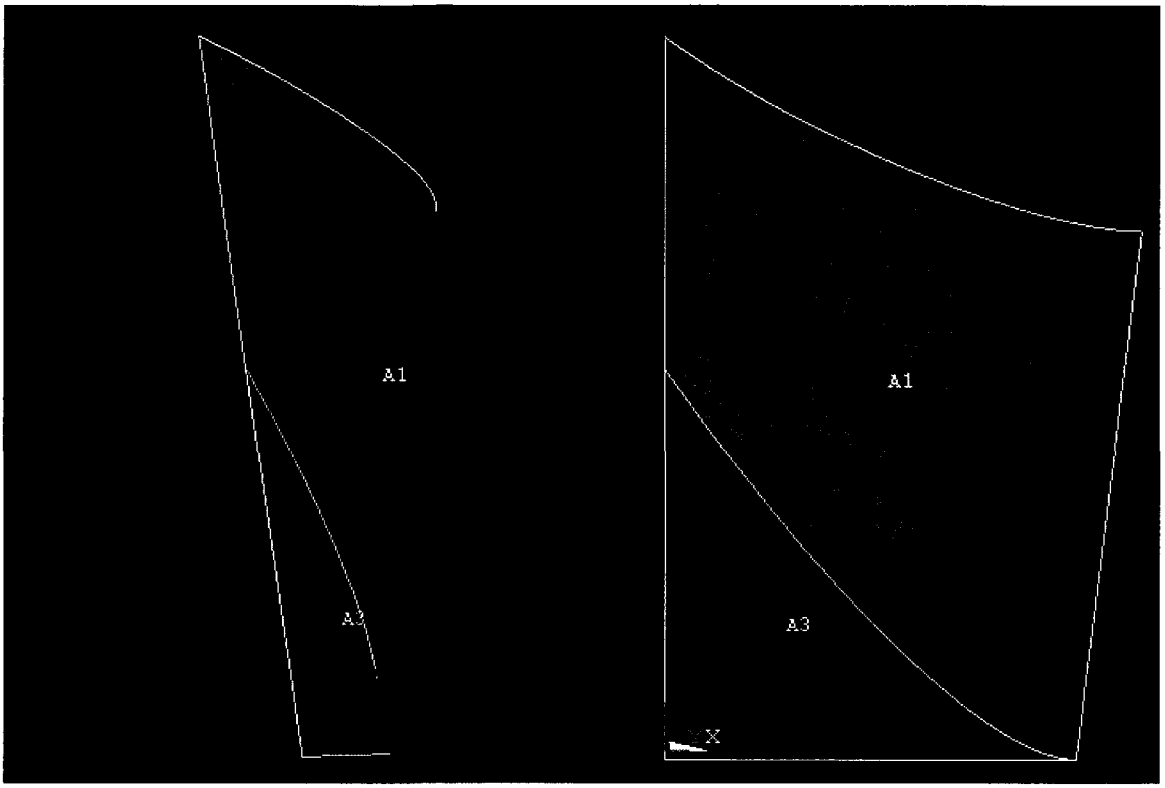

Figure 17 – Orthogonal views of the leaflet and LV tract.

The leaflet was then meshed with elements that were arranged to resemble the alignment of the underlying fibre bundles in natural valves (Billiar and Sacks, 2000), as illustrated in Fig. 18, right. The same construction was repeated at a distance of 0.5 mm from the first (inner) leaflet constructed to produce a solid leaflet of the same thickness.

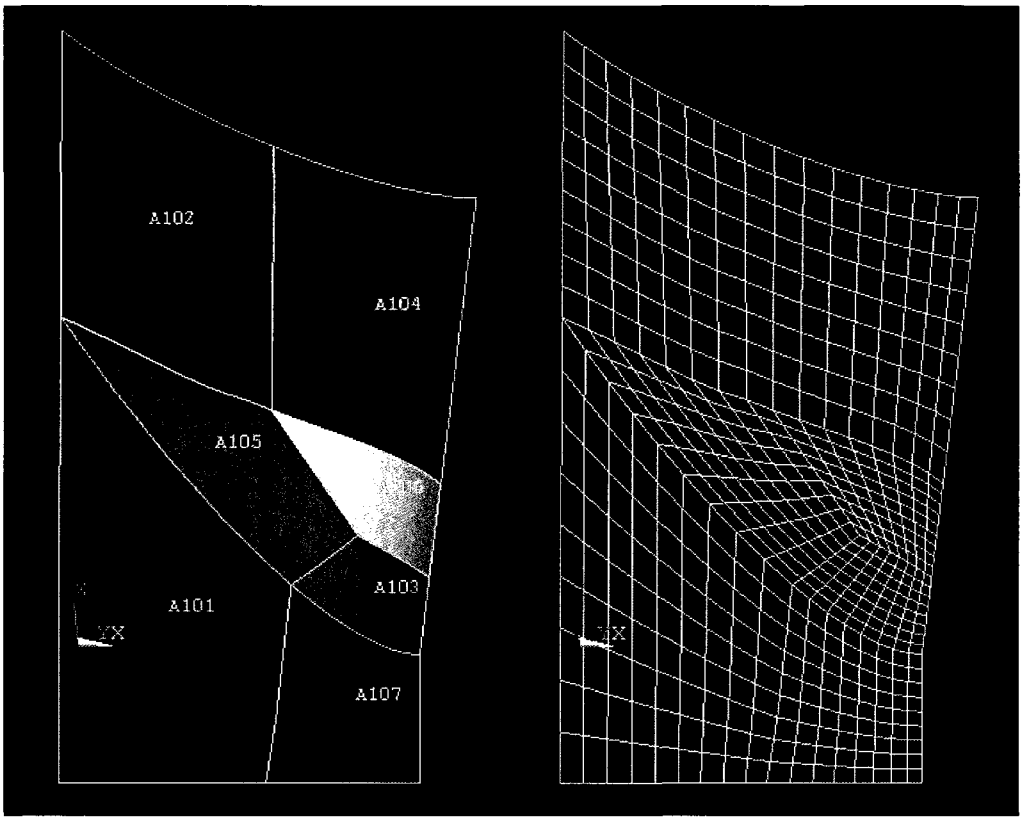

Figure 18 – The topical division of the leaflet (left) and the resulting fibre bundle orientation (right).

Construction of the sinus began by constructing a B-spline along the middle of the sinus where it would interface with the other half of the sinus. This sinus curve connects the sinotubular junction (STJ) to the leaflet attachment line. It is constructed to fit a curve specified by the sinus height h_s, the maximum sinus depth or out pocketing d_s and the location of maximum depth z_s. An arc was then constructed connecting the top of the sinus curve to the bottom of the commissure (i.e. top of the attachment line) (Fig. 19). ANSYS then lofted an area that fitted between the sinus curve, the leaflet attachment line, the commissures and the arc connecting the commissures and the sinus curve. Above the sinus area a cylindrical section was built representing the ascending aorta (Fig 19).

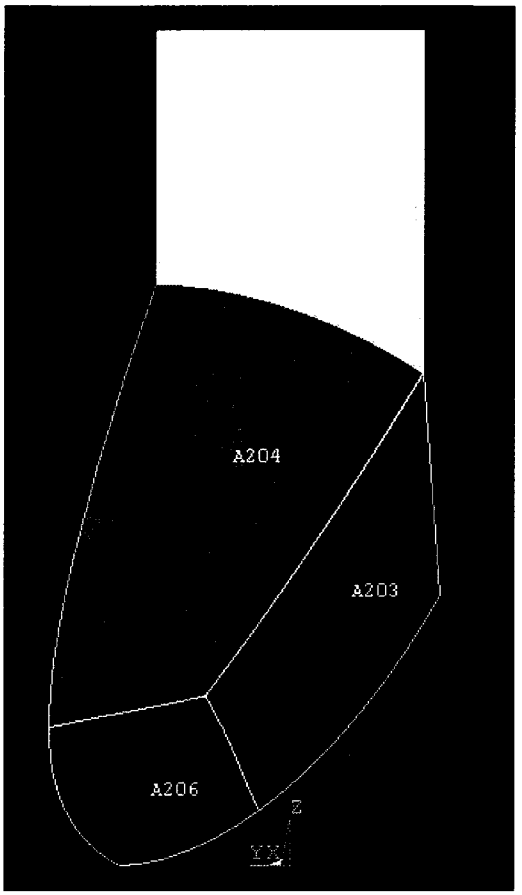

Figure 19 - A view of the inner sinus area. Notice the sinus curve on the left hand side, connecting to the STJ above and the leaflet attachment line at the bottom. The inner sinus area is composed of the green, pink and purple area whereas the ascending aorta is represented in orange. The sinus area is divided into three parts to better control meshing and the application of material properties.

This procedure was repeated with another sinus area created at a radial distance of 3.4 mm beyond the first sinus area. A complication, however, lay in the fact that there was no line of attachment to connect to the second (outer) sinus area. Therefore, the LVOT was rebuilt following the same procedure as when constructing the leaflet, only offset by a thickness of 3.4 mm from the original sinus wall built (Fig. 20, left). The outer area of the ascending aorta was then built connecting the STJ to the commissures. Then the outer sinus curve was built connecting the outer LVOT (and therefore outer line of attachment) to the ascending aorta. Both the outer and inner sinus areas were divided

into three parts to easily control solid meshing. Finally, a rigid wall was built along the commissural side of the model to simulate the presence of a neighbouring leaflet during valve closure (Fig. 20).

More preparation of the model was needed to ensure adequate transfer of information between the pre-processor (ANSYS) and the solver (LS-Dyna). Non-structural shell elements were built along the inner sinus wall and both the inner and outer surfaces of the leaflet mark these surfaces for pressure loading in LS-Dyna. Special nodes were arbitrarily labelled to easily locate them and implement prescribed motions or directional constraints on them in LS-Dyna. The nodes at the top of the ascending aorta were marked for prescribed motion in the longitudinal direction to simulate natural tethering conditions in the aortic root (labelled as master nodes or m-nodes in ANSYS). These nodes at the top of the aorta were designated as master nodes (m-nodes) so that they could later be used to apply a longitudinal stretch in LS-Dyna. Due to symmetry, nodes on the reflection plane of the leaflet and sinus (middle of the complete sinus and leaflet) were constrained to move only in this plane (labelled as d-nodes). Similarly, nodes along the commissural side of the model were constrained to move along the plane of the rigid wall and were consequently included in the d-node list. Nodes on the ventricular side of the leaflet were assigned to be contact nodes in order to coapt with the rigid wall rather than pass through it; these nodes were labelled as force nodes or f-nodes. The nodes at the base of the model were constrained in all directions to replicate the clamped condition found in the experimental procedure. They were added to the d-node list. In ANSYS, each geometric part was assigned its own material number, as parts and

material properties are hardly distinguishable in LS-Dyna. For example, referring to Fig. 19, the sinus and ascending aorta were divided into four distinct parts.

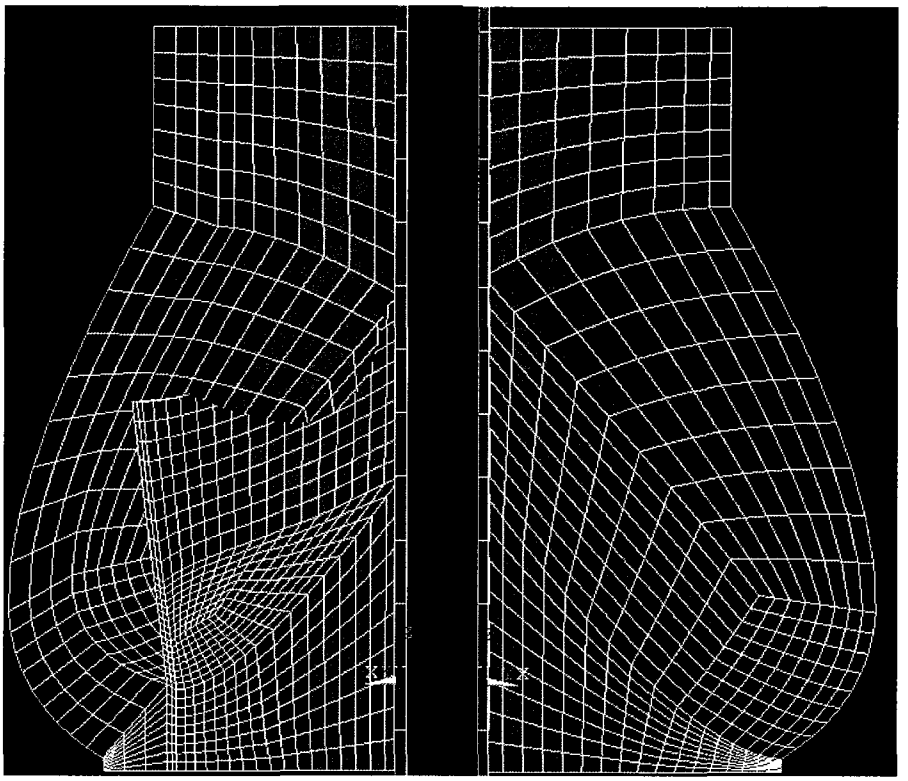

Figure 20 – Views of the completely meshed, unpressurized, geometry from the inside (left) and outside (right) of the valve. Note that the leaflet interferes with the sinus, but this problem disappears upon pressurization of the aortic root to physiological pressures.

4.4 Exporting the Geometry from Ansys 11.0 to LS-Dyna 971

The input format for LS-Dyna is different from ANSYS' and therefore must be formatted accordingly. The translation was performed using MATLAB numerical computing suite. As previously mentioned, the translation required some preparation of the ANSYS model. More specifically, during pre-processing in ANSYS, a number of lists and important figures were recorded. Tables for shell and solid elements (e-list), nodes (n-list), nodes with associated degree of freedom constraints (d-list), master nodes

(m-list) and nodes with associated forces (f-list) were recorded and read into MATLAB. At this point the ideal ventricular and aortic pressure curves are read into MATLAB. A MATLAB code was then written to reformat this information into an LS-Dyna specific data file. Below is a plain English description of the content of the LS-Dyna input deck given in Appendix B.

Following the definition of control parameters and database controls, individual model parts are defined based on the material numbers assigned in ANSYS. A summary of part numbers and names is found in Table 2. Having distinct part numbers helps in assigning material properties to groups of parts. Material properties for the sinus, aorta and LV tract are obtained from the pressurization experiment, and are assigned to parts 1, 2, and 8 to 13. Another set of material properties for the leaflet, obtained from Billiar and Sacks data (2000), is assigned to parts 3 to 7. The rigid wall, part 14, is assigned its own set of material properties. A detailed discussion of material properties follows in later sections.

Table 2 – LS-Dyna part identities

Part Number	Part Name
1	LV1
2	LV2
3	Leaflet1
4	Leaflet2
5	Leaflet3
6	Leaflet4
7	Leaflet5
8	LV3
9	LV4
10	Sinus1
11	Sinus2
12	Sinus3
13	Aorta
14	Rigidwall

Following the designation of material properties is the assignment of sections. Here each part is assigned to the use of a type of element. In this model, all parts are assigned to use solid elements with the exception of the rigid wall being assigned shell elements (as per ANSYS requirements for a rigid wall).

Next, the node list is written identifying each node by number and rectangular coordinates. Following the list of nodes is the list of elements identifying each element by number and all its associated nodes (8 nodes for solid elements and 4 for shell elements).

Before describing the loads that are to be applied to various parts of the valve, load curves must be assigned to the four nodes of each element face that is to be loaded. These elements are the shell elements along the inner sinus and aorta as well as the leaflet surfaces. In total, five load curves were defined; Table 3 outlines the load curves and their associated surfaces.

Table 3 – Load curve identities and locations

Load Curve ID	Surface
1	Inner sinus and aorta
2	Aortic side of leaflet
3	Ventricular side of leaflet
4	Inner LV tract
5	Top surface of aorta

MATLAB is used to define each of these load curves specifying a particular value for pressure (N/mm^2) at various times during the cycle. A detailed description of the load curves follows in the next sections.

Boundary conditions are specified in two manners: degree of freedom constraints and prescribed motion. Prescribed motion is used for nodes at the top surface of the aorta through load curve 5. These nodes are assigned a longitudinal displacement that results in a 20% longitudinal stretch of the entire model.

Six types of degree of freedom constraints are available: three translational motion constraints and three rotational motion constraints. For each node number a 0 is assigned to unconstrained directions and 1 is assigned to constrained directions. The top surface of the aorta is constrained in the longitudinal (z) direction once the 20% stretch is achieved. To simulate symmetry the nodes on the side of the sinus arc, from the aorta, sinus, LV tract and leaflet are constrained from translating in the circumferential (y) direction. All nodes along the commissural side of the aorta, sinus, LV tract and leaflet are constrained from translating across the rigid wall. For this a new coordinate system is defined using the plane of the rigid wall as its base. Finally the base of the valve is fixed to replicate a clamped condition.

CHAPTER 5 MATERIAL MODELING

While the material properties of the aortic tissue (including the ascending aorta and the sinuses) are different from those of the leaflet, the same material model was used for both, with different material constants. The material model is described in detail below as well as the acquisition of material constants and the data used to produce them.

The mechanical response of cardiovascular tissues to stress or stretch can be observed using different in vitro methods. One basic method is a uniaxial test in which tension is applied in one direction incrementally to a sample and the resulting strain is

recorded. While this method can reveal the nonlinear nature of the material, it cannot be used to characterize its anisotropic properties. Biaxial testing is an improvement over uniaxial testing in this regard. The sample is differentially loaded in two perpendicular directions and the strain in each direction can be observed, while the behaviour of the two directions is obviously coupled. One shortcoming of this method, however, is that it is not possible to preserve the natural curvature of blood vessel walls as the material is being stretched in a plane. Yet, biaxial testing is particularly well suited for observing the behaviour of the leaflets.

Pressurization testing is the preferred method to observe the dilation and extension of blood vessel sections under physiological loads (Humphrey, 2002). In essence, pressurization testing is to blood vessels what uniaxial testing is to steel. The equations describing the forces and deformations experienced by a standardized dog-bone sample for steel are known, and, as shown below, so are the equations of a closed-end blood vessel under pressure. In both cases, such equations are used to establish the material properties of the material, i.e. Young's modulus and Poisson's ratio in the case of steel, and different material constants in the case of cardiovascular tissue, depending on the constitutive equation used.

5.1 Mechanical Model of a Closed-End Blood Vessel Under Pressure

Arterial tissue, including the aortic tissue of interest here, has many unorthodox characteristics from an engineering perspective. Therefore, certain assumptions must be made prior to the derivation of modeling equations. The assumptions discussed here are for modeling a cylindrical aortic section. However, the constitutive equation used in

combination with these assumptions is also valid for non-cylindrical geometries, and was used for the leaflets as well.

The aortic geometry is first assumed to be axisymmetric: a straight, hollow, circular cylinder subjected to axial extension and internal pressures. The arterial wall has three concentric layers: intima, media, and adventitia. These layers have different compositions in terms of cell types and content of elastin and collagen fibres. While the intima is very thin and therefore usually not included in structural models, the media and adventitia are modelled together as one homogeneous layer for simplicity. In this analysis, the behaviour is being studied at the macroscopic level, and therefore observing individual layers is not yet necessary. In addition, the cylinder is assumed to be thick-walled. Under physiological pressure, the ratio of thickness to radius varies between 1/8 and 1/10 (McDonald, 1974), which would justify the use of a thin-walled cylinder theory. However, this would also neglect the stresses and deformations accumulated between the unpressurized state and the physiological range, and would make impossible any attempt to describe the stress distribution across the aortic wall. In the end, the unpressurized aortic wall exceeds a thickness-to-radius ratio that can be considered suitable for thin-walled theory; therefore it is assumed to be a thick-walled cylinder.

The stress state of a purely elastic material (including hyperelastic) is dependent on the state of strain at a given time and is identical when being loaded and unloaded using the same deformations. It has been demonstrated that in the physiological domain (Fung, 1984), arterial tissue also exhibits repeatable hyperelastic behaviour. These deformations are beyond the realm of linear elasticity, and require the use of a hyperelastic strain energy function W in combination with finite strains to characterize

the mechanical energy stored in the material during elastic deformation. There are many forms of strain energy functions, as will be discussed later.

For now, let us focus on the different deformations experienced by the aortic wall in different directions. In a cylindrical coordinate system, aortic tissue behaviour is different in the radial, circumferential, and longitudinal directions, but no twist is apparent upon pressurization (Patel and Fry, 1966). Thus, three preferred orthogonal directions characterize the anisotropic response of the aortic tissue: radial, circumferential and longitudinal.

Consider a material particle located at (r, θ, z) in the deformed arterial section that can be found at (R, Θ, Z) in the undeformed section where

$$r = r(R),\ \theta = \Theta,\ \text{and}\ z = z(Z).$$

Here, $A \le R \le B$, where A and B are the inner and outer radii respectively in the undeformed section. Also, $a \le r \le b$, where a and b are respectively the inner and outer radii in a deformed arterial section under an internal pressure p and an applied axial force F_z. It is assumed that there is no external pressure on the section.

A basic definition for deformation in this case is given by the deformation gradient tensor F as follows

$$[F] = \begin{bmatrix} \partial r/\partial R & 0 & 0 \\ 0 & r/R & 0 \\ 0 & 0 & \partial z/\partial Z \end{bmatrix},$$

where the components of this tensor are respectively the radial, circumferential and longitudinal stretch ratios

$$\lambda_{rr} = \frac{\partial r}{\partial R}, \lambda_{\theta\theta} = \frac{r}{R}, \lambda_{zz} = \frac{\partial z}{\partial Z}. \qquad \text{Eq. (8)}$$

These are used in describing the Cauchy-Green strain tensor defined as $\boldsymbol{C} = \boldsymbol{F}^T.\boldsymbol{F}$ or

$$[C] = \begin{bmatrix} \lambda_{rr}^2 & 0 & 0 \\ 0 & \lambda_{\theta\theta}^2 & 0 \\ 0 & 0 & \lambda_{zz}^2 \end{bmatrix}.$$

The Green-Lagrange strain tensor is also used in describing the material deformation and is defined as $\boldsymbol{E} = \frac{1}{2}(\boldsymbol{C} - \boldsymbol{I})$. This gives $\boldsymbol{E}$ as

$$[E] = \begin{bmatrix} E_{rr} = \frac{1}{2}(\lambda_{rr}^2 - 1) & 0 & 0 \\ 0 & E_{\theta\theta} = \frac{1}{2}(\lambda_{\theta\theta}^2 - 1) & 0 \\ 0 & 0 & E_{zz} = \frac{1}{2}(\lambda_{zz}^2 - 1) \end{bmatrix}.$$

Note that components of shear in the strain tensors are assumed to be zero because studies involving pressurization tests yielded negligible amounts of shear strain (Patel and Fry, 1966).

The description of stress most useful here is the Cauchy stress which characterizes the force per unit of deformed area at any given time. A traction vector $\boldsymbol{t}$ acting on a deformed material unit area *da* of normal vector $\boldsymbol{n}$ is defined using the Cauchy stress tensor $\boldsymbol{\sigma}$ as $\boldsymbol{t} = \boldsymbol{n}.\boldsymbol{\sigma}$. For convenience, let us define two additional stress tensors which will be used in the remainder of the thesis. The first and second Piola-Kirchoff stress tensors $\boldsymbol{P}$ and $\boldsymbol{S}$, respectively, which are related to the Cauchy stress tensor such that

$$\boldsymbol{\sigma} = J^{-1}\boldsymbol{F}.\boldsymbol{P}$$

$$\boldsymbol{\sigma} = \boldsymbol{J}^{-1}\boldsymbol{F}.\boldsymbol{S}.\boldsymbol{F}^{T}$$

where, $J \equiv \det \boldsymbol{F}$ is called the Jacobian of gradient tensor $\boldsymbol{F}$. Tensors $\boldsymbol{\sigma}$ and $\boldsymbol{S}$ are symmetric because there are no loads inducing moments per unit of volume.

Consider the static equilibrium of a volume element in the section given in cylindrical coordinates by

$$\begin{cases} \partial\sigma_{rr}/\partial r + \partial\sigma_{r\theta}/r\partial\theta + \partial\sigma_{zr}/\partial z + (\sigma_{rr} - \sigma_{\theta\theta})/r = 0 \\ \partial\sigma_{r\theta}/\partial r + \partial\sigma_{\theta\theta}/r\partial\theta + \partial\sigma_{z\theta}/\partial z + 2\sigma_{r\theta}/r = 0 \\ \partial\sigma_{rz}/\partial r + \partial\sigma_{\theta z}/r\partial\theta + \partial\sigma_{zz}/\partial z + \sigma_{rz}/r = 0 \end{cases}.$$

where σ_{ij} are components of the Cauchy stress tensor. Because $\boldsymbol{\sigma}$ is symmetric and shear components are assumed negligible, the remaining non-trivial equation is

$$\frac{\partial\sigma_{rr}}{\partial r} + \frac{(\sigma_{rr} - \sigma_{\theta\theta})}{r} = 0. \qquad \text{Eq. (9)}$$

Before proceeding, the strain energy function W should be described, as it is integral to relating the stresses and strains in a hyperelastic material. It is defined such that $\boldsymbol{S} = \partial W / \partial \boldsymbol{E}$, and in the case at hand (neglecting shear components)

$$dW = S_{rr}dE_{rr} + S_{\theta\theta}dE_{\theta\theta} + S_{zz}dE_{zz} \qquad \text{Eq. (10)}$$

where S_{ij} are the components of the second Piola-Kirchoff stress tensor.

The material unit is considered incompressible. Therefore the ratio of deformed to undeformed volume is one, or

$$dv/dV \equiv J \equiv \det F = 1 \qquad \text{Eq. (11)}$$

and since $\boldsymbol{C}$ and $\boldsymbol{F}$ are related by $\boldsymbol{C} = \boldsymbol{F}^{T}.\boldsymbol{F}$,

$$det\,\boldsymbol{C} = 1 \text{ and } \lambda_{rr}\lambda_{\theta\theta}\lambda_{zz} = 1. \qquad \text{Eq. (12)}$$

Note that Eq. 12 indicates that one stretch ratio (say λ_{rr}) can be written in terms of the other two (say $\lambda_{\theta\theta}, \lambda_{zz}$). Similarly, the strain energy function can be written in terms of $E_{\theta\theta}$ and E_{zz} only. Differentiating this function gives

$$dW = \frac{\partial W}{\partial E_{\theta\theta}} dE_{\theta\theta} + \frac{\partial W}{\partial E_{zz}} dE_{zz}. \qquad \text{Eq. (13)}$$

and the partial derivatives of the strain energy function can be expressed in terms of the second Piola-Kirchoff components as

$$\begin{cases} \dfrac{\partial W}{\partial E_{\theta\theta}} = S_{\theta\theta} - \dfrac{\lambda_{rr}^2}{\lambda_{\theta\theta}^2} S_{rr} \\ \dfrac{\partial W}{\partial E_{zz}} = S_{zz} - \dfrac{\lambda_{rr}^2}{\lambda_{zz}^2} S_{rr} \end{cases}, \qquad \text{Eq. (14)}$$

Using equation 14, $\boldsymbol{\sigma} = J^{-1}\boldsymbol{F}.\boldsymbol{S}.\boldsymbol{F}^T$ and $J = 1$, the Cauchy stresses can be expressed as

$$\begin{cases} \sigma_{\theta\theta} - \sigma_{rr} = \lambda_{\theta\theta}^2 \dfrac{\partial W}{\partial E_{\theta\theta}} \\ \sigma_{zz} - \sigma_{rr} = \lambda_{zz}^2 \dfrac{\partial W}{\partial E_{zz}} \end{cases}. \qquad \text{Eq. (15)}$$

To develop an equation for intramural radial stress, σ_{rr}, $\sigma_{\theta\theta} - \sigma_{rr}$ from Eq. 15 is substituted into Eq. 9. This expression is then integrated using the boundary conditions $\sigma_{rr}(a) = -p$ and $\sigma_{rr}(b) = 0$. The intramural radial stress is then given as

$$\sigma_{rr}(r) = \int_a^r \frac{1}{r} \lambda_{\theta\theta}^2 \frac{\partial W}{\partial E_{\theta\theta}} dr - p, \qquad \text{Eq. (16)}$$

where the internal pressure p is

$$p = \int_a^b \frac{1}{r} \lambda_{\theta\theta}^2 \frac{\partial W}{\partial E_{\theta\theta}} dr. \qquad \text{Eq. (17)}$$

Keeping this pressure in mind, it is also important that the longitudinal stresses in the arterial wall balance with any applied axial load and pressure on the end of the arterial section, assuming the section is closed. Therefore, this relation is written as

$$2\pi \int_a^b \sigma_{zz} r dr = F_z + \pi a^2 p. \qquad \text{Eq. (18)}$$

Equation 18 can then be rewritten with $\sigma_{zz} \equiv (\sigma_{zz} - \sigma_{rr}) + \sigma_{rr}$ and $\sigma_{zz} - \sigma_{rr}$ from Eq. 15 as

$$2\pi \int_a^b \lambda_{zz}^2 \frac{\partial W}{\partial E_{zz}} r dr + 2\pi \int_a^b \sigma_{rr} r dr = F_z + \pi a^2 p \qquad \text{Eq. (19)}$$

By integrating $2\pi \int_a^b \sigma_{rr} r dr$ in Eq. 19 by parts and using Eq. 16, the axial force can finally be described as

$$F_z = \pi \int_a^b \left(2\lambda_{zz}^2 \frac{\partial W}{\partial E_{zz}} - \lambda_{\theta\theta}^2 \frac{\partial W}{\partial E_{\theta\theta}} \right) r dr. \qquad \text{Eq. (20)}$$

Equations 17 and 20, given a material model, fully describe the equilibrium of a closed-end segment of aorta under pressure as was the case in the pressurization testing described in Chapter 3.

5.2 Mechanical Model of Membrane Sample under Biaxial Testing

The loads and deformations used to obtain the leaflet material properties were taken from biaxial testing data published by Billiar and Sacks (2000). Billiar and Sacks performed

biaxial loading of approximately 13 mm by 13 mm leaflet samples taken from fresh porcine aortic valves. The samples were loaded with Lagrangian membrane tensions ranging from 0 to 0.060 N/mm in the circumferential and radial directions simultaneously and the resulting experimental Green strains E_{ii} were recorded.

For determination of the material properties of the leaflets, the Lagrangian membrane tensions were converted to first Piola-Kirchhoff stresses by dividing them by the reported average leaflet thickness (0.466 mm), and then to Cauchy stresses by multiplying the first Piola-Kirchhoff stresses by the respective stretch ratios. This is because $\boldsymbol{\sigma} = J^{-1}\boldsymbol{F}.\boldsymbol{P}$ and, in biaxial planar testing, the deformation gradient tensor $\boldsymbol{F}$ is such that

$$[F] = \begin{bmatrix} \lambda_{11} & 0 & 0 \\ 0 & \lambda_{22} & 0 \\ 0 & 0 & \lambda_{33} \end{bmatrix}$$

where directions 1 and 2 are the directions of testing, and direction 3 is along the thickness of the sample. From the incompressibility of the leaflet tissue, $J = \lambda_{11}\lambda_{22}\lambda_{33} = 1$.

Stretch ratios λ_{11} and λ_{22} were determined from the Green strains reported by Billiar and Sacks using the relationship $E_{ii} = \frac{1}{2}\left(\lambda_{ii}^2 - 1\right)$ from $\boldsymbol{E} = \frac{1}{2}(\boldsymbol{C} - \boldsymbol{I})$.

Given the experimental Green strains, the Cauchy stresses predicted by the material model or strain energy function W were determined as $\sigma_{ii} = \frac{\partial W}{\partial E_{ii}}\lambda_{ii}^2$ since $\boldsymbol{\sigma} = J^{-1}\boldsymbol{F}.\boldsymbol{S}.\boldsymbol{F}^T$ and $\boldsymbol{S} = \partial W / \partial \boldsymbol{E}$.

5.3 Choice of a Constitutive Equation or Material Model

For both the aortic and leaflet tissues, a strain energy function W must be chosen that can most closely replicate the experimental data. Many strain energy functions have been developed over the years, for different types of biological tissues, for example by Takamizawa and Hayashi (1987), or Fung et al. (1979). A strain energy function introduced by Guccione et al. (1991) has been implemented in finite element software LS-DYNA, as is a variation of the widely accepted Fung model. The function is given as

$$W = \frac{C_1}{2}\left(e^{Q} - 1\right) + \frac{1}{2}P(J-1) \qquad \text{Eq. (21)}$$

where

$$Q = C_2 E_{\theta\theta}^2 + C_3\left(E_{zz}^2 + E_{rr}^2 + E_{rz}^2 + E_{zr}^2\right) + C_4\left(E_{z\theta}^2 + E_{\theta z}^2 + E_{\theta r}^2 + E_{r\theta}^2\right),$$

and the material constants are C_1, C_2, C_3 and C_4. Here, P is a Lagrange multiplier used to numerically enforce material near-incompressibility ($J \cong 1$) when it is not directly implemented through Eq. 12. The Green-Lagrange strain components are denoted as E_{ij}. Although Guccione's model was initially introduced for modelling heart muscle tissue, it has been shown to be a good candidate for modeling different cardiovascular tissues as well (Labrosse et al., 2009), and presents the unique advantage of having already been implemented and tested in a commercial finite element software.

5.4 Characterization and Validation of Material Constants

Characterization of the material constants is performed using data collected during experiments for which an analytical model exists, and where the constants can be

optimized so that the analytical model closely reproduces the experimental behaviour. Given the nonlinear nature of the optimization required, the classic Levenberg-Marquardt method is used, whose basic principles are detailed below (Humphrey, 2002).

Suppose m data points are available. Regardless of the type of data (e.g. stress, force, pressure) the difference between each experimental and theoretical quantity at each data point k must be reduced to obtain accurate material constants. In the case of the aortic tissue, a possible error function can be defined as

$$e = \sum_{k=1}^{m} \left(\left(\frac{p_{\text{theo}} - p_{\text{exp}}}{p_{\text{exp}}} \right)_k^2 + \left(\frac{F_{z\,\text{theo}} - F_{z\text{exp}}}{F_{z\text{exp}}} \right)_k^2 \right). \qquad \text{Eq. (22)}$$

where 'theo' refers to theoretical, 'exp' refers to experimental, p_{theo} is computed using Eq. 17, and F_{theo} is computed using Eq. 20. Similarly, for the leaflet tissue,

$$e = \sum_{k=1}^{m} \left(\left(\frac{\sigma_{11\text{theo}} - \sigma_{rr\text{exp}}}{\sigma_{22\text{exp}}} \right)_k^2 + \left(\frac{\sigma_{22\text{theo}} - \sigma_{\theta\theta\text{exp}}}{\sigma_{22\text{exp}}} \right)_k^2 \right)$$

The error function e being a function of c_i, it can be written more generally as $e = \vec{f}(\vec{c}) \cdot \vec{f}(\vec{c})$ or $e = f_k(c_i) f_k(c_i)$. Since $\vec{f}$ is a nonlinear function of the material constants c_i, these constants cannot be determined analytically and must be solved for numerically. Differentiating the error function with respect to the material parameters $\frac{\partial e}{\partial c_i} = 2 f_k \frac{\partial f_k}{\partial c_i} \equiv 2 f_k J_{ki}$ where J_{ki} is a Jacobian. Let $2 f_k J_{ki} = 2 r_i$, where r_i should ideally be zero, but usually is not in the first iteration as it is usually based upon a crude estimation for values of $\{\vec{c}\}$. Therefore an iterative solution is sought to drive r_i toward zero. At iteration j, $r_n^{j+1} = r_n^j + (c_i^{j+1} - c_i^j) \left. \frac{\partial r_n}{\partial c_i} \right|^j$. It is desired that $r_n^{j+1} = 0$ and $r_n^j = (f_k J_{kn})^j$.

Therefore, $-(f_k J_{kn})^j = (c_i^{j+1} - c_i^j)(\frac{\partial f_k}{\partial c_i} J_{kn} + f_k \frac{\partial J_{kn}}{\partial c_i})^j$, where $\frac{\partial f_k}{\partial c_i} = J_{ki}$ and $f_k = \frac{\partial J_{kn}}{\partial c_i}$ are replaced with λ, the Levenberg-Marquardt parameter. The full expression in matrix form is given as $([J]^T[J] + \lambda[I])^j(\{\vec{c}\}^{j+1} - \{\vec{c}\}^j) = -([J]^T\{\vec{f}\})^j$ (Humphrey, 2002).

To proceed with the minimization process, estimated values for $\{\vec{c}\}$ are assigned and iterations are performed until the difference between consecutive iterations for $\{\vec{c}\}$ is negligible. The method of minimization depends on the difference between λ and the norm of $J_{ki}J_{kn}$. As λ gets relatively larger, the minimization tends toward a method of steepest descent. This method converges as long as the error function e is convex or bounded from below, but may converge slowly. As λ becomes relatively small the minimization tends toward Newton's method. Newton's method may converge to a solution fairly quickly, but may not converge at all.

The Levenberg – Marquardt method is effective for the type of optimization to be performed here. It is available in Matlab as a multivariable function (lsqnonlin, see Appendix C) for which upper and lower bounds can be defined for $\{\vec{c}\}$. Enforcing boundaries for the optimization is useful for limiting the minimum values for the constants to those of the smallest usable in LS-Dyna (i.e. without crashing, as determined by practice and experience).

For the leaflets, the only significant constraints placed on the elements of $\{\vec{c}\}$ were that the constants should be positive and c_1 should have a value larger than 0.001. The constants obtained for the leaflet employing Guccione's material model were c_1 = 0.001 MPa, c_2 = 10.446, and c_3 = 1.925. Figure 21 shows the experimental and

theoretical Cauchy stresses against the Green strains with these constants. Note that the fourth material constant in Guccione's model is not calculated in Matlab. Because there was no shear deformation or force exerted on the leaflet sample in Billiar and Sacks' experiment, there was no relevant data to calculate this constant. It was therefore excluded from the model. However, a value for the constant is required to proceed in LS-Dyna. It was arbitrarily decided to set the fourth constant to the same value as the third constant. It was verified that other choices did not perceptibly influence the results, which was expected as long as the main mode of deformation of the tissue was not shear. This was also done for the aortic tissue for which no experimental behaviour in shear was available.

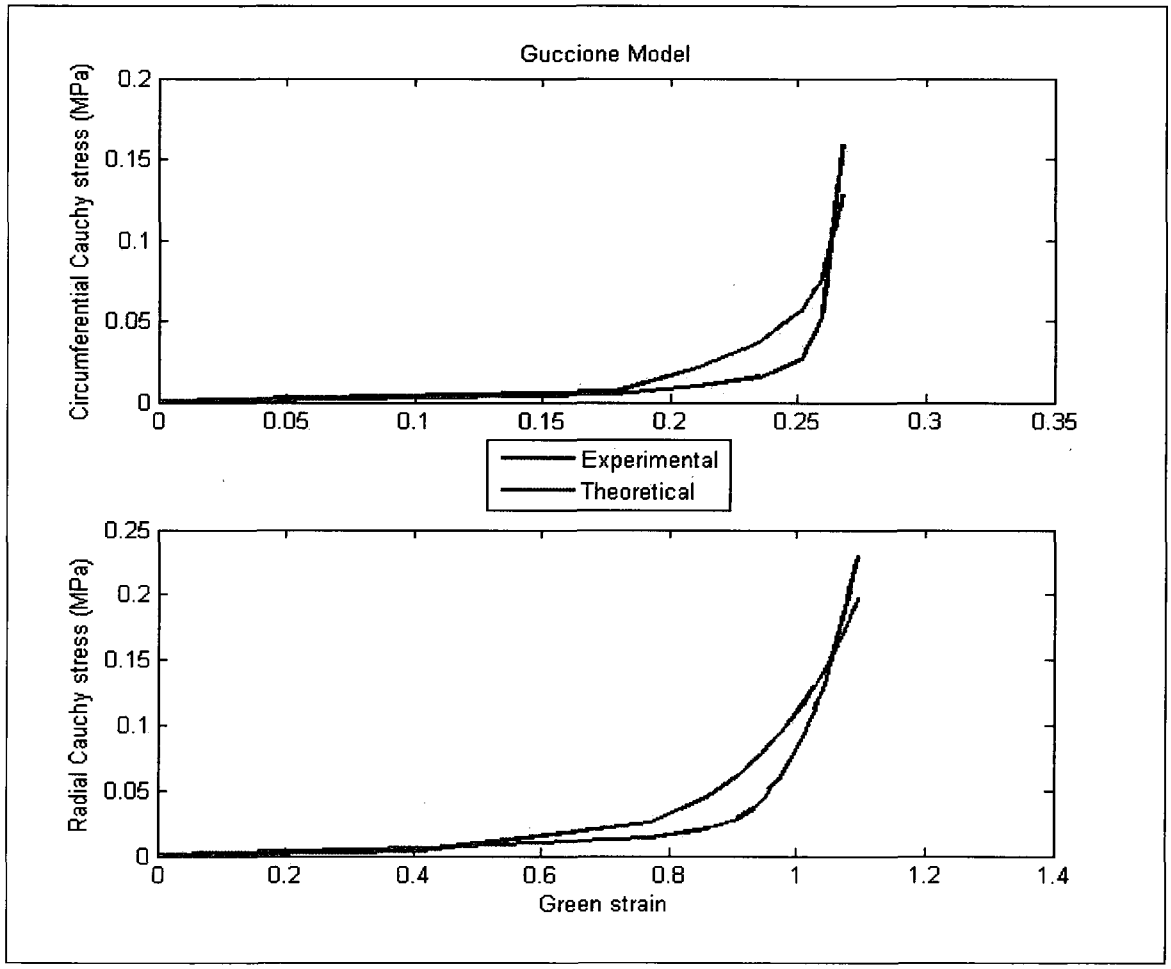

Figure 21 – Superimposed curves of the experimental and theoretically calculated Cauchy stresses and Green strains for the leaflet.

To validate the determination of these numerically optimized material constants, Billiar and Sacks experiment was recreated in LS-Dyna. A square material sample was constructed of thickness 0.5 mm and loaded with the same experimental membrane tensions in the radial and circumferential directions. The Cauchy stresses were then recorded and plotted against the Green strains. Figure 22 displays the various stresses obtained for comparison. The Cauchy stresses obtained from the LS-Dyna simulation confirm the validity of the material constants calculated for the leaflet.

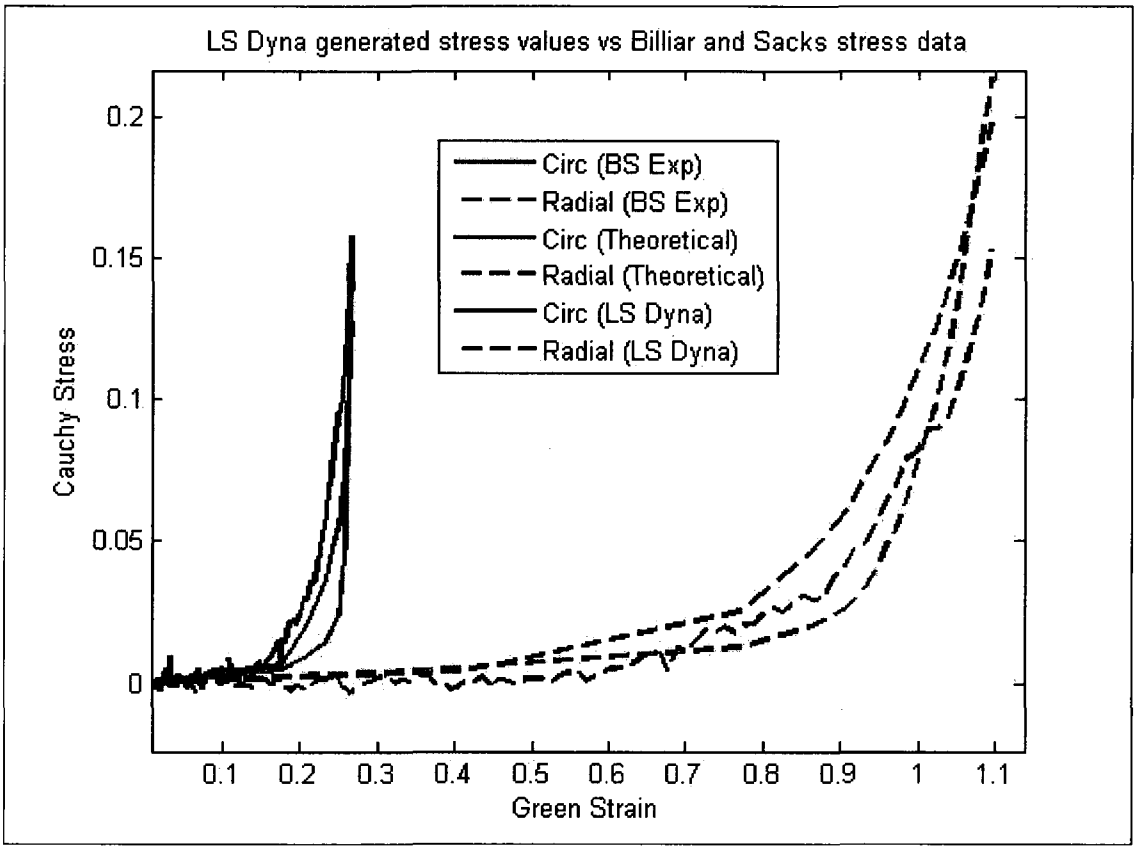

Figure 22 – A comparison of the theoretical, experimental (BS: Billiar and Sacks, 2000) and LS-Dyna generated stress-strain results for the leaflet material.

Another indication of how accurate the constants obtained are is to calculate the correlation coefficient R. Despite being a single value, the coefficient is representative of the total accuracy of the curves at all points. The coefficient R (Humphrey, 2002) is given by

$$R = \frac{\sum (y_k - \bar{y})_t (y_k - \bar{y})_e}{\sqrt{\sum (y_k - \bar{y})_t^2} \sqrt{\sum (y_k - \bar{y})_e^2}}$$

where t and e denote the theoretical and experimental values and the overbar denotes a mean value. The closer the value of R to unity, the more suitable the curve fit. For the leaflet values of 0.999, 0.999 and 0.998 were found for R corresponding to each material constant.

The material constants for the aortic tissue were calculated using the same Levenberg – Marquardt optimization method although a different set of inputs was used. The leaflet material optimization inputs were membrane tensions and Green strains, whereas the experimental inputs for the aortic tissue optimization were pressure, force, longitudinal stretch and inner radius at each pressure point (see Appendix D). Although pressure readings were only taken at intervals of 20 mmHg, the data were expanded to 81 data points from 0 to 160 mmHg for better accuracy of the Levenberg-Marquardt procedure. The material constants for the aorta were found as c_1 = 0.191 MPa, c_2 = 0.451, and c_3 = 0.184. The values for R were found to be 1.000, 0.999 and 0.998 for each constant respectively.

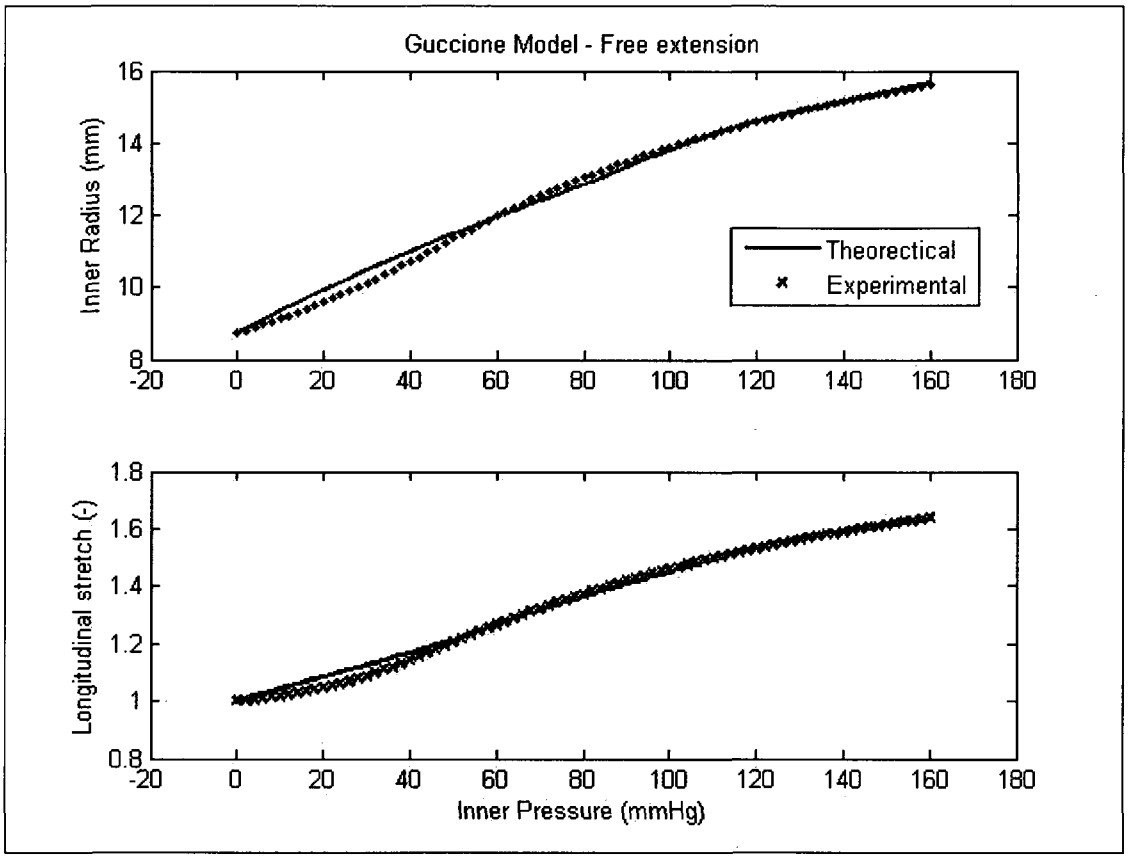

Figure 23 – Theoretical and experimental longitudinal stretch ratios (λ) and inner radius in the circumferential and radial directions.

Figure 23 displays the theoretical and experimental values of inner radius and longitudinal stretch ratio against pressure. As with the leaflet material properties, the theoretical results and experimental data agree well with each other. While these curves seemed favourable, the material constants had yet to be validated in a finite element analysis. Therefore, a simulation was performed in LS-Dyna replicating the experimental pressurization of the ascending aorta. A quarter of the aortic section from the STJ to the cannulated end of the ascending aorta was modeled. The cannulated end was constrained from expanding radially and the STJ was free to expand longitudinally, mirroring the situation in the actual experiment where the cannulated end was free to move

longitudinally and also constrained radially. The undeformed geometry of the aorta was determined from the experimental data at the STJ. Figure 24 shows the change in radii for the aorta from 0 to 120 mmHg during the pressurization experiment.

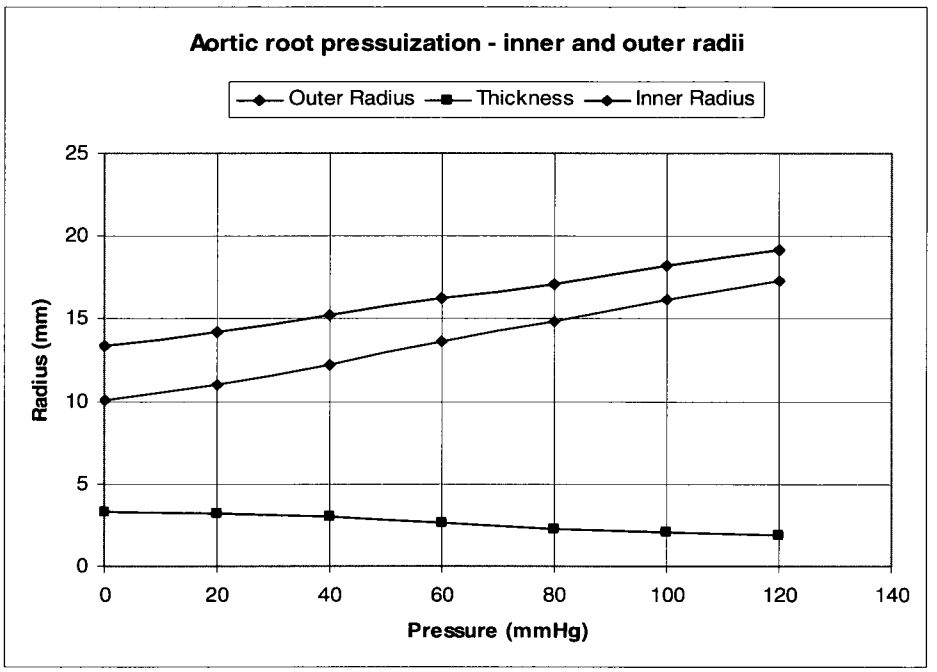

Figure 24 – Aortic root experimental pressurization from 0 to 120 mmHg. Note the decrease in thickness (difference between inner and outer radius) along the progression from 0 to maximum pressure.

Table 4 – Experimental and LS-Dyna aortic root radii compared

	Experimental		LS-Dyna	
	80 mmHg	100 mmHg	80 mmHg	100 mmHg
Outer Radius (mm)	17.11	18.19	16.43	17.09
Inner Radius (mm)	14.82	16.16	14.79	15.51
Thickness (mm)	2.29	2.03	1.64	1.58

Table 4 presents the values for inner and outer radii as well as thickness for two data points of interest: 80 mmHg and 100 mmHg pressure. Note the relatively large difference in thickness between the experimental results and the LS-Dyna simulation (28% and 22% respectively for 80 and 100 mmHg). However, Fig. 25 shows that the

aorta in the LS-Dyna simulation experiences more longitudinal stretch, which accounts for the relatively smaller thickness observed, given that the aortic material is incompressible. The simulated values for the outer radius (Fig. 25) are within an acceptable error from the experimental values, given the challenges posed by the finite element implementation of an anisotropic hyperelastic material model. Overall, these results validate the use of the material constants found and Guccione's material model in the aortic valve model.

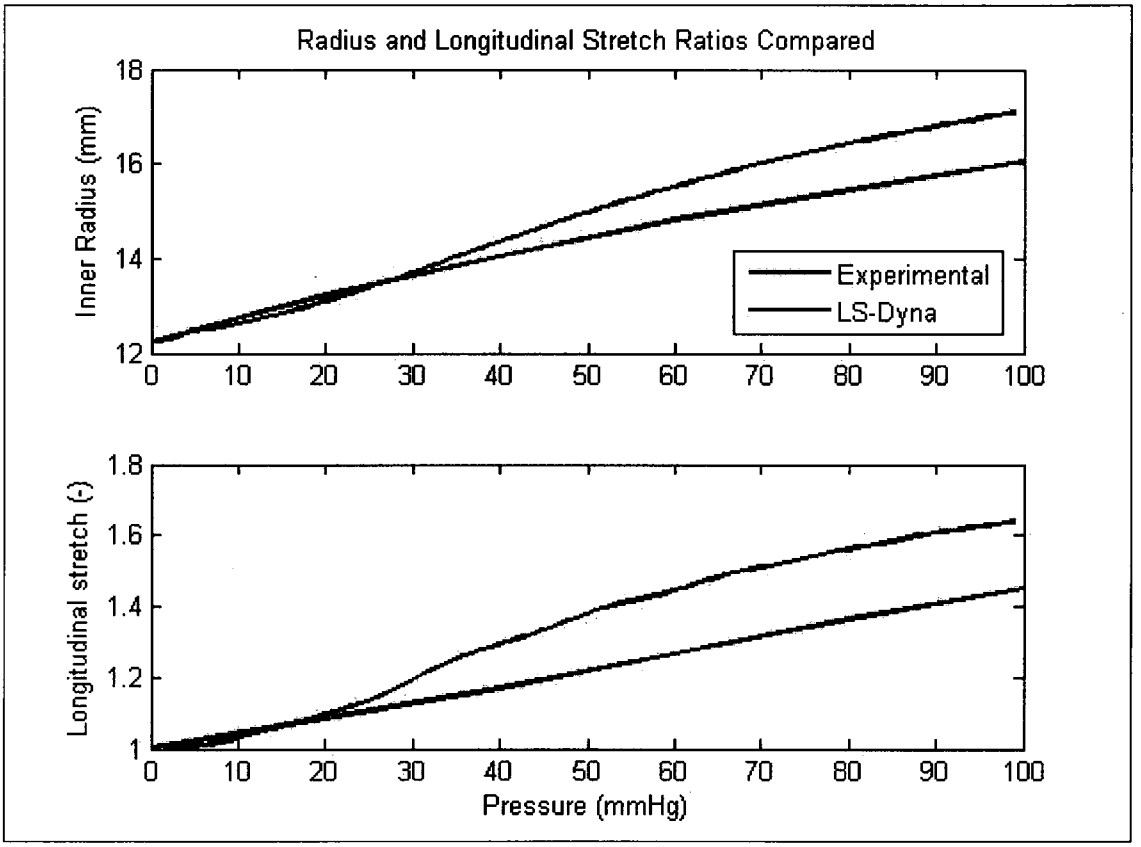

Figure 25 – Experimental and LS-Dyna results for the inner radius and longitudinal stretch compared.

5.5 Reordering of Constitutive Nodes

Now that the material model has been introduced, a specific implementation issue related to anisotropicity needs addressing. Consider a brick element from the aortic valve

finite element model with eight nodes (Fig. 26). Because of the anisotropicity, preferred directions need to be defined for each element. In LS-Dyna, this is done as follows: from node 1 to node 2 is the first preferred direction, from node 1 to node 4 is the second preferred direction, and from node 1 to node 5 is the third preferred direction. In Guccione's material model where the polynomial in the exponential is

$$Q = C_2 E_{\theta\theta}^2 + C_3\left(E_{zz}^2 + E_{rr}^2 + E_{rz}^2 + E_{zr}^2\right) + C_4(E_{z\theta}^2 + E_{\theta z}^2 + E_{\theta r}^2 + E_{r\theta}^2).$$

In the strain energy function, the influence of the circumferential Green strain is scaled by the second material constant whereas that of the longitudinal and radial Green strains are scaled by the third material constant. Therefore, the first preferred direction (node 1 to node 2) should be aligned with the circumferential direction. The second and third preferred directions will therefore be radial and longitudinal, not necessarily in that order.

During meshing of a volume, the preferred directions are generated arbitrarily because the meshing algorithm is not specifically written to mesh anisotropic material elements. Therefore, in some parts of the finite element model, the preferred directions in the biological tissue may not be described properly. For this reason, some node arrangements are rewritten to match the tissue preferred directions (see Appendix A). Consider Fig. 27 where element A is viewed from the centreline of the valve.

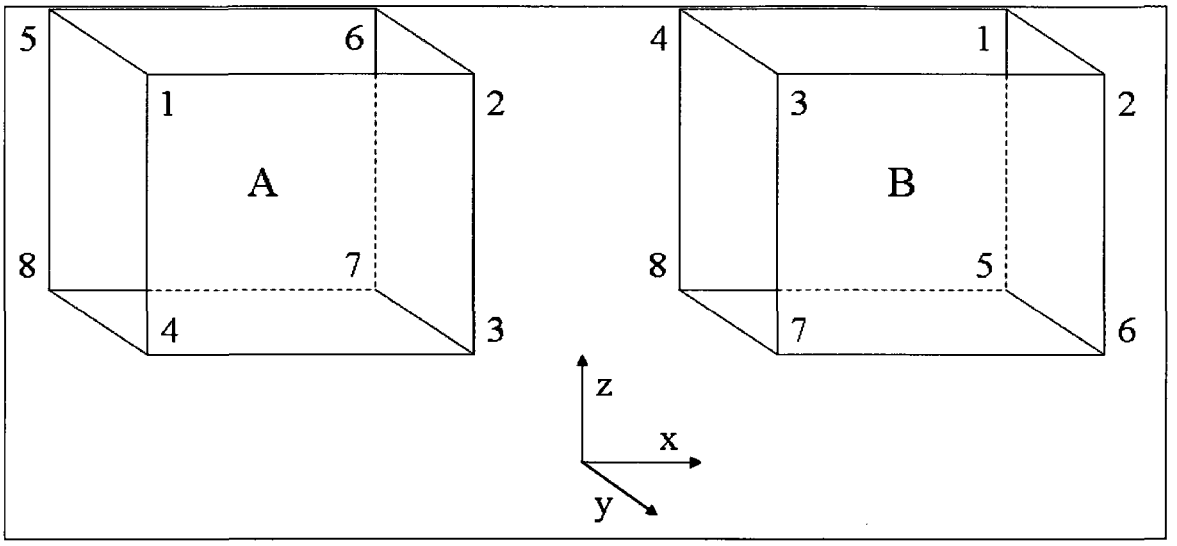

Figure 26 – Sample elements A and B. Element A has its preferred directions oriented with the orthogonal directions.

In element A the preferred directions are aligned with the correct orthogonal directions. However, in element B the directions are aligned incorrectly; node 1 to node 2 is along the radial direction. To correct this mismatch, nodes 4 and 2 cannot simply be switched to correct the problem. However, the element node numbers can be rearranged by rotating the element around its geometric center. For example, if element B is adjacent to element A in the aortic wall then it should have the same preferred directions. For this to be true, element B should be rotated 90 degrees about the x-axis once from the positive z-axis to the positive y-axis, and then rotated 90 degrees about the y-axis from the positive x-axis to the positive z-axis.

After meshing in ANSYS, a few parts required all of their element nodes to be reordered. All of these parts were meshed with the same preferred directions: longitudinal along nodes 1-2, circumferential along nodes 1-4 and radial along nodes 1-5 In all of these parts, element nodes were rearranged so that the circumferential and longitudinal directions were now the first and second preferred directions respectively.

As illustrated in Fig. 27, this was done by simply rotating element A 90 degrees about the y-axis from the positive z-axis to the positive x-axis. In the leaflet, parts 5, 6 and 7 were rearranged as discussed. In the sinus and aorta, parts 8, 11 and 13 were rearranged.

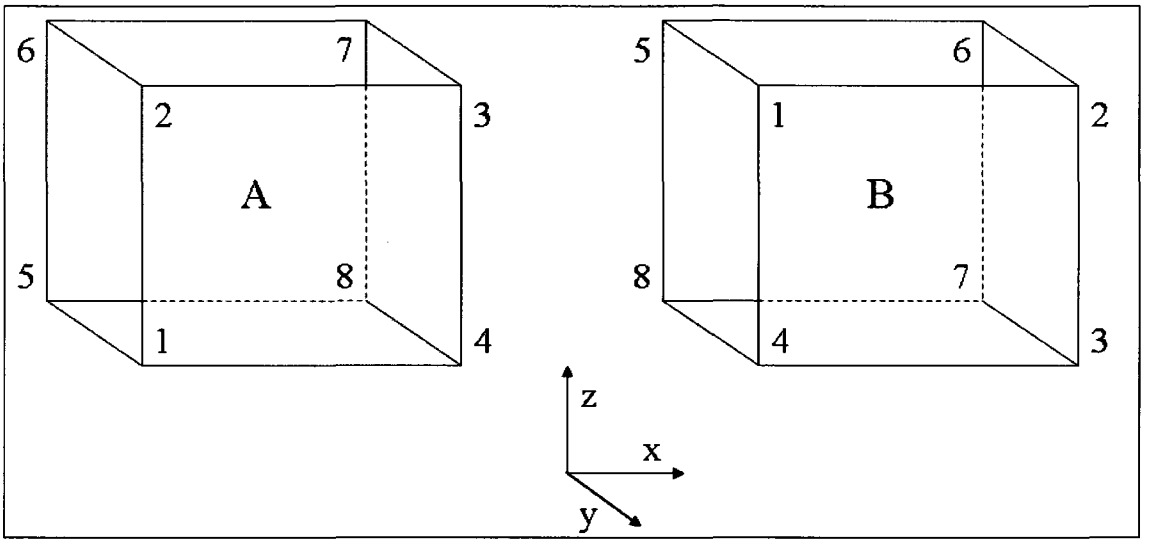

Figure 27 – Element A is rotated to have the node arrangements of element B in order to align the orthogonal directions along the corresponding preferred directions.

After these modifications, the lists of nodes, elements, forces and other important attributes were recorded and used to export the aortic valve geometry from ANSYS to LS-Dyna as discussed in Chapter 4.

CHAPTER 6 NUMERICAL SIMULATION

Chapters 3 to 5 presented the geometric modeling of the aortic valve and the determination and implementation of the material properties for its different constituents. As a continuation of the aortic valve model description, the present chapter will first detail what boundary conditions and loads were applied to the model, and then will present the results obtained from the numerical simulation of the entire cardiac cycle, starting from an unpressurized geometry. For consistency between simulations an idealized pressure curve was used for all variations.

6.1 Application of Boundary Conditions and Loads

Many boundary conditions applied to the aortic valve model were related to the valve symmetry. The most obvious was the constraints placed on the nodes along the plane that bisects the leaflet. In order to simulate symmetry of the leaflet, the nodes along the edge of the leaflet, sinus and aorta were constrained to motion within the radial-longitudinal plane.

To allow for quantitative comparison of the valve performance, the base of the aortic valve model was constrained to simulate a fixed base as was the case in the left-heart simulator. Although the base of the valve in vivo is normally unconstrained as it expands and contracts along with the left ventricle, no quantified data were available for validation of the numerical simulation, therefore a simplified fixed end condition was preferred. Accordingly, the base was constrained to its original radius and position in space

To simulate coaptation with the neighbouring leaflet, the nodes along the ventricular surface of the leaflet were specified as contact nodes, and were restricted from penetrating the surface of the rigid wall and the LVOT. The nodes contacting the rigid wall were allowed to slide on it without friction, thereby mimicking the simultaneous descent of two coapting leaflets. Real valves are rarely symmetric, which would lead to variations such as one leaflet stretching slightly further into the neighbouring leaflet. This is obviously dependent on geometric variations and local material properties, and can be seen as further second-order refinement when the present analysis aims at first-order behaviour.

At the top of the model, the nodes along the upper surface of the ascending aorta were moved longitudinally. A longitudinal stretch of 20 percent of the valve initial height was applied to the valve by displacing the top of the aorta. This was to account for the fact that the aorta and arteries retract when excised (Han and Fung, 1994; Dobrin, 1983) indicating that they are under longitudinal tethering *in situ*. Literature indeed suggests that the human body, as a whole, grows at a greater rate than the circulatory system, subjecting the vessels to longitudinal stretch (Dobrin, 1983). Han and Fung (1994) measured that *in situ* porcine aortas, from the aortic root to the iliac bifurcation, have a longitudinal stretch from approximately 1.2 to 1.5. To reproduce this type of tethering, a longitudinal stretch ratio of 1.2 was applied to the entire aortic valve model in the experiment and in the simulation. Variations of this longitudinal stretch ratio were examined in different models, for values ranging from 1.0 to 1.3.

One key feature of the present finite element model is that it starts from an unpressurized geometry. Assuming that the unpressurized geometry is stress and strain

free, this approach allows for the determination of the total stress and strain states once the model is pressurized to physiological conditions. Since the model has been created in open position, it implies that it should be loaded first to systolic pressure (120 mmHg) and then closed. This was done in two parts. First, a necessary (but non-physiologic) loading ramp lasting 0.04 s was used to bring the valve parts from the 0 to diastolic pressure (80 mmHg). The longitudinal stretch ratio of 1.2 was also applied during the ramp and held throughout the entire simulation. Then, following the pressurization ramp, the model entered a physiologic cardiac cycle, with the ventricular pressure starting to rise to 120 mmHg, as illustrated in Fig. 28. The pressures applied to the leaflet were obtained from the difference between the aortic and ventricular pressures. The pressure difference was applied to the ventricular side of the leaflet. This pressure difference was applied to only one side of the leaflet as opposed to the aortic and ventricular pressures being applied to their respective leaflet sides because this caused the leaflet elements to thin out and experience numerical problems. Also note that the diastolic phase was shortened in the simulation because extended period of high pressures caused the elements in the simulation to become numerically unstable (a result of software limitations), leading to undesirable jagged shapes that did not all recover upon pressure decrease. Although only for a shorter than physiological period of time, the maximum diastolic pressure difference was still applied to the leaflets.

In LS-Dyna finite element software, the time step is determined by the size of the smallest element. With this time step however, the computation time for each simulation was very long. For this reason the simulation time was scaled to 1/10 of the real time for the whole cardiac cycle in an attempt to speed up computation. However, one full

simulation was also carried out in real time and its results did not exhibit significant differences from those obtained with a scaled time cycle. Also, due to numerical instabilities witnessed in some elements, the diastolic period was shortened, having no effect on the stress and strain state of the model. Differences in stress, strain and overall dynamics from the simulations with short and full diastolic phases were negligible and therefore the short diastolic period was used in the simulation.

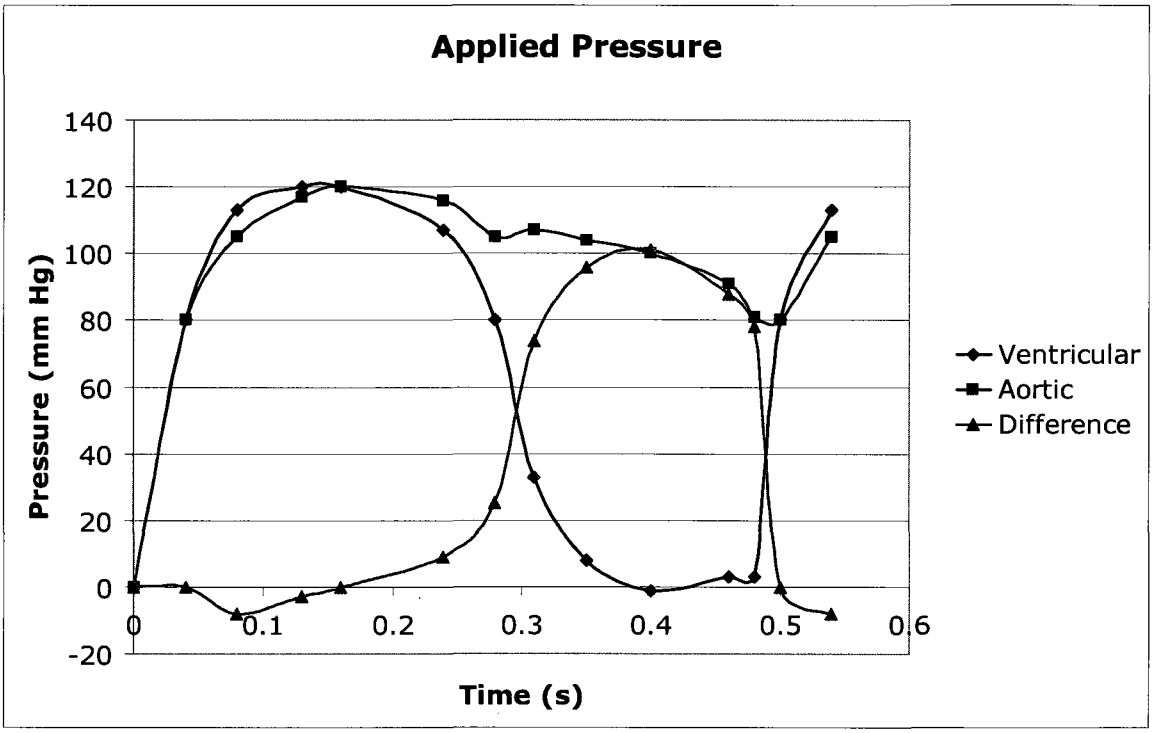

Figure 28 – The physiologic aortic and ventricular pressures applied, along with the unphysiologic loading ramp (Cheitlin et al., 2007).

Table 5 – Loading data used in the LS-Dyna simulation

Data Point	Time (s)	LV (mmHg)	Aorta (mmHg)	Ao-LV (mmHg)
1	0	0	0	0
2	0.04	80	80	0
3	0.08	113	105	-8
4	0.13	120	117	-3
5	0.16	120	120	0
6	0.24	107	116	9
7	0.28	80	105	25
8	0.31	33	107	74
9	0.35	8	104	96
10	0.4	-1	100	101
11	0.46	3	91	88
12	0.48	3	81	78
13	0.5	80	80	0
14	0.54	113	105	-8

6.2 Simulation Results

There are some crucial observations to be made from the simulation results. With regards to dynamic behaviour a number of qualities and quantities must be considered: shape and leaflet position, valve opening and closing times, as well as the geometric orifice area (which is an indicator of hemodynamic performance of the valve).

Refer to Fig. 29 for a composite view of the valve closing and then opening. At data point 2, the valve pressures have just been ramped to 80 mmHg, and the physiologic cardiac cycle starts. Data point 5 is the end of the systolic phase and the leaflets are about to start closing. At data point 8 the leaflets are in the process of fully closing, which they do at point 10 of the diastolic phase where they reach maximum deflection. Points 12 and 14 represent the leaflet opening and fully open in the next systolic phase, respectively.

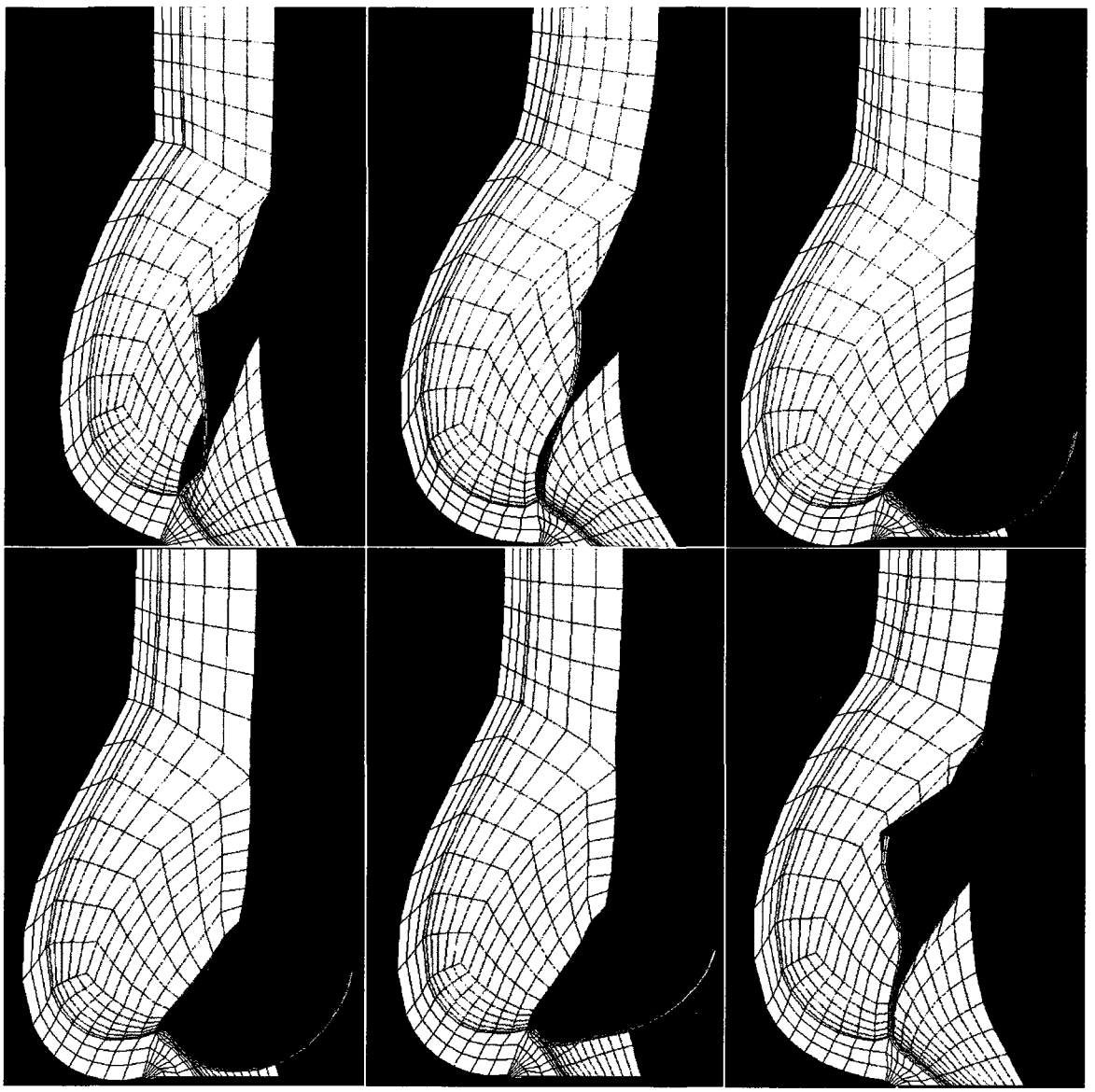

Figure 29 – From left to right, images taken at points 2, 5, 8, 10, 12 and 14 in Table 5 illustrating the simulated closing and opening of the aortic valve. The aortic and sinus tissues are represented in yellow, and the leaflet tissue is represented in red.

When the valve is fully closed (at and around point 10), the leaflet coaptation area near the free-edge is flat, indicating contact with the rigid wall representing the neighbouring leaflet. Despite a slight depression in the leaflet belly region, there is no indication of a future prolapse, which would be marked by the leaflet free edge starting to sag below the belly. The leaflet and sinus shapes during the diastolic phase are representative of an

average aortic valve during diastole. This is visualized in Fig. 30 in an oblique view of the aortic valve model for qualitative comparison with the anatomical description in Fig. 2.

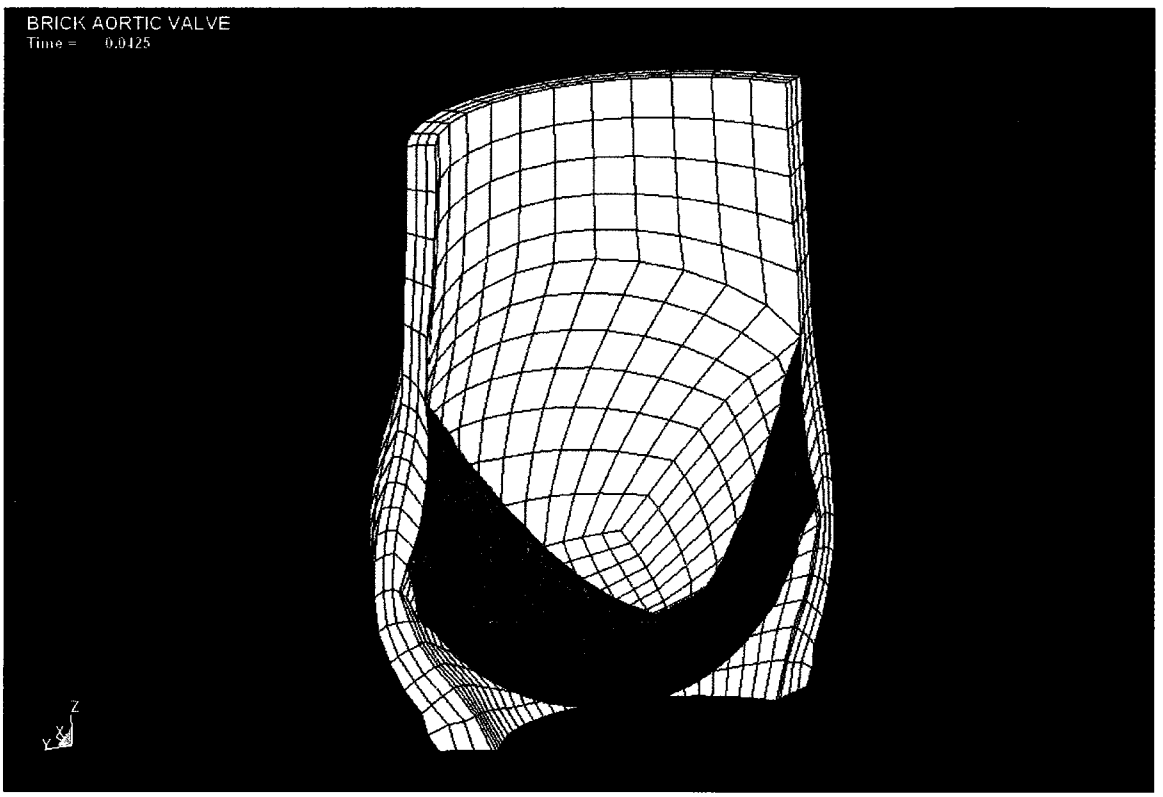

Figure 30 – An oblique view of one third of the aortic valve during simulation of the diastolic loading. This leaflet and sinus shapes are typical of those found in the aortic valve *in vivo*.

The time taken for the valve to open and to close was recorded, as appropriate closing and opening times are another strong indicator of proper valve function in clinical context. To help determine these parameters, a curve of the geometric orifice area (GOA) is commonly plotted against time (Thubrikar et al. 2000). The GOA is found by measuring the projected area created by the open leaflets. In the simulation and

experiment the GOA was calculated from still images taken from the top view of the valve from the ascending aorta.

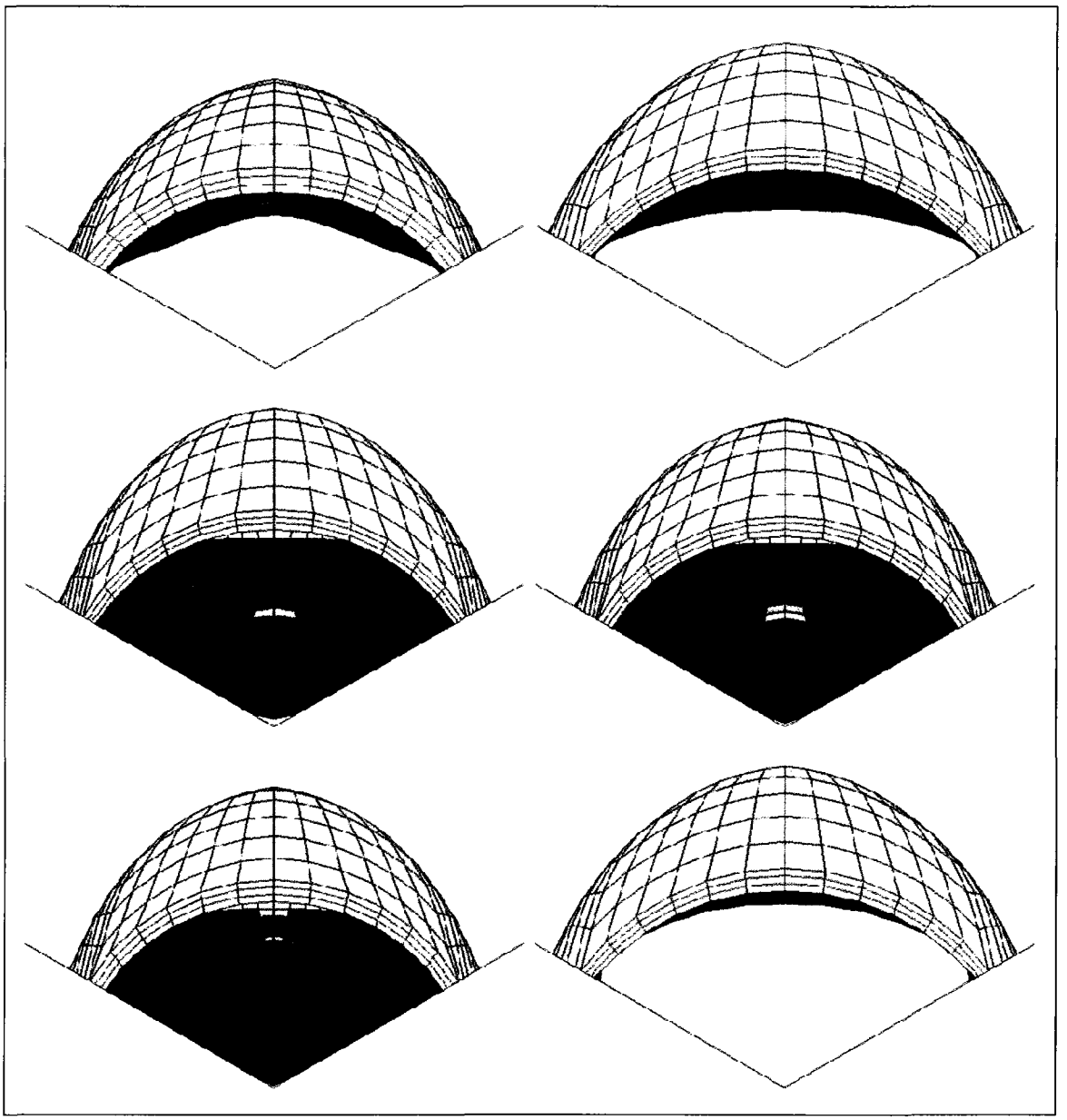

Figure 31 - From left to right and then top to bottom, an evolution of the simulated valve from open to closed position and then back to the open position. The images were taken at data points used for Fig. 29. Similar pictures, taken at much closer time intervals, were used to determine the geometric orifice area as a function of time as presented in Fig. 32.

Figure 32 displays the calculated geometric orifice areas of both the simulation and experiment.

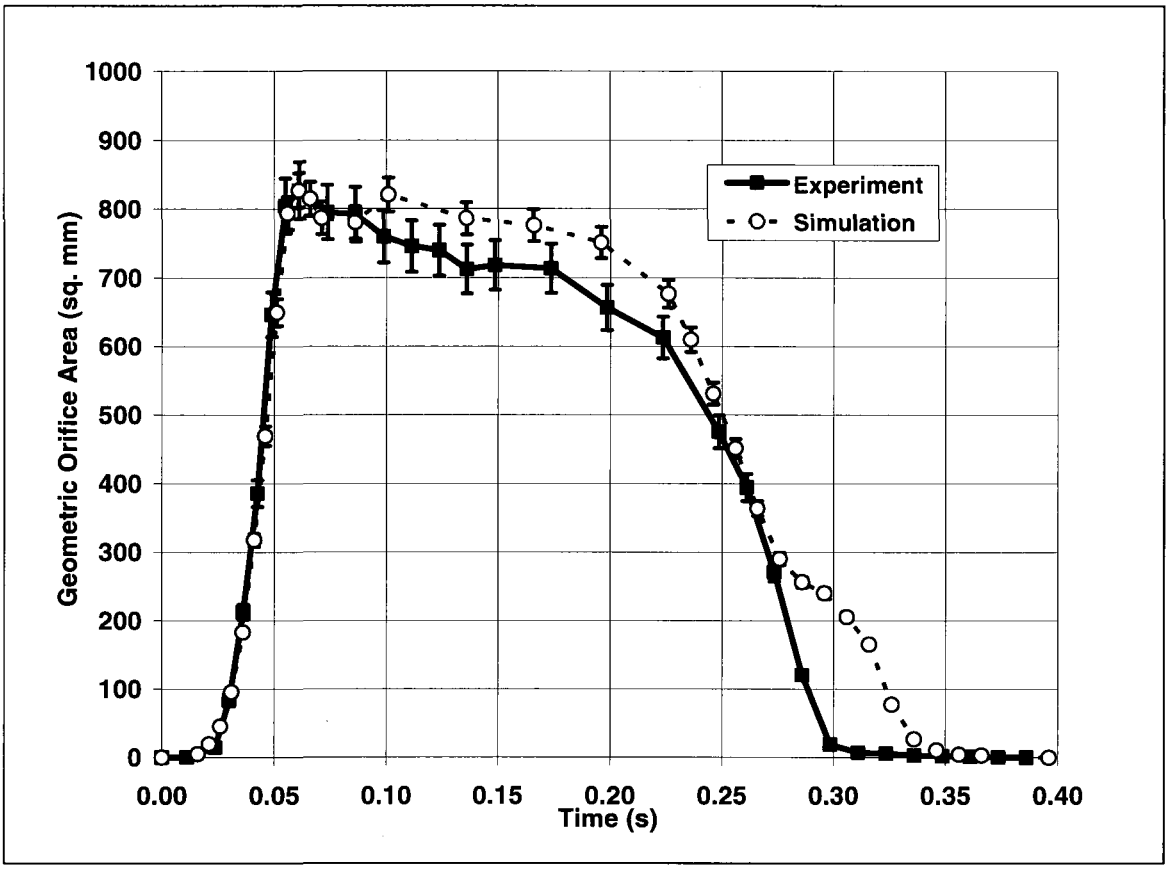

Figure 32 – Geometric orifice areas of the experimental and simulated valves. Note the error bars are not clearly visible in the plot, however they are present behind the data point markers. The timing in this plot does not correspond to the loading times used in the simulation: in this plot, the closed position was taken as time zero.

There is no set method for calculating GOA since the area is usually of irregular shape. Here, GOA was calculated by measuring the number of pixels in an area and then converting this figure to mm^2. Image processing was done using imaging software Image Tool 3.0 (The University of Texas Health Science Center in San Antonio). First a conversion from pixels to area must be established for the experiment and the simulation separately. In the simulation, a known base diameter of 23.5 mm for the LV tract yielded

an area of 433.74 mm^2. This area corresponds to 19650 $pixel^2$, with less than 1% relative error. In a similar fashion 39616 $pixel^2$ (less than 2% relative error) corresponded to 827.1 mm^2 in the experimental image. These calibrations were used to calculate the GOA at each time point shown in Fig. 32.

From the plots of the GOAs it is possible to compare the opening and closing behaviours of the experimental and simulated valves. From the curves it is observed that both valves take roughly 30 ms to open and remain completely or more than half open for almost 200 ms. At this point, the experimental valve begins to close steadily for approximately 30 ms till there is no orifice. After being open for 200 ms the simulated valve begins to close at a slower rate than the experimental valve for 25 ms and then continues to close at the same rate for another 25 ms.

Overall, there was less than 5% measurement error in the GOA measured for the experimental images and less than 3% measurement error in the GOA measured from the simulation. The scaling used to calculate these GOAs is sufficient; this is supported by the fact that the curves are very similar and the fact that there is only a 1.5% difference between the average GOAs of the two curves. These errors are differences in measurement betweein the GOAs of the simulation and those in the experiemental images; they are not actual errors in the simulation

6.3 Stress and Strain Behaviour

The aortic valve's function is to block the backward flow of blood into the left ventricle. This comes at the cost of being subjected to relatively large amounts of

mechanical stress. The distribution of stress in the valve varies with time and location; even within parts such as the leaflet there is a considerable amount of variation between such areas as the attachment line and the belly region.

There are a few areas in the valve that are important to observe that highly affect valve function, stress distribution and possible pathology. Therefore, stresses in these areas will be scrutinized throughout the evolution of the load cycle. The magnitude of stress experienced by the valve tissues is much greater during the diastolic phase than the systolic phase and more attention should be paid to stresses during diastole. However, the ability to monitor the valve behaviour in systole is also potentially important. Indeed, some diseased valves, especially stenotic aortic valves, do not open properly in systole and are subjected to tremendous loads then as well.

To illustrate the stress and strain results, specific elements in the leaflet belly, aorta, sinus, and at the line of attachment were monitored throughout the cardiac cycle. The stress and strain data were recorded in particular at three time points during the loading cycle: when the valve was fully open (systole), at maximum loading (diastole), and when the valve began to open again (start of next systole). Figure 33 and Table 6 indicate the regions and elements chosen to be recorded.

Table 6 – Elements for which stress and strain data are recorded

Valve Region	Element ID
Leaflet Belly	590
Leaflet Attachment (low)	466
Sinus	1137
Aorta	1277

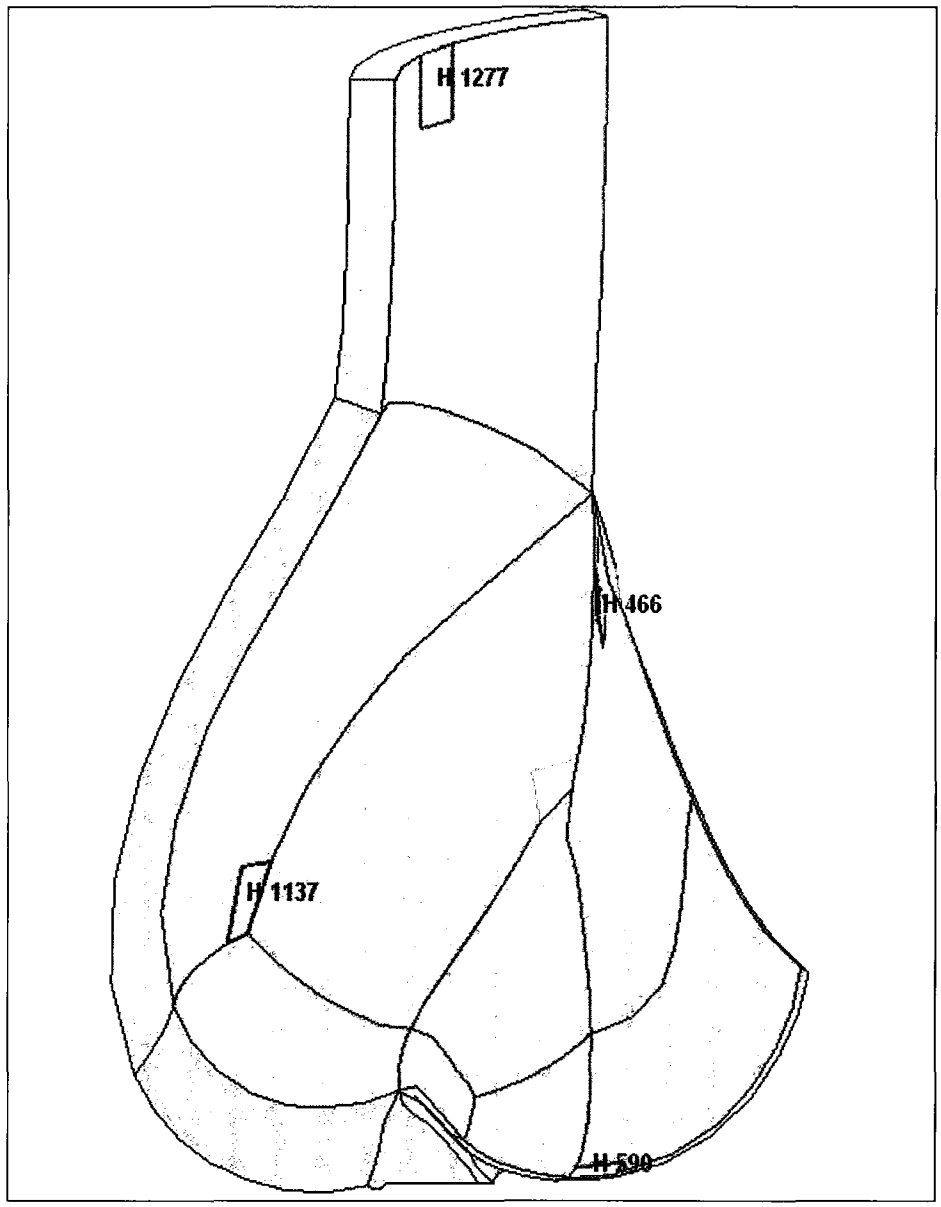

Figure 33 – The aortic valve model with highlighted elements for which Cauchy stresses and Green strains have been recorded.

Presenting the results is a challenge because giving a general stress plot of the principal stresses of the entire valve without vector directions would prove to hold little significance. But then, a vector plot would be just too messy and would not give the whole picture either. However, because the valve has many near cylindrical or spherical

features, it is expected that the principal stresses will generally be along the local circumferential direction. In Fig. 34, element 590 from the leaflet belly is shown with its first and second principal stresses. Note that the principal stresses are not perfectly aligned with the element edges; however, they are generally carried in the circumferential (orange) and radial (light blue) directions. A summary of the Cauchy stresses and Green strains of the highlighted elements can be found in Table 7.

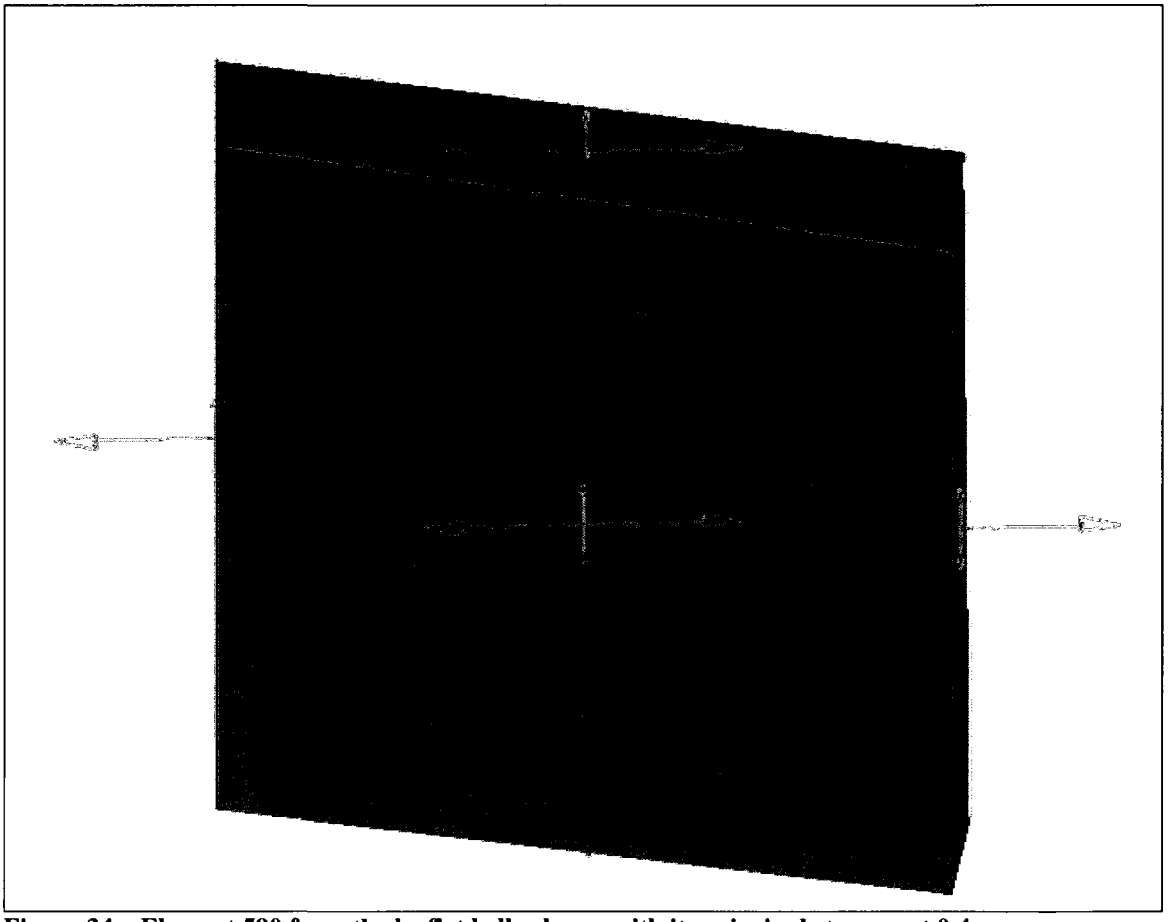

Figure 34 – Element 590 from the leaflet belly shown with its principal stresses at 0.4 *s*.

Table 7 – Each of the elements along with their principal Cauchy stresses and Green strains. All of the first principal Cauchy stresses and second principal Green strains were in the circumferential direction, as expected. Note that elements 590 and 466 are on the leaflet, whereas elements 1137 and 1277 are in the sinus and aorta. All Cauchy stress values are given in MPa.

Element	0.06 s		0.4 s		0.48 s	
	1^{st} P Stress	2^{nd} P Strain	1^{st} P Stress	2^{nd} P Strain	1^{st} P Stress	2^{nd} P Strain
	2^{nd} P Stress	1^{st} P Strain	2^{nd} P Stress	1^{st} P Strain	2^{nd} P Stress	1^{st} P Strain
590	0.3957	0.3254	0.5737	0.568	0.5116	0.3295
	0.0961	0.795	0.1779	1.075	0.0413	0.7588
466	0.0243	0.2697	0.7416	0.3533	0.243	0.2597
	0.0065	0.5813	-0.0352	1.193	-0.0249	0.8758
1137	0.1575	0.5314	0.0687	0.3729	0.0552	0.3236
	0.0701	0.6894	0.0372	0.5375	0.0295	0.4751
1277	0.075	0.0961	0.1689	0.465	0.1335	0.4351
	-0.0041	0.5607	0.0372	0.6015	0.0311	0.5249

At the maximum load during diastolic phase, there was a large amount of stress on the leaflet along the attachment line and in the belly region. Figure 35 displays the principal Cauchy stress vectors for the leaflet at that time. The first principal Cauchy stress is carried generally parallel to the free-edge, which corresponds to the circumferential direction in the leaflet. In the sinus and aorta (Fig. 36), the first principal Cauchy stress is again primarily circumferential and the largest stresses are along the leaflet attachment line.

The results obtained from the numerical simulations, along with the whole modeling procedure, will be discussed in Chapter 7.

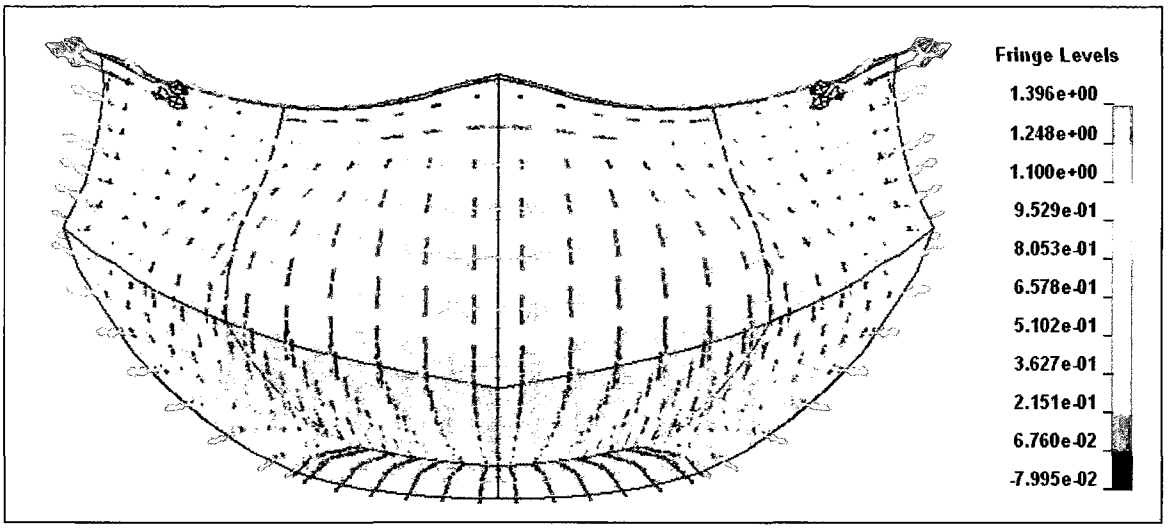

Figure 35 – A view of the leaflet from the sinus wall at maximum pressure difference, with principal Cauchy stress vectors displayed.

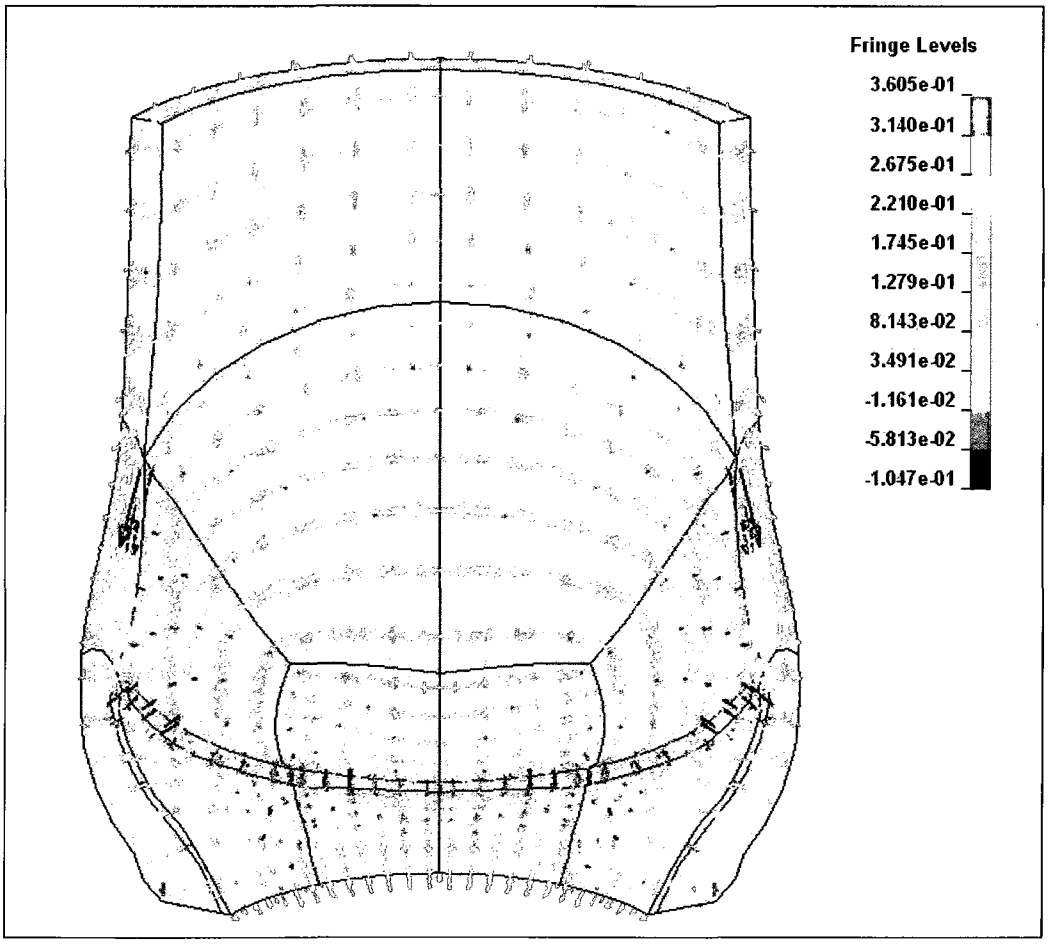

Figure 36 – A view of the sinus and aorta from the valve centreline at maximum diastolic pressure, with principal Cauchy stress vectors shown.

CHAPTER 7 DISCUSSION AND CONCLUSIONS

The numerical simulation of the aortic valve produced in the present work was developed based on a combination of data obtained from experiments that were carried out especially, as well as from published data. The dimensions used to establish the geometry of the aortic root were measured from a silicone rubber mould and were supplemented when needed using published data (Swanson and Clark, 1974). Prior to the silicone rubber being injected, the root was observed in a left-heart simulator to collect data about its dynamics. The aortic root was also quasi-statically pressurized and data collected regarding its dilation and longitudinal extension to obtain the material properties for the aortic tissue used in the numerical model. The numerical model developed can be used to display the distributions of stress and strain in the leaflet as well as in the surrounding aortic root. It can also be used to visualize the aortic root shape and dynamics over the cardiac cycle, and for validation purposes, such results can be compared to those obtained from the experiments in the left-heart simulator and the static pressurization system. Below is a discussion of the results from the numerical simulations, with an emphasis on dynamics and stress and strain distributions. Then, comments about possible improvements and extensions of the present work will follow, along with concluding remarks.

7.1 A Discussion of Simulated Results

Qualitatively, the shape of the sinus and leaflet at various time points throughout the cardiac cycle corresponded to typical shapes observed in the left-heart simulator *in*

vitro. Recalling Figs. 29 and 30, note that the shape of the sinus was characterized by a rounded, outward bulge as pressure was applied. This occurred in the simulation as expected and depicted in Fig. 30 at the maximum pressure difference. Figures 29 and 31, display the leaflet at maximum deflection and its evolution from open to closed configurations, respectively. The shape of the leaflet was characterized by the triangular closing shape seen from the ascending aorta. This matched well with the closed geometry recorded from the left-heart simulator (see Figs. 9 and 31).

In the previous chapter, the outer radius of the ascending aorta was recorded during static pressurization and an LS-Dyna simulation of just a thick-walled, closed-end cylinder was performed to validate the material properties used in the aortic valve model. The outer radius of the ascending aorta in the aortic valve model was recorded at various pressures and compared to the outer radii of the ascending aorta in the experimental aortic root and the LS-Dyna simulation, as illustrated in Fig. 37.

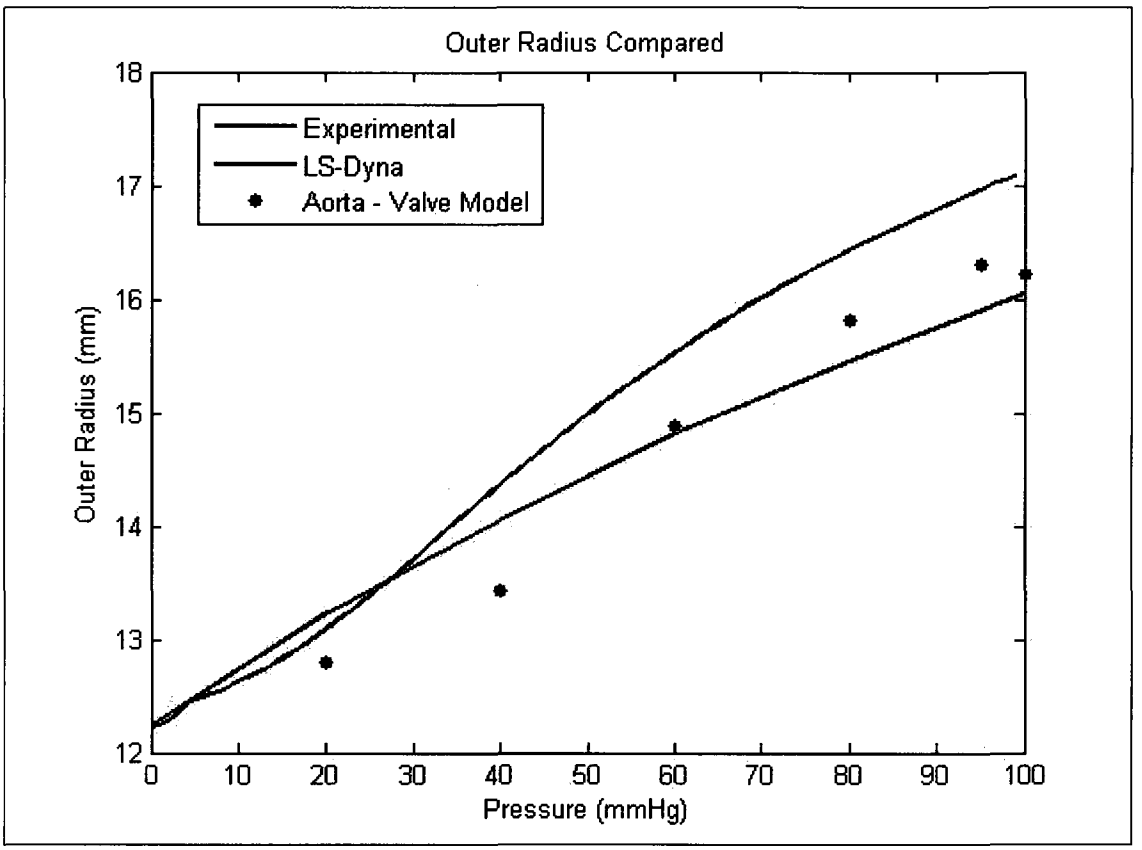

Figure 37 - Radii for the ascending aorta are compared between the experimental pressurization, a simulation for a thick-walled closed-end cylinder, and the complete aortic valve model. The black markers are instantaneous values for radii recorded at various pressures during the simulation of the aortic valve.

The radii for the simulated cylindrical ascending aorta lay within 7% of maximum relative error of the experimental values, and the readings for the outer radius of the aorta in the whole valve model also agreed very well with the experimental values. This indicates that the material properties used for the aorta were well chosen and lead to a predictable response from the aorta and sinus in the numerical simulation of the aortic valve.

When constructing the valve in ANSYS, a coaptation height of 3.9 mm was specified on the basis of a purely geometric (i.e. unstretchable) model. In the actual

aortic valve simulation, the resulting coaptation height along the bisecting plane of the leaflet was 2.9 mm when the maximum diastolic load was applied. Despite this smaller coaptation height along the centreline of the valve, the rest of the leaflet towards the commissure coapted well with the neighbouring surface, with much larger coaptation heights. Therefore, the model credibly represented sealing of the valve during diastole. Nevertheless, it can be noted that the coaptation height along the valve centreline could be influenced by the initial leaflet geometry. As discussed in section 4.3, the leaflet parameters used in the model were taken from Swanson and Clark (1974) for an aortic root of similar basal and STJ radii. The leaflet was constructed in the open position, whereas the values were measured in the closed position. While the values used in the open and closed positions should ideally be the same or fairly close at zero pressure, any difference may have affected the coaptation height in the model.

Another important issue is the construction and loading of the aortic valve model. There is no standard procedure for constructing and solving a numerical model of the aortic valve. Some authors (Nicosia et al. 2003; Howard et al. 2003; De Hart et al. 2003; Grande et al. 2000) have constructed the aortic valve in the closed configuration using data collected during diastolic loading and proceeded to apply this loading while considering the already loaded geometry as stress-free. This is incorrect, as it does not allow for the model to include the initial stresses that are inherent in natural valves. These initial stresses are accumulated by loading the valve from 0 to 80 mmHg pressure, which happens in the embryo. By constructing the valve in the closed position and applying diastolic loads, the initial stress accumulated from 0 to 80 mmHg of pressure is removed, thereby reducing the total amount of stress in the valve. Other authors (Chew

et al. 1999) constructed their models in the open configuration using data from the systolic phase, which is also incorrect and also has the effect of eliminating initial stress. In the present model, specific attention was paid to constructing the model in the stress free state (i.e. 0 mmHg pressure), so that the initial stresses could be included before starting a physiological load cycle. The radii chosen for the aortic root base and STJ were taken from the ultrasound images obtained in static pressurization under zero pressure. As discussed in the previous paragraph, the leaflet dimensions were taken from an aortic root of similar dimensions recorded by Swanson and Clark (1974) at zero pressure. The leaflet was built in the open position, and the whole aortic valve was pressurized from a good approximation of the stress-free state.

One of the easiest ways to evaluate the dynamics of the aortic valve model is to compare the geometric orifice area calculated for the simulated valve and that obtained from an aortic valve tested in the left-heart simulator over one cardiac cycle. As illustrated in Fig. 38, the rapid opening and gradual closing of the experimental valve was well matched by the simulation. Figure 38, however, shows one slight inconsistency: at approximately 0.275 s, the closing in the simulation was slowed and then proceeded again at approximately 0.30 s. The origin of this delay in closure is unclear. Perhaps inclusion of fluid-structure interactions would help close the valve at this particular point. Despite this deviation, the rate at which the leaflet closes in the simulation is the same as in experimental conditions, and overall, the simulation provides an excellent replication of the closing and opening motions of the valve, both in timing and quantity.

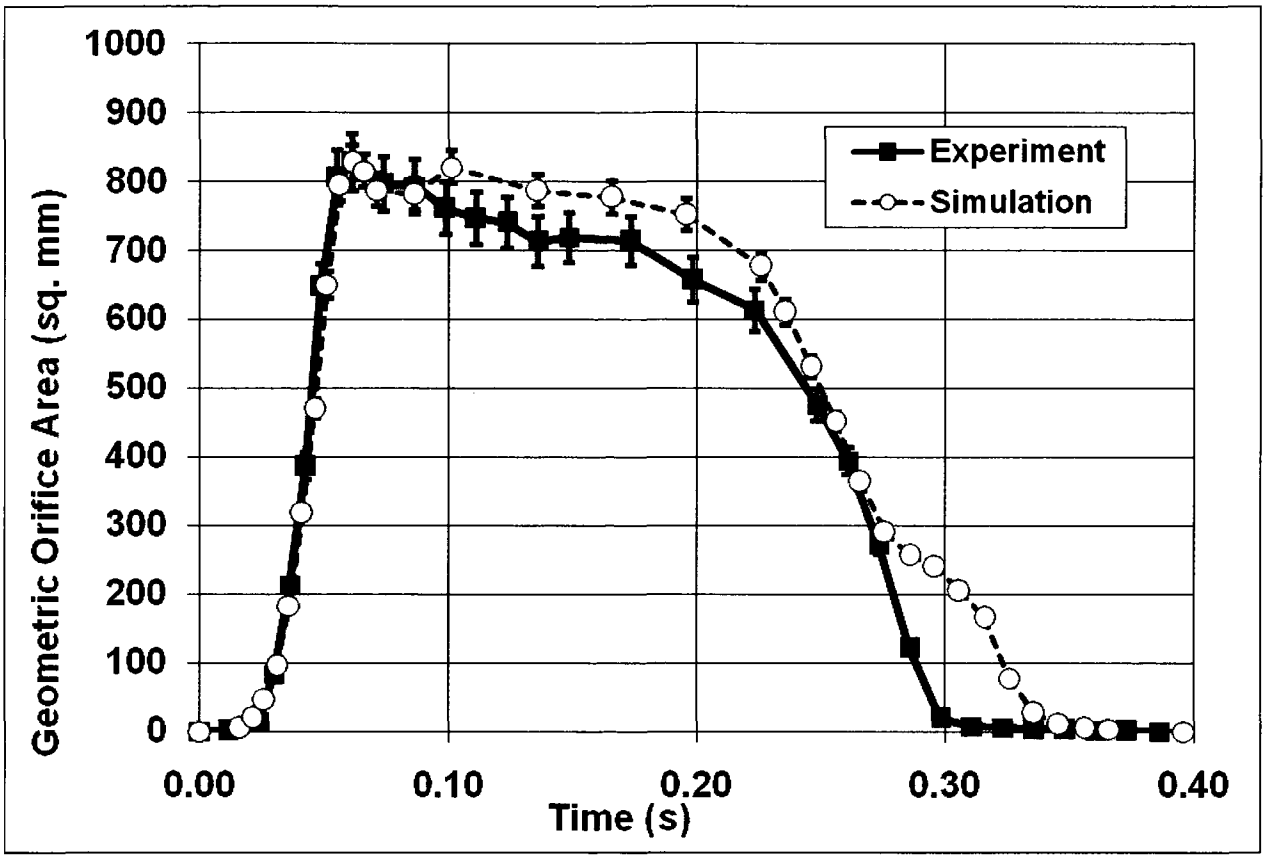

Figure 38 – Geometric orifice areas of the experimental and simulated valves.

Some authors (Ranga et al. 2004) have argued that the leaflet holds physiological pressures without bulging downward toward the left ventricle in the belly region. This however was not verified as the leaflet was clearly seen to continue bulging well after complete closure in the high-speed video taken in the left-heart simulator via endoscopy. The same behaviour was observed in the numerical solution after the GOA became 0, as illustrated in Fig. 29, where the bottom left and centre left pictures display the leaflet at two different times both having a GOA of 0. Also, the leaflet expectedly exhibits a cylindrical shape during diastolic loading as mentioned in the geometric assumptions when building the model.

Due to surrounding tissues, it is difficult to decipher the exact shape or position of the aortic sinuses *in vivo*. In the simulation, the sinus sagged slightly to the level of the basal plane. This slight depression in the sinus was also seen in the left-heart simulator however, not to the same extent. Because the simulation aimed at reproducing conditions in the left-heart simulator, the base of the valve and the top of the ascending aorta were constrained from radial motion in the simulation. The sag in the sinus could be attributed to this constraint. Indeed, a simulation was performed with the basal plane constrained only in the longitudinal direction, and in the resulting simulation, the sinus did not sag as much. This may be closer to an aortic root *in vivo*, which has no radial constraint at the base, despite the contraction of the heart on approximately two-thirds of the basal circumference during systole.

In the model, three elements were used across the thickness of the sinus and two elements were used across the thickness of the leaflet. This configuration was found through varying the number of elements across the thickness. It was observed that less than three elements across the thickness produced results that did not clearly depict the distribution of stresses in the sinus wall and similarly in the leaflet. A model with more than three elements in the sinus wall gives an accurate representation of stress variation across the thickness but also increases the computation time required.

While a longitudinal stretch ratio of 1.2 was found to be the natural configuration in vivo, ratios of 1.0 to 1.3 were also investigated in intervals of 0.1. It was found that adding longitudinal stretch reduced the sag in the sinus, and a stretch ratio of 1.2 (physiologically correct for a porcine aortic root according to Han and Fung, 1994) adequately modeled the sinus shape seen in the left-heart simulator.

The following in this section deals with stress and strain results throughout the model. Recall the stress and strain data collected from elements 590 (belly region) and 466 (attachment) in the leaflet at various times during the load cycle, and shown in Table 7. The Cauchy stress values are plotted against the Green strain values in Figs. 40 and 41. They are plotted along with the stress-strain curves from Billiar and Sacks (2000) used to calculate the material constants for the leaflet and the stress-strain relationship enforced in LS-Dyna for the leaflet. Figure 39 displays the comparison of radial stresses from elements 590 and 466. In the radial direction, stresses in element 590 were low, pointing to the possibility that the loaded leaflet belly does not experience an equibiaxial state of stress or strain. However, it seems that both elements were generally governed by the stress-strain curve enforced.

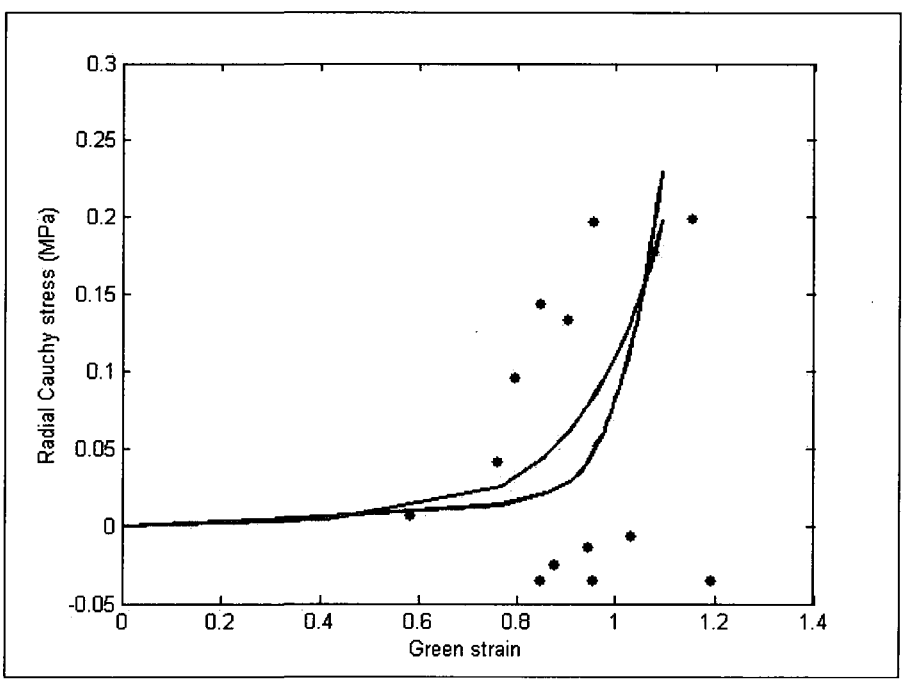

Figure 39 – Cauchy stress vs Green strain in the radial direction, in the leaflet. Blue curve: Equibiaxial stress-strain relationship established by Billiar and Sacks (2000); green curve: equibiaxial stress-strain relationship enforced in the leaflets parts in LS-Dyna; black markers: stress values for element 590 (belly region); red markers: element 466 (attachment).

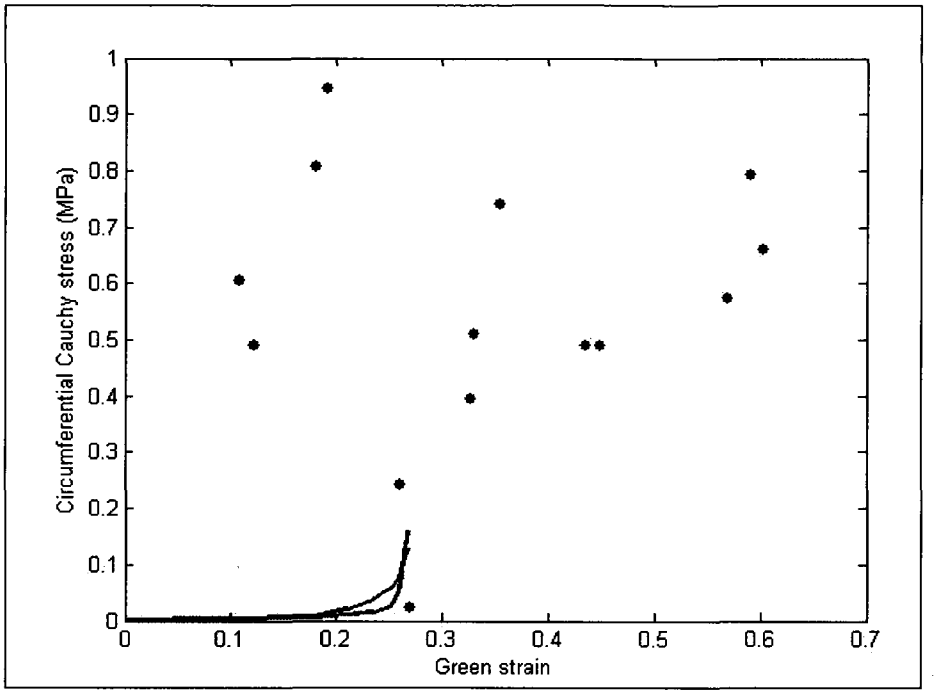

Figure 40 - Cauchy stress vs. Green strain in the circumferential direction. Same colour convention for the markers as in Fig. 39.

In the circumferential direction (Fig. 40), the strain values are well out of the normal range seen in most studies. The elements along the commissural attachment experienced abnormal amounts of strain only in the circumferential direction.

The specific material model used was optimized according to an equibiaxial test. The stress-strain curves found for the equibiaxial test were compared to a simulated uniaxial test in the circumferential direction for the same leaflet sample in LS-Dyna. It was found that the sample is much more compliant in a uniaxial test as seen in Fig. 41. This indicates that the material model used cannot completely describe the leaflet behaviour. The material model properly replicates the leaflet behaviour near biaxial conditions however, fails to adequately reproduce the leaflet behaviour in conditions that are nearly uniaxial. This probably explains the abnormal amount of strain observed in

the leaflet near the commissures where the load was mostly uniaxial (circumferential) in nature.

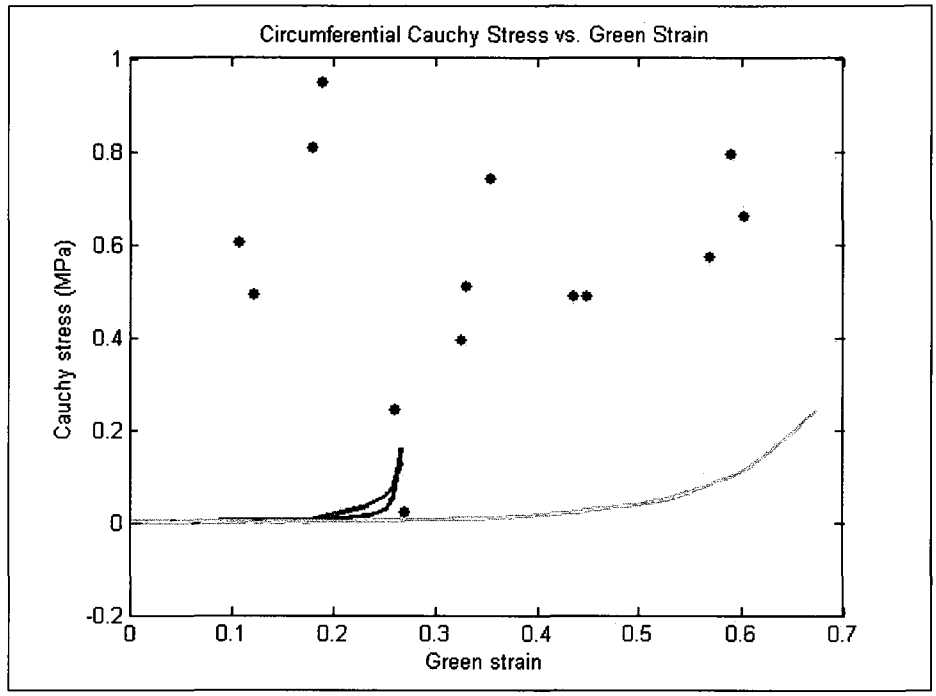

Figure 41 – Cauchy stress vs Green strains in the circumferential direction including a uniaxial loading of a leaflet sample in LS-Dyna (orange).

There may also have been some contributing factors to the elevated stress levels. The experiment from which the material properties were obtained was a biaxial mechanical test with no bending. Bending was not included in the test due to the added complexity it would have posed in the experiment. In the simulation of the entire valve however, the elements in the leaflet experienced bending stresses which contributed to the overall magnitude of stresses. Additionally, according to the Laplace Law $\left(\sigma = \frac{PR}{t}\right)$ decreasing the thickness (t) of the leaflet wall increases the amount of circumferential stress considerably. The initial thickness of the leaflet was 0.5 mm. At element 590 the

leaflet thickness became 0.16 mm, which dramatically increased stress. This change in thickness also indicated that the elements have flattened out, increasing the strain in the radial and circumferential directions. Overall, it was verified that the numerical simulation was able to maintain local mechanical equilibrium even though the material response was not entirely expected in the circumferential direction of the leaflet. In other words, the numerical results for stress are not believed to occur out of numerical problem or instability, but as a limitation of the material model itself.

The main objectives of this study were to construct a numerical model of the aortic valve, and simulate the dynamics and stress and strain distributions occurring in the valve through the length of a cardiac cycle. The dynamic motion was captured and the stress distributions were obtained. One major issue for the present study was validation of the accuracy of the model, because very few precedents have been set in this area of research. The dynamics of the valve was validated by qualitatively comparing the sinus and leaflet shapes of the valve to *in vitro* simulations, as well as quantitatively measuring the GOA of the simulation and experimental aortic root. The accuracy of material modeling was also validated by showing that the stress and strain values obtained were consistent with those used initially to calculate the material constants. These facts all indicate that the model of the aortic valve is reasonably accurate.

7.2 Improvements, Modifications and Possible Future Studies

Now that the original objectives of the thesis have been met, there are many new studies that can be undertaken. A number of modifications could be done to study various situations or to improve the performance and accuracy of the model.

Guccione's material model was chosen because it was the only strain energy density function available for use in LS-Dyna. The usability of this material model was affected by the limitations of the software. For example, for the leaflets, the first optimized material constant calculated would have been less than 0.001 MPa. However, this was the smallest valve usable in LS-Dyna and therefore the first constant had to be greater than this value, potentially affecting the accuracy of the resulting stress-strain behaviour.

Also, the inadequacy of the material model is an issue yet to be explored. Currently, no other hyperelastic strain energy models are available when modeling non-linear dynamics in a large range of motion. Improving the versatility of the material model to be able to replicate conditions that are closer to both equibiaxial and uniaxial would be a major improvement.

The high levels of stress could also be alleviated by artificially increasing the thickness of the leaflet, assuming other dynamic characteristics of the valve would not be affected by this change. Also, similar material properties as in the circumferential direction were assumed through the thickness of the leaflet and aortic wall (transverse isotropicity). This was done because it was not possible to obtain data for the material properties through the thickness of the valve, experimentally or from the literature. In future modeling, the fully three-dimensional anisotropic response of the tissues could be incorporated for a more accurate result. This may also help improve the large amounts of strain experienced in the leaflet. Having a stiffer thickness would reduce the amount of strain experienced in the radial and circumferential directions.

The ability to precisely measure dimensions in the valve is also much needed. Swanson and Clark (1974) were able to measure dimensions inside the valve with precision tools that are not commonly and readily available. Developing methods of measurement that are accurate, precise and widely available would benefit studies such as this in many ways. Measuring leaflet dimensions seems to be problematic at lower pressures because it is difficult to inject moulds and obtain a favourable product because of the small amount of pressure applied to the valve. Improving capabilities to measure valve dimensions at lower pressures or zero pressure would enhance the accuracy of the model in the stress-free state.

The aortic valve model developed herein clearly demonstrated that dry-models are adequate to analyze valve dynamics and stress distributions. Although some authors prefer FSI models, none have been successful so far in developing one that properly models the response of the aortic root (De Hart et al. 2003; Nicosia et al. 2003; Ranga et al. 2004). These authors argue that fluid-structure interactions should be included because only then would one be able to obtain a clear idea of the shear stresses present along the surfaces in the valve. However, the normal stress values resulting from physiologic loading turn out to be about five orders of magnitude larger than shear stresses (Humphrey, 2002, pg. 533), demonstrating that in fact, shear stresses are negligible from a structural point of view. It remains that the cells lining the surface of the aortic valve are highly sensitive to shear stresses and may induce remodelling of the aortic valve tissues if excessive values are reached (Vesely and Boughner, 1989).

Some authors also argue that the opening and closing motions of the valve are a result of the fluid dynamics in the valve. For example, Ranga et al. (2004) state that the

closing of the leaflet is a result of the fluid vortex produced in the sinus from the flow curling back off the leaflet free-edge. While there may be dynamic pressure exerted on the leaflets by the velocity of the fluid flow, it is likely to be insignificant compared to the difference in total pressure between the aorta and left ventricle. The dry model produced in the present work was able to provide a sound understanding of the distribution of stress in the aortic valve without including fluid structure interactions, clearly demonstrating that an FSI model is not required to study principal stresses and the dynamic motion of the aortic valve.

While an FSI model was not necessary for the original objectives of the thesis, the current model may be extended to include fluid-structure interactions if an analysis of shear is required or other dynamic events would need to be explored, such as fluid velocity profiles through the valve and the coronary arteries, or sinus vortices and eddies from the leaflet free-edge.

The assumption of symmetry was adequate to represent the workings of the entire valve. However, it would be interesting to observe the changes in simulated results that would occur without symmetry, i.e. if an entire valve were to be created with unequal dimensions for each third. Adding to asymmetry, the coronary ostia may also be included to observe what effects their presence has on the distribution of stress in the sinus walls.

There are many avenues opened by the present study that would be of interests to physicians and surgeons. The aortic valve model presented can be modified to replicate situations a surgeon would typically come across. One such case of particular interest is aortic valve stenosis (AS). This occurs when the leaflets of the aortic valve thicken and the orifice presented by the valve from the left ventricle to the aorta is narrower. The

most common type of AS is calcific where the leaflets thicken from calcium depositing in the leaflets thereby stiffening and swelling them. A stenotic aortic valve leads to problems within the myocardium, as it must work harder to push the same amount of blood through the valve and aorta. This type of stenosis can be replicated in the model by increasing the thickness or additionally stiffening the leaflet material properties appropriately. Properties of a calcific leaflet will need to be characterized as well. To some extent the calcifications can also be localized because the valve model is divided into 13 parts, and calcification could also be defined at the element level. The simulation of calcifications may reveal some insight into the dynamics of stenotic valves and how to possibly treat them while leaving most of the original tissue in place, for the benefit of the patient.

Simulating a malfunctioning valve may also reveal further pathologies to be considered. For example, abnormally high amounts of stress carried by the leaflet can lead to a tear at the commissural attachment or in the belly. Perhaps loading a valve with extreme pressures could indicate where such tears may occur. Sutures to repair the tear could be included in the model using two-dimensional elements. The type and placement of the sutures would change the stress distribution in the region of the sutures. This may help provide some guidelines for where sutures could be placed to alleviate the amount of stress carried by the leaflet or even how many sutures are necessary (Avanzini, 2008; Dal Pan et al. 2005).

In some cases, surgeons may want to perform repairs and reconstructions on valve leaflets. This is a very difficult procedure and very few surgeons attempt it since a slight inconsistency in repair could have major repercussions due to the close relationship

between the aortic valve's geometry and function (Labrosse et al., 2006). Some repairs to alter valve geometries could be simulated prior to surgical repairs to gather some foresight into the result of the final product. A surgeon would then be able to know well before hand the effect on function of altering basic valve dimensions. For example, with a "leaky" valve, would the valve close completely if the aortic diameter was reduced by 4 mm or is any change in the leaflet dimensions necessary for the valve to be competent? Currently, many such questions remain unanswered until during the procedure and it would be advantageous to have some basic foresight prior to the procedure.

This study was undertaken primarily to provide a numerical model to study the effects and correlations between stress distribution and aortic valve pathologies. It is evident that there is much knowledge to be gained from this study in the future. Not only has it demonstrated the challenges associated with modeling such a complex structure, but displayed that the relationships between geometry, function, and load bearing capabilities in the aortic valve are very complex and cannot easily be isolated. This will take considerable efforts, but will undoubtedly be valuable and significantly contribute to advanced knowledge about the aortic valve. With this knowledge, the ability to understand the development and progression of disease and problematic function will improve, and from there it will be possible to gain a better perspective of how to deal with such cases and hopefully serve those in need of aid.

REERENCES

Avanzini, A., *A computational procedure for prediction of structural effects of edge-to-edge repair on mitral valve.* Journal of Biomechanical Engineering, 130 (3): 031015.

Beck, A., Thubrikar, M.J., Robicsek F., *Stress analysis of the aortic valve with and without the sinuses of Valsalva.* Journal of Heart Valve Disease, 2001, 10(1): 1 – 11.

Billiar, K., Sacks, M., *Biaxial Mechanical Properties of the Natural and Glutaraldehyde Treated Aortic Valve Cusp – Part I: Experimental Results*, Journal of Biomechanical Engineering, 2000, 122 (1): 23 – 30.

Billiar, K., Sacks, M., *Biaxial Mechanical Properties of the Natural and Glutaraldehyde Treated Aortic Valve Cusp – Part II: Experimental Results*, Journal of Biomechanical Engineering, 2000, 122 (4): 327 – 335.

Burriesci, G., Howard, I., Patterson, E., *Influence of anisotropy on the mechanical behaviour of bioprosthetic heart valves*, Journal of Medical Engineering & Technology, 1999, 23 (6): 203 – 215.

Cacciola, G., *Design, Simulation and manufacturing of fiber reinforced polymer heat valves*, Ph.D. Thesis, Eindhoven University of Technology, Eindhoven, 1998.

Cacciola, G., Peters, G.W.M., Schreurs, P.J.G., *A three-dimensional mechanical analysis of a stentless fibre-reinforced aortic valve prosthesis*, Journal of Biomechanics, 2000, 33 (5): 521 – 530.

Carmody, C., Burriesci, G., Howard, I., Patterson, E., *An approach to the simulation of fluid-structure interaction in the aortic valve*, Journal of Biomechanics, 2006, 39 (1): 158 – 169.

Cheitlin, M.D., Sokolow, M., McIlroy, M.B., *Clinical Cardiology, 6th Edition*, Appleton and Lange, Norwalk, Connecticut, USA, 1993, pg: 18.

Chew, G., Howard, I., Paterson, E., *Non-linear Finite Element Modelling of Porcine Bioprosthetic Valves*, Engineering Failure Analysis, 1994, 1 (3): 231 – 242.

Chew, G., Howard, I., Paterson, E., *Simulation of damage in a porcine prosthetic heart valve*, Journal of Medical Engineering & Technology, 1999, 23 (5): 178 – 189.

Dal Pan, F., Donzella, G., Fucci, C., Schreiber, M., *Structural effects of an innovative surgical technique to repair heart valve defects*, Journal of Biomechanics, 2005, 38 (12): 2460 – 2471.

De Hart, J., Peters, G.W.M., Schreurs, P., Baaijens, F., *A two-dimensional fluid-structure interaction model of the aortic valve*, Journal of Biomechanics, 2000, 33 (9): 1079 – 1088.

De Hart, J., Peters, G.W.M., Schreurs, P., Baaijens, F., *A three-dimensional computational analysis of fluid-structure interaction in the aortic valve*, Journal of Biomechanics, 2003, 36: 103 – 112.

De Hart, J., Peters, G.W.M., Schreurs, P., Baaijens, F., *A computational fluid-structure interaction analysis of a fiber-reinforced stentless aortic valve*, Journal of Biomechanics, 2003, 36: 699 – 712.

Dobrin, P.B., *Handbook of Physiology: Vascular Mechanics (Peripheral Circulation and Organ Blood Flow).* Williams and Wilkins, 1983.

Einstein, D., Reinhall, P., Nicosia, M., Cochran, R., Kunzelman, K., *Dynamic Finite Element Implementation of Nonlinear Anisotropic Hyperelastic Biological Membranes*, Computer Methods in Biomechanics and Biomedical Engineering, 2002, 6(1): 33 – 44.

Ethier, C. R., Simmons, C. A., *Introductory Biomechanics*, Cambridge University Press, Cambridge, UK, 2007, pg: 421.

Ferraresi, C., Bertetto, A., Mazza, L., Maffiodo, D., Franco, W., *One-dimensional experimental mechanical characterisation of porcine aortic root wall*, Medical & Biological Engineering & Computing, 1999, 37: 202 – 207.

Fung, Y.C., *Biodynamics: Circulation.* Springer Verlag, New York, 1984.

Garcia, D., Kadem, L., *What do You mean by Aortic Valve Area: Geometric Orrifice Area, Effective Orifice Area, or Gorlin Area?* Journal of Heart Valve Disease, 2006, 15: 601 – 608.

Grande, K., Cochran, R., Reinhall, P., Kunzelman, K., *Stress Variations in the Human Aortic Root and Valve: The Role of Anatomic Asymmetry*, Annals of Biomedical Engineering, 1998, 26: 534 – 545.

Grande, K., Cochran, R., Reinhall, P., Kunzelman, K., *Mechanisms of Aortic Valve Incompetence Finite Element Modeling of Aortic Root Dilation*, Annals of Biomedical Engineering, 2000, 69 (6): 1851 – 1857.

Guccione, J.M., McCulloh, A.D., Waldman L.K., *Passive material properties of intact ventricular myocardium determined from a cylindrical model.* Journal of Biomechanical Engineering, 1991, 113 (1): 42 – 55.

Han, H-C., Fung, Y-C., *Longitudinal Strain of Canine and Porcine Aortas*, Journal of Biomechanics, 1994, 28 (5): 637 – 641.

Howard, I., Patterson, E., Yoxall, A., *On the opening mechanism of the aortic valve: some observations from simulations*, Journal of Medical Engineering & Technology, 2003, 27 (6) 259 – 266.

Huang, X., Black, M. Howard, I., Patterson, E., *A two-dimensional finite element analysis of a bioprosthetic heart valve,* Journal of Biomechanics, 1990, 23 (8): 753 – 762.

Humphrey, J.D., *Cardiovascular Solid Mechanics: Cells, Tissues and Organs.* Springer Verlag, New York, 2002.

Kunzelman, K. S., Grande, K. J., David, T.E., Cochran, R. P., Verrier, E. D., *Aortic root and valve relationships. Impact on surgical repair.* Journal of Thoracic and Cardiovascular Surgery, 1994, 107 (1): 162 – 170.

Labrosse, M., Beller, C. J., Mesana, T., Veinot, J. P., *Mechanical behavior of human aortas : Experiments, material constants and 3 – D finite element modeling including residual stress*, Journal of Biomechanics, 2009, 42 (8): 996 – 1004.

Labrosse, M. R., Beller, C., Robicsek, F., Thubrikar M., *Geometric modeling of functional trileaflet aortic valves: Development and clinical applications*, Journal of Biomechanics, 2006, 39: 2665 – 2672.

Lzeik, M., *Undergraduate Thesis: Left-Heart Simulator and Patient-Prosthesis Mismatch.* University of Ottawa, Department of Mechanical Engineering, 2007.

McDonald, D.A., *Blood Flow in Arteries, 2nd Ed.* Williams and Wilkins, Baltimore, 1974.

Mercer, J., Benedicty, M., Bahnson, H.T., *The geometry and construction of the aortic leaflet.* Journal of Thoracic and Cardiovascular Surgery, 1973, 65 (4): 511 – 518.

Merryman, W., Huang H-Y., Schoen, F., Sacks, M., *The effects of cellular contraction on aortic valve leaflet flexural stiffness*, Journal of Biomechanics, 2006, 39: 88 – 96.

Mirnafaji, A., Raymer, J., McClure, L., Sacks, M., *The flexural rigidity of the aortic valve leaflet in the commissural region.* Journal of Biomechanics, 2006, 39 (16): 2966 – 2973.

Mitimo, Y., Nakao, K., Angrist, A., *The fine structure of the heart valves in the chicken*, American Journal of Anatomy, 1969, 125 (2): 147 – 167.

Mori, Y., Bashey, R.I., Angrist, A., *The in vivo biosynthesis of collagen of bovine heart valves*, 1967, 1 (3): 295 – 304.

Nicosia, M., Cochran, R., Einstein D., Rutland, C., Kunzelman, K., *A Coupled Fluid-Structure Finite Element Model of the Aortic Valve and Root*, Journal of Heart Valve Disease, 2003, 12: 781 – 789.

Patel, D. J., Fry, D. L., *Longitudinal Tethering of Arteries in Dogs.* Circulation Research, 1966, 19 (6): 1011 – 1021.

Peskin, C. S., McQueen, D. M., *A general method for the computer simulation of biological systems interacting with fluids*, Symposia of the Society for Experimental Biology, 1995, 49: 265 – 276.

Ranga, A., Mongrain, R., Mendes Galaz, R., Biadillah, Y., Cartier, R., *Large-displacement 3D structural analysis of an aortic valve model with nonlinear material properties*, Journal of Medical Engineering & Technology, 2004, 28 (3): 95 – 103.

Shoen, F. J., Levy, R.J., *Calcification of tissue heart valve substitutes: progress towards understanding and prevention*, Annals of Thoracic Surgery, 2005, 79 (3): 1072 – 1080.

Stella, J., Sacks, M., *On the Biaxial Mechanical Properties of the Layers of the Aortic valve Leaflet,* Journal of Biomechanical Engineering, 2007, 129 (5): 757 – 766.

Swanson, W., Clark, R., *Dimensions and Geometric Relationships of the Human Aortic Valve as a Function of Pressure*, Circulation Research, 1974, 35 (6): 871 – 882.

Takamizawa, K., and Hayashi, K. *Strain energy density function and uniform strain hypothesis for arterial mechanics.* Journal of Biomechanics, 1987, 20 (1): 7 – 17.

Thornton, M. A., Howard, I. C., Patterson, E. A., *Three dimensional stress analysis of polypropylene leaflets for prosthetic heart valves*, Medical Engineering and Physics, 1997, 19 (6): 588 – 597.

Thubrikar, M.J., *The Aortic Valve,* CRC Press Inc., Boca Raton, Florida, 1990.

Thubrikar, M.J., Gong, G., Konstantinov, I., Selim, G., Fowler, B., Robicsek, F., *Influence of sizing and subcoronary implantation technique on the function of porcine aortic homografts*, Journal of Medical Engineering & Technology, 2000, 24 (4): 173 – 180.

Thubrikar, M.J., Gong, G., Fowler, B., Robicsek, F., *A New Aortic Root Prosthesis With Compliant Sinuses for Valve-Sparing Operations*, The Society of Thoracic Surgeons, 2001, 71 (5): S318 – S322.

Tong, P., Fung, Y.C., *Classical and Computational Solid Mechanics.* World Scientific Publishing, 2001.

Trowbridge, E. A., Black, M. M., Daniel, C. L., *The mechanical response of glutaraldehyde-fixed bovine pericardium to uniaxial load.* Journal of Material Science, 1985, 20 (1): 114 – 140.

Vesely, I., Boughner, D., *Analysis of the bending behaviour of the porcine xenograft leaflets and of natural aortic valve material: bending stiffness, neutral axis and shear measurements.* Journal of Biomechanics, 1989, 22 (6 – 7): 655 – 671.

Vesely, I., Noseworthy, R., *Micromechanics of the Fibrosa and the Ventricularis in Aortic Valve Leaflets.* Journal of Biomechanics, 1992, 25 (1): 101 – 113.

APPENDIX A – ANSYS 11.0 Input

The input commands in ANSYS 11.0 to construct the three-dimensional finite element model of the aortic valve, with controlled meshing and constitutive node reordering are presented in this appendix.

```
! See characteristics below and in "datansys.txt"
/prep7
/graphics,power

! Defining the attributes

layer_inleaf = 1
layer_outleaf = 1
layer_insinus = 1
layer_outsinus = 1

stop = 0


et,1,solid45
et,3,conta173
real,2
et,2,shell63

/pnum,kp,1
/pnum,line,1
/pnum,area,1

tleaf=0.5       ! leaflet thickness
tao=3.4                 ! aortic thickness
t1=0.5*sqrt(tao)

ratio=0.65

nc=3
nc1=5+nc
nc2=6+nc
nl1=6+nc
nl2=6+nc
nl3=4+nc
nr1=2       !elements across leaflet
nr2=3       !elements across sinus wall

depth=-4
```

```
/input,datansys_swan,txt
pi=4.*atan(1.)
beta=beta*pi/180.
omega=atan((lw*cos(beta)-h)/(rb+lw*sin(beta)-0.5*rc))
xb=(lw*cos(beta)-h)/sin(omega)
xa=(3*rc**2/4-xb**2)/(2*xb)
r1=xa+xb
*if,cone,eq,0,then
dist=rc
*endif
*if,cone,eq,1,then
dist=rb+(rc-rb)*(1.-hhs/h)
*endif

*if,layer_inleaf,eq,1,then

!                    Inner layer: leaflet and LV tract only

! Defining the geometry
csys,1
k,1,0,0,-10
k,2,0,0,2.*h
k,3,rb,-60,-0.25
k,4,dist,-60,h-hhs-0.25
lstr,3,4
! basic valve cone
arotat,1,,,,,,1,2,60,1

! plane where the attachment line lies
csys,0
k,7,rb,-1.2*max(rb,rc),-0.25
k,8,rb,0,-0.25
k,9,0.5*dist,-1.2*max(rb,rc),h-hhs-0.25
k,10,0.5*dist,0,h-hhs-0.25
a,7,8,10,9


! defining line of attachment
asba,1,2
adele,4,,,1

! defining the commissures
csys,1
k,12,rc,-60,h
lstr,4,12
```

```
! defining the free edge
csys,0
k,13,rb+lw*sin(beta),0,lw*cos(beta)
lstr,5,13
csys,1
k,14,rc,60,h
larc,12,13,14,r1

! creating the open leaflet surface
al,2,5,4,9



! reshaping the LV outflow tract

adele,3
ldele,3
csys,1
k,15,0,0,depth
k,16,rb,-60,depth
k,17,rb,0,depth
larc,16,17,15,rb
lstr,5,17
lstr,3,16
lcomb,1,7          !lcomb cannot be removed because the area cannot be created without it
ln1=_return
al,ln1,3,6,9

! cut along the attachment line
ldiv,9,ratio,,,keep
! cut along leaflet height
ldiv,4,1-distkp(12,4)/distkp(13,5),,,keep
larea,4,6,1
ldiv,10,0.5,,,keep
ldiv,4,0.45,,,keep       ! lower vertical part of leaflet
larea,7,5,1
ldiv,13,0.5,,,keep
ldele,14
larea,3,9,1
larea,9,8,1
ldiv,5,0.5,,,keep
larea,10,7,1
lsel,s,line,,10,11,1
lsel,a,line,,13,15,1
lsel,a,line,,17
btol,0.001
```

```
asbl,1,all,,,keep
allsel
*get,nl,line,0,count
*if,nl,eq,19,then
lsel,s,line,,18,19,1
asll,s,0
adele,all
ldele,18
ldele,19
allsel
al,13,10,9,14
al,11,13,15,12
al,15,14,7,4
*endif

ldiv,3,0.5,,,keep
larea,11,3,2
btol,0.1
asbl,2,19

numcmp,all

csys,1

*get,nl,line,0,count

*if,nl,eq,24,then
lsel,s,line,,17,24,1
asll,s,0
adele,all
ldele,19,23,3
lcomb,18,23
lcomb,17,20
lcomb,24,21
allsel
al,18,2,17,7
al,17,16,21,5
*endif

numcmp,all
btol,defa

ksel,s,kp,,11,17,6
lslk,s,1
lesize,all,,,nc1
ksel,s,kp,,3,5,2
```

```
lslk,s,1
lesize,all,,,nc1
ksel,s,kp,,8,9,1
lslk,s,1
lesize,all,,,nc1
ksel,s,kp,,6,7,1
lslk,s,1
lesize,all,,,nc1
ksel,s,kp,,10,13,3
lslk,s,1
lesize,all,,,nc1

ksel,s,kp,,10,12,2
lslk,s,1
lesize,all,,,nc1
ksel,s,kp,,4,7,3
lslk,s,1
lesize,all,,,nc1
ksel,s,kp,,3,9,6
lslk,s,1
lesize,all,,,nc1
ksel,s,kp,,5,8,3
lslk,s,1
lesize,all,,,nc1

ksel,s,kp,,4,12,8
lslk,s,1
lesize,all,,,nl1
ksel,s,kp,,7,10,3
lslk,s,1
lesize,all,,,nl1
ksel,s,kp,,6,13,7
lslk,s,1
lesize,all,,,nl1

ksel,s,kp,,16
ksel,a,kp,,11
lslk,s,1
lesize,all,,,nc2
ksel,s,kp,,4
ksel,a,kp,,3
lslk,s,1
lesize,all,,,nc2
ksel,s,kp,,7,9,2
lslk,s,1
lesize,all,,,nc2
```

```
ksel,s,kp,,6,8,2
lslk,s,1
lesize,all,,,nc2

ksel,s,kp,,4,16,12
lslk,s,1
lesize,all,,,nl2
ksel,s,kp,,3,11,8
lslk,s,1
lesize,all,,,nl2
ksel,s,kp,,5,17,12
lslk,s,1
lesize,all,,,nl2

anorm,1
type,2
amesh,all
allsel

numoff,kp,100
numoff,line,100
numoff,area,100
numoff,volu,100
numoff,node,1000
numoff,elem,1000

!                    the inner leaflet is done at this point

*endif

*if,layer_outleaf,eq,1,then

!                    Second layer: outer leaflet, middle LV tract

! Defining the geometry
csys,1
k,1,0,0,-10
k,2,0,0,2.*h
k,3,rb+tleaf,-60,0
*if,cone,eq,0,then
dist=rc+tleaf
*endif
*if,cone,eq,1,then
dist=rb+tleaf+(rc-rb)*(1.-hhs/h)
*endif
k,4,dist,-60,h-hhs
```

```
lstr,3,4
! basic valve cone
arotat,1,,,,,,1,2,60,1
! plane where the attachment line lies
csys,0
k,7,rb+tleaf,-1.2*max(rb+tleaf,rc+tleaf),0
k,8,rb+tleaf,0,0
k,9,0.5*dist,-1.2*max(rb+tleaf,rc+tleaf),h-hhs
k,10,0.5*dist,0,h-hhs
a,7,8,10,9
! defining line of attachment
asba,1,2
adele,4,,,1
! defining the commissures
csys,1
k,12,rc+tleaf,-60,h
lstr,4,12
! defining the free edge
csys,0
k,13,rb+tleaf+lw*sin(beta),0,lw*cos(beta)
lstr,5,13
csys,1
k,14,rc+tleaf,60,h
r2=r1+tleaf
larc,12,13,14,r2
! creating the open leaflet surface
al,2,5,4,9

! reshaping the LV outflow tract

adele,3
ldele,3
csys,1
k,15,0,0,depth
k,16,rb+tleaf,-60,depth
k,17,rb+tleaf,0,depth
larc,16,17,15,rb+tleaf
lstr,5,17
lstr,3,16
lcomb,1,7
al,1,3,6,9
! cut along the attachment line
ldiv,9,ratio,,,keep
! cut along leaflet height
ldiv,4,1-distkp(12,4)/distkp(13,5),,,keep
larea,4,6,1
```

```
ldiv,10,0.5,,,keep
ldiv,4,0.45,,,keep        ! lower vertical part of leaflet
larea,7,5,1
ldiv,13,0.5,,,keep
ldele,14
larea,3,9,1
larea,9,8,1
ldiv,5,0.5,,,keep
larea,10,7,1
lsel,s,line,,10,11,1
lsel,a,line,,13,15,1
lsel,a,line,,17
btol,0.001
asbl,1,all,,,keep
allsel

*get,nl,line,0,count
*if,nl,eq,38,then
lsel,s,line,,18,19,1
asll,s,0
adele,all
ldele,18
ldele,19
allsel
al,13,10,9,14
al,11,13,15,12
al,15,14,7,4
*endif

ldiv,3,0.5,,,keep
larea,11,3,2
btol,0.1
asbl,2,19

numcmp,kp
numcmp,line

csys,1

*get,nl,line,0,count
*if,nl,eq,43,then
lsel,s,line,,17,24,1
asll,s,0
adele,all
ldele,19,23,3
lcomb,18,23
```

```
lcomb,17,20
lcomb,24,21
allsel
al,18,2,17,7
al,17,16,21,5
*endif

numcmp,kp
btol,defa

v,20,21,33,28,3,4,16,11
v,22,20,28,34,5,3,11,17
v,24,21,20,26,7,4,3,9
v,25,26,20,22,8,9,3,5
v,23,24,26,25,6,7,9,8
v,27,29,21,24,10,12,4,7
v,30,27,24,23,13,10,7,6

ksel,s,kp,,3,20,17
lslk,s,1
lesize,all,,,nr1
ksel,s,kp,,4,21,17
lslk,s,1
lesize,all,,,nr1
ksel,s,kp,,5,22,17
lslk,s,1
lesize,all,,,nr1
ksel,s,kp,,6,23,17
lslk,s,1
lesize,all,,,nr1
ksel,s,kp,,7,24,17
lslk,s,1
lesize,all,,,nr1
ksel,s,kp,,8,25,17
lslk,s,1
lesize,all,,,nr1
ksel,s,kp,,9,26,17
lslk,s,1
lesize,all,,,nr1
ksel,s,kp,,10,27,17
lslk,s,1
lesize,all,,,nr1
ksel,s,kp,,11,28,17
lslk,s,1
lesize,all,,,nr1
ksel,s,kp,,12,29,17
```

```
lslk,s,1
lesize,all,,,nr1
ksel,s,kp,,13,30,17
lslk,s,1
lesize,all,,,nr1
ksel,s,kp,,16,33,17
lslk,s,1
lesize,all,,,nr1
ksel,s,kp,,17,34,17
lslk,s,1
lesize,all,,,nr1

*do,i,1,7
mat,i
type,1
vmesh,i
aclear,100+i
*enddo

allsel
numcmp,all

numoff,kp,100
numoff,line,100
numoff,area,100
numoff,volu,100
numoff,node,2000
numoff,elem,2000

!                    The outer leaflet is done at this point

*endif

*if,layer_insinus,eq,1,then

!                          Third layer: inner sinus and aorta

! Defining the geometry
csys,1
k,1,0,0,-10
k,2,0,0,2.*h
k,3,rb+tleaf,-60,0
*if,cone,eq,0,then
dist=rc+tleaf
*endif
*if,cone,eq,1,then
```

```
dist=rb+tleaf+(rc-rb)*(1.-hhs/h)
*endif
k,4,dist,-60,h-hhs
lstr,3,4
! basic valve cone
arotat,1,,,,,,1,2,60,1
! plane where the attachment line lies
csys,0
k,7,rb+tleaf,-1.2*max(rb+tleaf,rc+tleaf),0
k,8,rb+tleaf,0,0
k,9,0.5*dist,-1.2*max(rb+tleaf,rc+tleaf),h-hhs
k,10,0.5*dist,0,h-hhs
a,7,8,10,9
! defining line of attachment
asba,1,2
adele,4,,,1
! defining the commissures
csys,1
k,12,rc+tleaf,-60,h
lstr,4,12

! reshaping the LV outflow tract

adele,3
ldele,3
csys,1
k,15,0,0,depth
k,16,rb+tleaf,-60,depth
k,17,rb+tleaf,0,depth
larc,16,17,15,rb+tleaf
lstr,5,17
lstr,3,16
lcomb,1,5
al,1,3,4,9

! creating the ascending aorta
k,13,rc+tleaf,-60,hs+rc
lstr,12,13
arotat,5,,,,,,1,2,60,1
! creating the sinus-aorta intersection
csys,0
k,32,0.5*(rc+tleaf),0,h
k,33,rc+tleaf,0,hs
k,34,rc+tleaf,-rc-tleaf,hs
a,12,32,33,34
asba,2,3
```

```
adele,4,,,1
! creating the sinus shape
k,35,ds,0,zs
flst,3,3,2
fitem,3,33
fitem,3,35
fitem,3,5
bsplin,,p51x
csys,1
al,2,9,6,15

! modifications to control meshing

! cut along the attachment line
ldiv,9,ratio,,,keep
ldiv,6,0.40,,,keep
larea,3,7,2
ldiv,11,0.40,,,keep
larea,8,12,2
ldel,12
lcomb,6,10,keep
! cut along the sinus
ldiv,6,0.70,,,keep
larea,8,7,2
btol,0.1
lsel,s,line,,11,13,1
asbl,2,all,
allsel
ldiv,3,0.5,,,keep
larea,9,3,1
btol,0.1
asbl,1,17

*get,nl,line,0,count
*if,nl,eq,73,then
!*if,nl,eq,22,then
lsel,s,line,,18,25,1
asll,s,0
adele,all
ldele,20,23,3
lcomb,19,24
lcomb,18,21
lcomb,25,22
allsel
al,9,19,3,18
al,18,14,22,7
```

```
*endif

ksel,s,kp,,9,17,8
lslk,s,1
lesize,all,,,nc1
ksel,s,kp,,3,5,2
lslk,s,1
lesize,all,,,nc1
ksel,s,kp,,7,8,1
lslk,s,1
lesize,all,,,nc1
ksel,s,kp,,12,33,21
lslk,s,1
lesize,all,,,nc1
ksel,s,kp,,6,13,7
lslk,s,1
lesize,all,,,nc1

ksel,s,kp,,9,16,7
lslk,s,1
lesize,all,,,nc2
ksel,s,kp,,3,4,1
lslk,s,1
lesize,all,,,nc2
ksel,s,kp,,8,12,4
lslk,s,1
lesize,all,,,nc2
ksel,s,kp,,7,33,26
lslk,s,1
lesize,all,,,nc2

ksel,s,kp,,12,13,1
lslk,s,1
lesize,all,,,nl3
ksel,s,kp,,6,33,27
lslk,s,1
lesize,all,,,nl3

ksel,s,kp,,4,16,12
lslk,s,1
lesize,all,,,nl2
ksel,s,kp,,3,9,6
lslk,s,1
lesize,all,,,nl2
ksel,s,kp,,5,17,12
lslk,s,1
```

```
lesize,all,,,nl2

ksel,s,kp,,4,12,8
lslk,s,1
lesize,all,,,nl1
ksel,s,kp,,3,8,5
lslk,s,1
lesize,all,,,nl1
ksel,s,kp,,5,7,2
lslk,s,1
lesize,all,,,nl1

numcmp,area
*do,i,1,6
type,2
amesh,i
*enddo
allsel

numcmp,all

numoff,kp,200
numoff,line,200
numoff,area,200
numoff,volu,200
numoff,node,4000
numoff,elem,4000

!                    The inner sinus is complete at this point

*endif



*if,layer_outsinus,eq,1,then

!                              Fourth layer: outer sinus and aorta

! Defining the geometry
csys,1
k,1,0,0,-10
k,2,0,0,2.*h
k,3,rb+tleaf+tao,-60,-tao
*if,cone,eq,0,then
dist=rc+tleaf+tao
*endif
```

```
*if,cone,eq,1,then
dist=rb+tleaf+tao+(rc-rb)*(1.-hhs/h)
*endif
k,4,dist,-60,h-hhs-t1
lstr,3,4
! basic valve cone
arotat,1,,,,,,1,2,60,1
! plane where the attachment line lies
csys,0
k,7,rb+tleaf+tao,-1.2*max(rb+tleaf+tao,rc+tleaf+tao),-tao
k,8,rb+tleaf+tao,0,-tao
k,9,0.5*dist,-1.2*max(rb+tleaf+tao,rc+tleaf+tao),h-hhs-t1
k,10,0.5*dist,0,h-hhs-t1
a,7,8,10,9
! defining line of attachment
asba,1,2
adele,4,,,1
! defining the commissures
csys,1
k,12,rc+tleaf+tao,-60,h+t1
lstr,4,12

! reshaping the LV outflow tract

adele,3
ldele,3
csys,1
k,15,0,0,depth
k,16,rb+tleaf+tao,-60,depth
k,17,rb+tleaf+tao,0,depth
larc,16,17,15,rb+tleaf+tao
lstr,5,17
lstr,3,16
lcomb,1,5
al,1,3,4,9

! creating the ascending aorta
k,13,rc+tleaf+tao,-60,hs+rc
lstr,12,13
arotat,5,,,,,,1,2,60,1
! creating the sinus-aorta intersection
csys,0
k,32,0.5*(rc+tleaf+tao),0,h+tao
k,33,rc+tleaf+tao,0,hs+t1
k,34,rc+tleaf+tao,-rc-tleaf-tao,hs+t1
a,12,32,33,34
```

```
asba,2,3
adele,4,,,1

! creating the sinus shape
k,35,ds+tao,0,zs-t1
flst,3,3,2
fitem,3,33
fitem,3,35
fitem,3,5
bsplin,,p51x
csys,1
al,2,9,6,15

! modifications to control meshing

! cut along the attachment line
ldiv,9,ratio,,,keep
ldiv,6,0.40,,,keep
larea,3,7,2
ldiv,11,0.40,,,keep
larea,8,12,2
ldel,12
lcomb,6,10,keep
! cut along the sinus
ldiv,6,0.70,,,keep
larea,8,7,2
btol,0.1
lsel,s,line,,11,13,1
asbl,2,all,
allsel
ldiv,3,0.5,,,keep
larea,9,3,1
btol,0.1
asbl,1,17

*get,nl,line,0,count
*if,nl,eq,90,then
!*if,nl,eq,39,then
lsel,s,line,,18,25,1
asll,s,0
adele,all
ldele,20,23,3
lcomb,19,24
lcomb,18,21
lcomb,25,22
allsel
```

```
al,9,19,3,18
al,18,14,22,7
*endif

numcmp,kp
btol,defa


v,19,20,29,25,3,4,13,9
v,21,19,25,30,5,3,9,14
v,24,26,20,19,8,10,4,3
v,23,24,19,21,7,8,3,5
v,31,26,24,23,15,10,8,7
v,22,27,26,31,6,11,10,15


ksel,s,kp,,3,19,16
lslk,s,1
lesize,all,,,nr2
ksel,s,kp,,4,20,16
lslk,s,1
lesize,all,,,nr2
ksel,s,kp,,5,21,16
lslk,s,1
lesize,all,,,nr2
ksel,s,kp,,6,22,16
lslk,s,1
lesize,all,,,nr2
ksel,s,kp,,7,23,16
lslk,s,1
lesize,all,,,nr2
ksel,s,kp,,8,24,16
lslk,s,1
lesize,all,,,nr2
ksel,s,kp,,9,25,16
lslk,s,1
lesize,all,,,nr2
ksel,s,kp,,10,26,16
lslk,s,1
lesize,all,,,nr2
ksel,s,kp,,11,27,16
lslk,s,1
lesize,all,,,nr2
ksel,s,kp,,13,29,16
lslk,s,1
lesize,all,,,nr2
```

```
ksel,s,kp,,14,30,16
lslk,s,1
lesize,all,,,nr2
ksel,s,kp,,15,31,16
lslk,s,1
lesize,all,,,nr2

*do,i,1,6
mat,7+i
type,1
vmesh,i
*enddo

*do,i,1,6
aclear,200+i
*enddo
numcmp,all

nummrg,node,0.05      ! to merge 2 layers of LV tract

*get,nelem0,elem,0,count

!                     The outer sinus is complete at this point

*endif




! re-ordering of constitutive nodes of brick elements
! for proper orientation of preferred direction

modmsh,nocheck                ! Do this before B.C. are set
*do,i,1,nelem0
 *get,nmat,elem,i,attr,mat
 *if,nmat,eq,4,then
  i1=nelem(i,1)
  i2=nelem(i,2)
  i3=nelem(i,3)
  i4=nelem(i,4)
  i5=nelem(i,5)
  i6=nelem(i,6)
  i7=nelem(i,7)
```

```
 i8=nelem(i,8)
 mat,4
 type,1
 emodif,i,1,i2,i3,i4,i1,i6,i7,i8,i5
*endif
*if,nmat,eq,5,then
 i1=nelem(i,1)
 i2=nelem(i,2)
 i3=nelem(i,3)
 i4=nelem(i,4)
 i5=nelem(i,5)
 i6=nelem(i,6)
 i7=nelem(i,7)
 i8=nelem(i,8)
 mat,5
 type,1
 emodif,i,1,i4,i1,i2,i3,i8,i5,i6,i7
*endif
*if,nmat,eq,6,then
 i1=nelem(i,1)
 i2=nelem(i,2)
 i3=nelem(i,3)
 i4=nelem(i,4)
 i5=nelem(i,5)
 i6=nelem(i,6)
 i7=nelem(i,7)
 i8=nelem(i,8)
 mat,6
 type,1
 emodif,i,1,i4,i1,i2,i3,i8,i5,i6,i7
*endif
*if,nmat,eq,7,then
 i1=nelem(i,1)
 i2=nelem(i,2)
 i3=nelem(i,3)
 i4=nelem(i,4)
 i5=nelem(i,5)
 i6=nelem(i,6)
 i7=nelem(i,7)
 i8=nelem(i,8)
 mat,7
 type,1
 emodif,i,1,i4,i1,i2,i3,i8,i5,i6,i7
*endif
*if,nmat,eq,8,then
 i1=nelem(i,1)
```

```
i2=nelem(i,2)
i3=nelem(i,3)
i4=nelem(i,4)
i5=nelem(i,5)
i6=nelem(i,6)
i7=nelem(i,7)
i8=nelem(i,8)
mat,8
type,1
emodif,i,1,i4,i1,i2,i3,i8,i5,i6,i7
*endif
*if,nmat,eq,10,then
i1=nelem(i,1)
i2=nelem(i,2)
i3=nelem(i,3)
i4=nelem(i,4)
i5=nelem(i,5)
i6=nelem(i,6)
i7=nelem(i,7)
i8=nelem(i,8)
mat,10
type,1
emodif,i,1,i4,i1,i2,i3,i8,i5,i6,i7
*endif
*if,nmat,eq,11,then
i1=nelem(i,1)
i2=nelem(i,2)
i3=nelem(i,3)
i4=nelem(i,4)
i5=nelem(i,5)
i6=nelem(i,6)
i7=nelem(i,7)
i8=nelem(i,8)
mat,11
type,1
emodif,i,1,i4,i1,i2,i3,i8,i5,i6,i7
*endif
*if,nmat,eq,13,then
i1=nelem(i,1)
i2=nelem(i,2)
i3=nelem(i,3)
i4=nelem(i,4)
i5=nelem(i,5)
i6=nelem(i,6)
i7=nelem(i,7)
i8=nelem(i,8)
```

```
  mat,13
  type,1
  emodif,i,1,i4,i1,i2,i3,i8,i5,i6,i7
 *endif
*enddo

modmsh,check




! boundary conditions and loading
! some B.C. are decoded later by the interface between Ansys and LS-Dyna

! symmetry conditions
csys,0
nsel,s,loc,y,0
d,all,uy,0
*get,dn,node,0,count

csys,1
nsel,s,loc,y,-60
f,all,fx,1
*get,fnode,node,0,count

! restraining the root base
csys,0
nsel,s,loc,z,depth
d,all,all,0
*get,dnode,node,0,count
dnode=6*dnode+dn-(nr1+nr2+1)

! top displacement
csys,0
nsel,s,loc,z,hs+rc
m,all,uz
*get,mnode,node,0,count

! surface elements for sinus and aorta
asel,s,area,,27,30,1
nsla,s,1
type,3
mat,100
```

```
esurf,
*get,nelem1,elem,0,count
nelem1=nelem1-nelem0


! surface elements for aortic side of leaflet
ksel,s,kp,,35,42,1
ksel,a,kp,,44,45,1
lslk,s,1
asll,s,1
nsla,s,1
type,3
mat,100
esurf,
*get,nelem2,elem,0,count
nelem2=nelem2-nelem1-nelem0

! surface elements for ventricular side of leaflet
ksel,s,kp,,52,59,1
ksel,a,kp,,61,62,1
lslk,s,1
asll,s,1
nsla,s,1
type,3
mat,100
esurf,
*get,nelem3,elem,0,count
nelem3=nelem3-nelem2-nelem1-nelem0

! surface elements for LV tract
ksel,s,kp,,52,54,1
ksel,a,kp,,60
ksel,a,kp,,65,66,1
lslk,s,1
asll,s,1
nsla,s,1
type,3
mat,100
esurf,
*get,nelem4,elem,0,count
nelem4=nelem4-nelem3-nelem2-nelem1-nelem0

! target surface
csys,0
k,102,0,0,-5
k,103,0,0,h+15
```

```
k,104,0.5*2.0*max(rb,rc),-0.5*sqrt(3)*2.0*max(rb,rc),-5
k,105,0.5*2.0*max(rb,rc),-0.5*sqrt(3)*2.0*max(rb,rc),h+15
a,102,103,105,104
area=_return
mat,14
type,2
r,2,tleaf
aesize,area,3
amesh,area
*get,nelem5,elem,0,count
nelem5=nelem5-nelem4-nelem3-nelem2-nelem1-nelem0
/eshape,1

allsel
*get,nelem,elem,0,count
*get,nnode,node,0,count

!calculating model height for 20% vertical stretch in Matlab translation
lstr,11,13
ln=_return
*get,length,line,ln,leng

*msg,note,nnode,nelem,dnode,fnode,mnode
There are %I nodes and %I elements in the model, %/&
with dnode=%I, fnode=%I, mnode=%I.

*msg,note,nelem0,nelem1,nelem2,nelem3,nelem4,nelem5
Info: nelem0=%I, nelem1=%I, nelem2=%I, %/&
nelem3=%I, nelem4=%I, nelem5=%I.

*msg,warning
See model parameters in output window

*msg, note, length
model height is %I

*if,stop,eq,1,then
*endif
```

APPENDIX C – Interface Between ANSYS and LS-Dyna performed by MATLAB

```
% This program reads in NLIST.LIS, ELIST.LIS, DLIST.LIS, FLIST.LIS and
% MLIST.LIS from ANSYS and converts the data into an input deck for
% LS-Dyna.
% The program is specifically written for brick elements loaded with
% pressure. Three types of boundary conditions are applied: one through
% DLIST, one through FLIST, and one through MLIST.
clc;
clear;

% Get nelem values from ANSYS
nelem0 = 2312;
nelem1 = 281;
nelem2 = 352;
nelem3 = nelem2;
nelem4 = 153;
nelem5 = 104;

nmax = 4000;        % >= highest node number in model (get from ANSYS)
stop = 0;           %turned on if = 0, loop found at end of program
ramptime = 0.05;     %time taken to load to 80mmHg
stabtime = 0.06;

npart = 14;         % number of parts in LS-Dyna, i.e. materials in
ANSYS
part = cell(1,npart);
part(1) = cellstr('LV1');
part(2) = cellstr('LV2');
part(3) = cellstr('Leaflet1');
part(4) = cellstr('Leaflet2');
part(5) = cellstr('Leaflet3');
part(6) = cellstr('Leaflet4');
part(7) = cellstr('Leaflet5');
part(8) = cellstr('LV3');
part(9) = cellstr('LV4');
part(10) = cellstr('Sinus1');
part(11) = cellstr('Sinus2');
part(12) = cellstr('Sinus3');
part(13) = cellstr('Aorta');
part(14) = cellstr('RigidWall');

% Import all elements and their connectivity tables from ELIST
% Note that shell elements are just used for load segment definition
readfile = 'ELIST.LIS';
fid = fopen(readfile, 'rt');
c = textscan(fid, '%f %f %*f %*f %*f %*f %f %f %f %f %f %f %f %f',
'headerLines', 5,'commentStyle', 'ELEM');
[nel,j] = size(c{1});
nel2 = nelem1+nelem2+nelem3+nelem4+nelem5;        % number of shell
elements (get from ANSYS)
nel1 = nel-nel2;
for i = 1:nel1+nel2
```

```
    if i <= nel1
        e(i) = c{1}(i);
        m(i) = c{2}(i);
        n1(i) = c{3}(i);
        n2(i) = c{4}(i);
        n3(i) = c{5}(i);
        n4(i) = c{6}(i);
        n5(i) = c{7}(i);
        n6(i) = c{8}(i);
        n7(i) = c{9}(i);
        n8(i) = c{10}(i);
    else
        e(i) = c{1}(i);
        m(i) = c{2}(i);
        n1(i) = c{3}(i);
        n2(i) = c{4}(i);
        n3(i) = c{5}(i);
        n4(i) = c{6}(i);
    end
end
fclose(fid);

% Import all nodes and their coordinates from NLIST
readfile = 'NLIST.LIS';
fid = fopen(readfile, 'rt');
c = textscan(fid, '%f %f %f %f', 'headerLines', 5,'commentStyle',
'NODE');
[nnode,j] = size(c{1});
for i = 1:nnode
    n(i) = c{1}(i);
    xn(i) = c{2}(i);
    yn(i) = c{3}(i);
    zn(i) = c{4}(i);
end
fclose(fid);


% Import nodes with prescribed DOFs in DLIST (non-special boundary
conditions)
readfile = 'DLIST.LIS';
fid = fopen(readfile, 'rt');
c = textscan(fid, '%f %s %*f %*f', 'headerLines', 5,'commentStyle',
'NODE');
[dnode,j] = size(c{1});
dn = zeros(1,dnode);
dof = cell(1,dnode);
dofx = zeros(1,nmax);
dofy = zeros(1,nmax);
dofz = zeros(1,nmax);
dofrx = zeros(1,nmax);
dofry = zeros(1,nmax);
dofrz = zeros(1,nmax);
for i = 1:dnode
    dn(i) = c{1}(i);
    dof(i) = c{2}(i);
end
```

```
for i = 1:dnode
   if strcmp(dof(i),'UX') == 1
      dofx(dn(i)) = 1;
   end;
   if strcmp(dof(i),'UY') == 1
      dofy(dn(i)) = 1;
   end;
   if strcmp(dof(i),'UZ') == 1
      dofz(dn(i)) = 1;
   end;
   if strcmp(dof(i),'ROTX') == 1
      dofrx(dn(i)) = 1;
   end;
   if strcmp(dof(i),'ROTY') == 1
      dofry(dn(i)) = 1;
   end;
   if strcmp(dof(i),'ROTZ') == 1
      dofrz(dn(i)) = 1;
   end
end
fclose(fid);

% Import nodes with prescribed DOFs in FLIST
% Symmetry conditions in coaptation plane
readfile = 'FLIST.LIS';
fid = fopen(readfile, 'rt');
c = textscan(fid, '%f %*s %*f %*f', 'headerLines', 5,'commentStyle',
'NODE');
[fnode,j] = size(c{1});
for i = 1:fnode
   dfn(i) = c{1}(i);
end                                %line can be removed
for i = 1:fnode                    %line can be removed
   dofy(dfn(i)) = 1;
   dofrx(dfn(i)) = 1;
   dofrz(dfn(i)) = 1;
end;
fclose(fid);


% Import nodes with prescribed DOFs in MLIST
% Displacement of top nodes
readfile = 'MLIST.LIS';
fid = fopen(readfile, 'rt');
c = textscan(fid, '%f %*s', 'headerLines', 4,'commentStyle', 'NODE');
[mnode,j] = size(c{1});
for i = 1:mnode
   mn(i) = c{1}(i);
end
fclose(fid);


% Ideal pressure curve, 1 cycle
readfile = 'timing.dat';
fid = fopen(readfile, 'rt');
press = textscan(fid, '%f %f %f %f', 'headerlines',1);
```

```
[time_max,j] = size(press{1});
for i = 1:time_max
    time(i) = press{1}(i)/10;
    lvp(i) = press{2}(i)*0.0133/100;
    aop(i) = press{3}(i)*0.0133/100;
end
fclose(fid);

readfile = 'timing.dat';
fid = fopen(readfile, 'rt');
press = textscan(fid, '%f %f %f %f', 'headerlines',1);
[time_max,j] = size(press{1});
for i = 1:time_max
    time(i) = press{1}(i)/10;
    lvp(i) = press{2}(i)*0.0133/100;
    aop(i) = press{3}(i)*0.0133/100;
end
fclose(fid);

savefile = 'BrickValve_LSDynaInput.dyn';
fid = fopen(savefile, 'wt');
user_entry = input('Analysis identifier?:','s');
fprintf(fid, '$ Identifier : %s\n', user_entry);
fprintf(fid, '*KEYWORD\n');
fprintf(fid, '$---+----1----+----2----+----3----+----4----+----5----+--
--6----+----7----+----8\n');
fprintf(fid, '$                    (1) TITLE CARD\n');
fprintf(fid, '$---+----1----+----2----+----3----+----4----+----5----+--
--6----+----7----+----8\n');
fprintf(fid, '*TITLE\n');
fprintf(fid, 'Brick Aortic Valve\n');
fprintf(fid, '$---+----1----+----2----+----3----+----4----+----5----+--
--6----+----7----+----8\n');
fprintf(fid, '$                    (2) CONTROL CARDS\n');
fprintf(fid, '$---+----1----+----2----+----3----+----4----+----5----+--
--6----+----7----+----8\n');
fprintf(fid, '*CONTROL_TERMINATION\n');
fprintf(fid, '$   ENDTIM    ENDCYC     DTMIN    ENDNEG    ENDMAS\n');
fprintf(fid, '%10f         0       0.0       0.0       0.0\n',
time(time_max));
fprintf(fid, '*CONTROL_TIMESTEP\n');
fprintf(fid, '$   DTINIT      SCFT      ISDO    TSLIMT      DTMS
LCTM     ERODE     MS1ST\n');
fprintf(fid, '      0.00       0.9         0\n');
fprintf(fid, '*CONTROL_HOURGLASS\n');
fprintf(fid, '$      IHQ        QH\n');
fprintf(fid, '         1       0.1\n');
fprintf(fid, '*CONTROL_BULK_VISCOSITY\n');
fprintf(fid, '$       Q2        Q1\n');
fprintf(fid, ' 0.150E+01 0.600E-01\n');
fprintf(fid, '*CONTROL_OUTPUT\n');
fprintf(fid, '$    NPOPT    NEECHO    NREFUP    IACCOP     OPIFS
IPNINT    IKEDIT\n');
fprintf(fid, '         0         0         0         0 0.000E+00
0         0\n');
fprintf(fid, '*CONTROL_ENERGY\n');
```

```
fprintf(fid, '$     HGEN      RWEN    SLNTEN     RYLEN\n');
fprintf(fid, '         1         2         1         1\n');
fprintf(fid, '$---+----1----+----2----+----3----+----4----+----5----+--
--6----+----7----+----8\n');
fprintf(fid, '$                    (4) DATABASE CONTROL CARDS FOR ASCII
FILE\n');
fprintf(fid, '$---+----1----+----2----+----3----+----4----+----5----+--
--6----+----7----+----8\n');
fprintf(fid, '*DATABASE_GLSTAT\n');
fprintf(fid, '   0.12E-3\n');
fprintf(fid, '*DATABASE_RCFORC\n');
fprintf(fid, '   0.12E-3\n');
fprintf(fid, '$---+----1----+----2----+----3----+----4----+----5----+--
--6----+----7----+----8\n');
fprintf(fid, '$                    (5) DATABASE CONTROL CARDS FOR
BINARY FILE\n');
fprintf(fid, '$---+----1----+----2----+----3----+----4----+----5----+--
--6----+----7----+----8\n');
fprintf(fid, '*DATABASE_BINARY_D3PLOT\n');
fprintf(fid, '   0.10E-3\n');
fprintf(fid, '*DATABASE_BINARY_D3THDT\n');
fprintf(fid, '   0.10E-3\n');
fprintf(fid, '*DATABASE_EXTENT_BINARY\n');
fprintf(fid, '         0         0         3         0         1
1         1         1\n');
fprintf(fid, '         0         0         0         0         0
0\n');
fprintf(fid, '$---+----1----+----2----+----3----+----4----+----5----+--
--6----+----7----+----8\n');
fprintf(fid, '$                      (6) DEFINE PARTS CARDS\n');
fprintf(fid, '$---+----1----+----2----+----3----+----4----+----5----+--
--6----+----7----+----8\n');
for i = 1:npart
   fprintf(fid, '*PART\n');
   fprintf(fid, '$ HEADING\n');
   fprintf(fid, ' PART PID =      %2i PART NAME : %s\n',
i,char(part(i)));
   fprintf(fid, '$      PID       SID       MID     EOSID      HGID
GRAV    ADPOPT      TMID\n');
   fprintf(fid, '%10i %9i %9i\n', i,i,i);
end
fprintf(fid, '$---+----1----+----2----+----3----+----4----+----5----+--
--6----+----7----+----8\n');
fprintf(fid, '$                     (7) MATERIAL CARDS\n');
fprintf(fid, '$---+----1----+----2----+----3----+----4----+----5----+--
--6----+----7----+----8\n');
for i = 1:2
   fprintf(fid, '*MAT_HEART_TISSUE\n');
   fprintf(fid, '$ MATERIAL NAME :%s\n', char(part(i)));
   fprintf(fid, '$      MID        RO         C        B1         B2
B3         P\n');
   fprintf(fid, '%10i    0.1E-8  1.913E-1  4.509E-1  1.835E-1  1.835E-1
0.513E+4\n', i);
   fprintf(fid, '$     AOPT\n');
   fprintf(fid, '         0\n');
   fprintf(fid, '$       XP        YP        ZP        A1        A2
A3\n\n');
```

```
   fprintf(fid, '$       V1        V2        V3        D1        D2
D3      BETA\n\n');
end
for i = 3:7
   fprintf(fid, '*MAT_HEART_TISSUE\n');
   fprintf(fid, '$ MATERIAL NAME :%s\n', char(part(i)));
   fprintf(fid, '$      MID        RO         C        B1        B2
B3         P\n');
   fprintf(fid, '%10i    0.1E-8  0.001E+0  10.45E+0  1.925E+0  1.925E+0
7.000E+3\n', i);
   fprintf(fid, '$     AOPT\n');
   fprintf(fid, '         0\n');
   fprintf(fid, '$       XP        YP        ZP        A1        A2
A3\n\n');
   fprintf(fid, '$       V1        V2        V3        D1        D2
D3      BETA\n\n');
end
for i = 8:13
   fprintf(fid, '*MAT_HEART_TISSUE\n');
   fprintf(fid, '$ MATERIAL NAME :%s\n', char(part(i)));
   fprintf(fid, '$      MID        RO         C        B1        B2
B3         P\n');
   fprintf(fid, '%10i    0.1E-8  1.913E-1  4.509E-1  1.835E-1  1.835E-1
0.513E+4\n', i);
   fprintf(fid, '$     AOPT\n');
   fprintf(fid, '         0\n');
   fprintf(fid, '$       XP        YP        ZP        A1        A2
A3\n\n');
   fprintf(fid, '$       V1        V2        V3        D1        D2
D3      BETA\n\n');
end
for i = 14
   fprintf(fid, '*MAT_RIGID\n');
   fprintf(fid, '$ MATERIAL NAME :%s\n', char(part(i)));
   fprintf(fid, '$      MID        RO         E        PR         N
COUPLE         M\n');
   fprintf(fid, '%10i 0.100E-08 0.400E+02 0.490E+00 0.000E+00 0.000E+00
0.000E+00\n', i);
   fprintf(fid, '$      CMO      CON1      CON2\n');
   fprintf(fid, '         1         7         7\n\n');
end
fprintf(fid, '$---+----1----+----2----+----3----+----4----+----5----+--
--6----+----7----+----8\n');
fprintf(fid, '$                      (7.1) SECTION CARDS\n');
fprintf(fid, '$---+----1----+----2----+----3----+----4----+----5----+--
--6----+----7----+----8\n');
for i = 1:npart-1
   fprintf(fid, '*SECTION_SOLID\n');
   fprintf(fid, '$    SECID    ELFORM       AET\n');
   fprintf(fid, '%10i %9i\n', i,1); % 1 means constant stress elements;
2 would mean constant pressure elements
end
fprintf(fid, '$---+----1----+----2----+----3----+----4----+----5----+--
--6----+----7----+----8\n');
for i = 14
   fprintf(fid, '*SECTION_SHELL\n');
```

```
   fprintf(fid, '$      SID    ELFORM      SHRF       NIP      PROPT
QR/IRID     ICOMP\n');
   fprintf(fid, '%10i %29i\n', i,2); % 1 means constant stress
elements; 2 would mean constant pressure elements
   fprintf(fid, '$       T1         T2         T3         T4
NLOC\n');
   fprintf(fid, ' 0.100E+01 0.100E+01 0.100E+01 0.100E+01\n');
end
fprintf(fid, '$---+----1----+----2----+----3----+----4----+----5----+--
--6----+----7----+----8\n');
fprintf(fid, '$                      (8) NODAL POINT CARDS\n');
fprintf(fid, '$---+----1----+----2----+----3----+----4----+----5----+--
--6----+----7----+----8\n');
fprintf(fid, '*NODE\n');
fprintf(fid, '$   NODE               X               Y               Z
TC      RC\n');
for i = 1:nnode
    fprintf(fid, '%8i %15.9f %15.9f %15.9f\n',n(i),xn(i),yn(i),zn(i));
end
fprintf(fid, '$---+----1----+----2----+----3----+----4----+----5----+--
--6----+----7----+----8\n');
fprintf(fid, '$                      (11) SOLID ELEMENT CARDS\n');
fprintf(fid, '$---+----1----+----2----+----3----+----4----+----5----+--
--6----+----7----+----8\n');
fprintf(fid, '*ELEMENT_SOLID\n');
fprintf(fid, '$    EID     PID      N1      N2      N3      N4      N5
N6      N7      N8\n');
for i = 1:nel1
    fprintf(fid, '%8i %7i %7i %7i %7i %7i %7i %7i %7i
%7i\n',e(i),m(i),n1(i),n2(i),n3(i),n4(i),n5(i),n6(i),n7(i),n8(i));
end
fprintf(fid, '$---+----1----+----2----+----3----+----4----+----5----+--
--6----+----7----+----8\n');
fprintf(fid, '$                      (12) SHELL ELEMENT CARDS\n');
fprintf(fid, '$---+----1----+----2----+----3----+----4----+----5----+--
--6----+----7----+----8\n');
fprintf(fid, '*ELEMENT_SHELL\n');
fprintf(fid, '$    EID     PID      N1      N2      N3      N4\n');
for i = nelem0+nelem1+nelem2+nelem3+nelem4+1:nel
    fprintf(fid, '%8i %7i %7i %7i %7i
%7i\n',e(i),14,n1(i),n2(i),n3(i),n4(i));
end
fprintf(fid, '*LOAD_SEGMENT\n');
fprintf(fid, '$     LCID        SF        AT        N1        N2
N3        N4\n');
for i = nelem0+1:nelem0+nelem1
    fprintf(fid, '%10i %9.1i %9.1i %9i %9i %9i
%9i\n',1,1,0,n1(i),n2(i),n3(i),n4(i));
end
for i = nelem0+nelem1+1:nelem0+nelem1+nelem2
    fprintf(fid, '%10i %9.1i %9.1i %9i %9i %9i
%9i\n',2,1,0,n1(i),n2(i),n3(i),n4(i));
end
for i = nelem0+nelem1+nelem2+1:nelem0+nelem1+nelem2+nelem3
    fprintf(fid, '%10i %9.1i %9.1i %9i %9i %9i
%9i\n',3,1,0,n1(i),n2(i),n3(i),n4(i));
end
```

```
for i =
nelem0+nelem1+nelem2+nelem3+1:nelem0+nelem1+nelem2+nelem3+nelem4
    fprintf(fid, '%10i %9.1i %9.1i %9i %9i %9i
%9i\n',4,1,0,n1(i),n2(i),n3(i),n4(i));
end
fprintf(fid, '$---+----1----+----2----+----3----+----4----+----5----+--
--6----+----7----+----8\n');
fprintf(fid, '$                    (16) BOUNDARY CONDITION CARDS\n');
fprintf(fid, '$---+----1----+----2----+----3----+----4----+----5----+--
--6----+----7----+----8\n');
fprintf(fid, '*BOUNDARY_SPC_NODE\n');
fprintf(fid, '$ NID/NSID       CID      DOFX      DOFY      DOFZ
DOFRX     DOFRY     DOFRZ\n');
fprintf(fid, '%10i %9i %9i %9i %9i %9i %9i
%9i\n',dn(1),0,dofx(dn(1)),dofy(dn(1)),dofz(dn(1)),dofrx(dn(1)),dofry(d
n(1)),dofrz(dn(1)));
% CID 0 is the global coordinate system
for i = 2:dnode
    if dn(i) ~= dn(i-1)
    fprintf(fid, '%10i %9i %9i %9i %9i %9i %9i
%9i\n',dn(i),0,dofx(dn(i)),dofy(dn(i)),dofz(dn(i)),dofrx(dn(i)),dofry(d
n(i)),dofrz(dn(i)));
    end
end
% CID 1 needs to be defined for use below;
% It represents the plane of symmetry (coaptation)
fprintf(fid, '*BOUNDARY_SPC_NODE\n');
fprintf(fid, '$ NID/NSID       CID      DOFX      DOFY      DOFZ
DOFRX     DOFRY     DOFRZ\n');
for i = 1:fnode
    test = 1;
    for k = 1:dnode
        if dfn(i) == dn(k)
        test = 0;
        end
    end
    if test == 1
        fprintf(fid, '%10i %9i %9i %9i %9i %9i %9i
%9i\n',dfn(i),1,dofx(dfn(i)),dofy(dfn(i)),dofz(dfn(i)),dofrx(dfn(i)),do
fry(dfn(i)),dofrz(dfn(i)));
    end
end
fprintf(fid, '*BOUNDARY_PRESCRIBED_MOTION_NODE\n');
fprintf(fid, '$      NID       DOF       VAD      LCID        SF
VID     DEATH     BIRTH\n');
% LCID 5 needs to be defined for use below
for i = 1:mnode
    fprintf(fid, '%10i %9i %9i %9i\n',mn(i),3,2,5);
end
fprintf(fid, '*SET_PART_LIST\n');
fprintf(fid, '         1\n');
fprintf(fid, '$     PID1      PID2      PID3      PID4      PID5
PID6      PID7      PID8\n');
fprintf(fid, '         6         7         5         3\n');
fprintf(fid, '*CONTACT_NODES_TO_SURFACE\n');
fprintf(fid, '         1        14         2         3\n\n\n');
fprintf(fid, '*SET_PART_LIST\n');
```

```
fprintf(fid, '         2\n');
fprintf(fid, '$     PID1       PID2       PID3       PID4       PID5
PID6       PID7       PID8\n');
fprintf(fid, '         1          2\n');
fprintf(fid, '*SET_PART_LIST\n');
fprintf(fid, '         3\n');
fprintf(fid, '$     PID1       PID2       PID3       PID4       PID5
PID6       PID7       PID8\n');
fprintf(fid, '         3          4\n');
fprintf(fid, '*CONTACT_AUTOMATIC_NODES_TO_SURFACE\n');
fprintf(fid, '         3          2          2          2\n\n\n');
fprintf(fid, '$---+----1----+----2----+----3----+----4----+----5----+--
--6----+----7----+----8\n');
fprintf(fid, '$                      (17) LOCAL COORDINATE SYSTEM\n');
fprintf(fid, '$---+----1----+----2----+----3----+----4----+----5----+--
--6----+----7----+----8\n');
fprintf(fid, '*DEFINE_COORDINATE_SYSTEM\n');
fprintf(fid, '$       CID        XO         YO         ZO         XL
YL         ZL\n');
fprintf(fid, '         1 0.000E+00 0.000E+00 0.000E+00 0.500E+01-
0.866E+01 0.000E+00\n');
fprintf(fid, '$       XP         YL         ZL\n');
fprintf(fid, ' 0.866E+01 0.500E+01 0.000E+00\n');

%Load Curves
fprintf(fid, '*DEFINE_CURVE\n');
fprintf(fid, '$     LCID       SIDR       SCLA       SCLO       OFFA
OFFO\n');
fprintf(fid, '         1          0\n');
fprintf(fid, '$                   A1                    O1\n');
fprintf(fid, '                    0                     0\n');
%fprintf(fid, '%20f %19f\n',ramptime/10, aop(1));%
for i = 2:time_max
    fprintf(fid, '%20f %19f\n',time(i), aop(i));
end
fprintf(fid, '*DEFINE_CURVE\n');
fprintf(fid, '$     LCID       SIDR       SCLA       SCLO       OFFA
OFFO\n');
fprintf(fid, '         2          0\n');
fprintf(fid, '$                   A1                    O1\n');
fprintf(fid, '                    0                     0\n');
%fprintf(fid, '%20f %19f\n',(ramptime+stabtime)/10,0);%
for i = 2:time_max
    fprintf(fid, '%20f %19f\n',time(i), -lvp(i)+aop(i));
end
fprintf(fid, '*DEFINE_CURVE\n');
fprintf(fid, '$     LCID       SIDR       SCLA       SCLO       OFFA
OFFO\n');
fprintf(fid, '         3          0\n');
fprintf(fid, '$                   A1                    O1\n');
fprintf(fid, '                    0                     0\n');
fprintf(fid, '%20f %19.9f\n', time(time_max),0.*0.0133/100);

fprintf(fid, '*DEFINE_CURVE\n');
fprintf(fid, '$     LCID       SIDR       SCLA       SCLO       OFFA
OFFO\n');
```

```
fprintf(fid, '         4         0\n');
fprintf(fid, '$                 A1                  O1\n');
fprintf(fid, '                  0                   0\n');
%fprintf(fid, '%20f %19f\n',ramptime/10, lvp(1));%
for i = 2:time_max
    fprintf(fid, '%20f %19f\n',time(i), lvp(i));
end

% Calculate longitudinal stretch to be applied
coef = 0;
hmax = zn(1809);
hmin = zn(269);
ho = hmax-hmin;
lambda = 1.2;
hs = ho*lambda;
h = hs-ho;

fprintf(fid, '*DEFINE_CURVE\n');
fprintf(fid, '$     LCID      SIDR      SCLA      SCLO      OFFA
OFFO\n');
fprintf(fid, '         5         0\n');
fprintf(fid, '$                 A1                  O1\n');
fprintf(fid, '                  0                   0\n');
%fprintf(fid, '%20f %19.9f\n',ramptime/10, h);%
fprintf(fid, '%20f %19.9f\n', time(2),h);
fprintf(fid, '%20f %19.9f\n', time(time_max),h);
fprintf(fid, '*END\n');
fclose(fid);

if stop == 1
end
```

APPENDIX B – MATLAB Code for Material Constant Identification

This appendix presents the routine developed to numerically optimize the material constants. This particular code optimizes the material constants for the leaflet based on the biaxial test performed by Billiar and Sacks in 2000.

```
% The Guccione material constants are determined using the Levenberg-
Marquardt
% method. Data from Billiar and Sacks II.

clc   % clears command window
clear % clears all variables
format long
load data.dat; % loads the experimental data file

global sig11exp sig22exp E11exp E22exp sig11t sig22t Constants
       % declares constants shared with other m-files

t0=0.466; % initial thickness (mm)
sig11exp=data(:,1)/t0; % experimental Piola-Kirchhoff stress (MPa)
sig22exp=data(:,1)/t0;
E11exp=data(:,2); % experimental circumferential Green strain
E22exp=data(:,3); % experimental radial Green strain
sig11exp=sig11exp.*sqrt(1+2.*E11exp); % experimental Cauchy stress
(MPa)
sig22exp=sig22exp.*sqrt(1+2.*E22exp);

options=optimset('largescale','off','MaxFunEvals',1e100,'tolFun',...
    1e-7,'TolX',1e-30,'MaxIter',5e3,'LevenbergMarquardt','on'); % turns
on
% Levenberg-Marquardt method of solution
iniconstants=[0.01 1 1]; % initial guesses for material constants
lb=[0.001; 0; 0];
ub=[1; 100; 100];
[Constants]=lsqnonlin(@errSC,iniconstants,lb,ub,options)
% the optimizer calls the @errSC m-file

function error=errSC(C)

global sig11exp sig22exp E11exp E22exp sig11t sig22t
c1=C(1);
c2=C(2);
c3=C(3);

E11=E11exp;
E22=E22exp;

delta=(1+2.*E11).*(1+2.*E22);
q=c2.*E11.^2+c3.*(E22.^2+(0.5.*(1./delta-1)).^2);
dW11=2.*c2.*E11-c3.*(1./delta-1)./(delta.*(1+2.*E11));
dW11=0.5.*c1.*dW11.*exp(q);
```

```
dW22=2.*c3.*E22-c3.*(1./delta-1)./(delta.*(1+2.*E22));
dW22=0.5.*c1.*dW22.*exp(q);

sig11t=(2.*E11+1).*dW11; % theoretical s11
sig22t=(2.*E22+1).*dW22; % theoretical s22
errs11=(sig11t-sig11exp);
errs22=(sig22t-sig22exp);
error=[errs11;errs22]; % combines errs11 and errs22 into one vector
```

APPENDIX D – Data collected from the aortic root pressurization

Table 8 – Experimental data collected from the aortic root pressurization. Pressure, outer diameter (OD), inner diameter (ID), and length (L), respectively.

Pressure	OD	ID	L
mmHg	mm	mm	mm
0	26.70	20.18504	9.29
20	28.32	21.99613	9.95
40	30.49	24.46265	10.71
60	32.51	27.17494	11.61
80	34.23	29.64006	12.74
100	36.39	32.31182	13.82
120	38.43	34.59541	14.77